PROBLEMY EKSPLOATACJI

MAINTENANCE PROBLEMS

No 3/2015

Contents

Andrzej MAJCHER

Institute for Sustainable Technologies – National Research Institute, Radom

andrzej.majcher@itee.radom.pl

BATCH CONTROL OF MICROWAVE HYDROTHERMAL SYNTHESIS OF NANOPOWDERS PROCESS

Key words

Batch control of chemical processes, microwave hydrothermal synthesis, stop-flow mode, nanopowders.

Abstract

Microwave hydrothermal synthesis processes allow to obtain the nanopowders of extremely high quality. However, their disadvantage in terms of industrial applications is low productivity. The article presents a technological system that breaks this barrier. A novel chemical reactor is described. The reactor has a unique design of process chamber, which used in conjunction with a batch control system allows highly efficient production of nanopowders to be obtained. The design of the reactor together with new principles of operation, structural materials, and distribution of electromagnetic field are described. The paper also presents a control system for the reactor, which allows for automatic operation in the stop-flow mode, control of process pressure, continuous monitoring of process parameters and safe operation of the device.

Introduction

Microwave hydrothermal synthesis is one of hydrothermal processes that are used for the procurement of nanopowders with controlled chemical content and morphology characterised by minor differences in the size of the grains [1]. Application of microwaves significantly increases the speed at which synthesis takes place for ceramic materials (e.g. titanium oxide and oxides of other metals, hematite, barium titanate, lead zirconate titanate, lead titanate, potassium niobate) and metal powders including: nickel, cobalt, platinum, palladium, gold, silver and others [2]. Organic syntheses in which microwave radiation is applied form a separate group of synthesis reaction. This type of processes lead to the generation of, inter alia, various bioactive heterocyclic compounds, azides, thiocyanates and sulfones, or bimetallic systems including Pt–In, Ag–Pt, Pt–Fe, Cu–Pd, Pt–Pd, Pd–Fe, single and polyhedral nanotubes, composite materials [3, 4, 5, 6]. Majority of these materials are characterised by a high commercial potential, and can be applied particularly in electronic, optoelectonic, pharmaceutical, chemical, cosmetic, ceramic and machine industries.

Increase in the process kinetics by means of micro-waves, which from the point of view of mass production is of great advantage, is unfortunately hampered by the lack of proper apparatus. Most of microwave hydrothermal synthesis reactions still take place in laboratory in modified microwave ovens. Commercial devices for microwave thermal syntheses with greater efficiency can be divided into: large closed vessel reactors, stop-flow reactors and flow reactors [7–10]. The advantages and limitations of all these types of reactors are present in numerous publications [11–16]. Main drawbacks of existing solutions from the point of view of mass production are as follows: low efficiency (in the case of large vessel reactors and stop- flow reactors), low flow of the substrate and the product of particularly thick suspensions in flow reactors.

1. A novel reactor with a moveable process batch

The reactor (Fig. 1a, b) is a stop-flow type reactors. Substrates are fed through the dosing pump (PM) from the container equipped with a mechanical mixing system and a level sensor (CK1). Pressure (P) in the chamber is measured with the use of a strain gauge force sensor (CTa), and temperature with the use of thermocouples located on the outside of the top (Tpg) and bottom (Tpd) wall of the chamber and the thermocouple that is in contact with the Teflon batch in the chamber. The outflow of the product can take place at the temperature and pressure of the reaction, which introduces an additional effect of quick drying. At low pressure of the product, the emptying of the chamber is supported by the neutral gas pressure pressure or pressure of the air coming through the electromagnetic valve (ZP3) and the return valve (ZZ).

The explosion protection system scatters kinetic energy of the bottom plunger and is controlled by the sensor (CK2).

a)

b)

c)
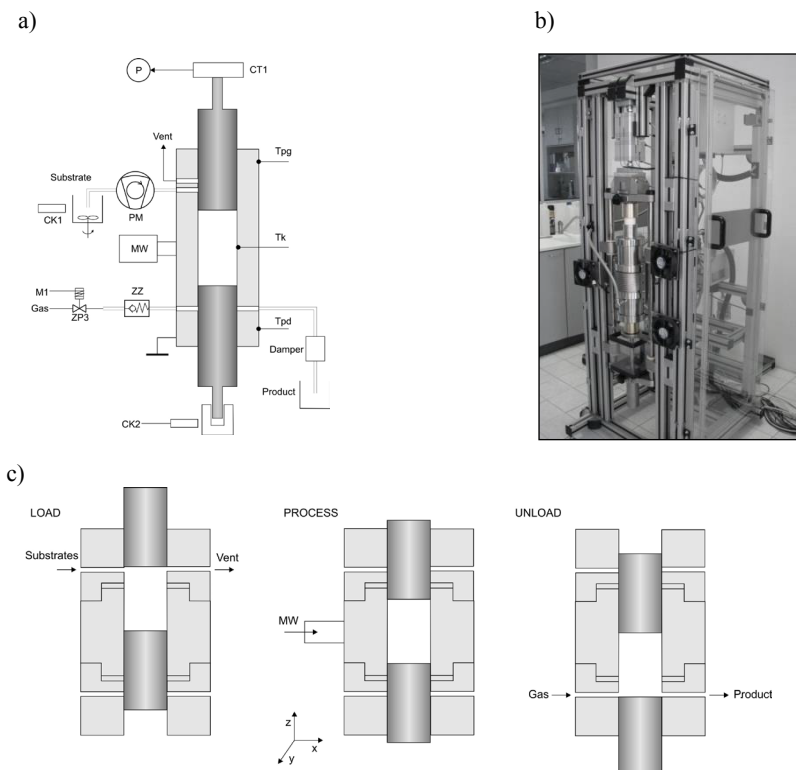
Fig. 1. General draft of the reactor (a), view of the prototype with the front cover taken off (b) principle of operation of the load and unload system (c)

A unique structure of the process chamber, uncommon for other solutions of this type, was applied in the reactor presented (Fig. 1c). The structure is close on both sides with moveable plungers, which in consecutive stages of the process position the batch at the level of load slots of the microwave waveguide (MW) and chamber unload slots.

All the elements that are in contact with the substrate and the product are made of chemically resistant materials – PTFE Teflon (connection lines, head of the dosing pump, middle part of the process chamber, seals) and Al_2O_3 ceramics (plungers, top and bottom part of the process chamber). Reaction pressure amounts to 6 MPa, which is obtained through the heating of the batch, however operation at higher pressure (up to 20 MPa), obtained with the application of the suitable dosing pump or the external source of compressed air, is also possible. The allowed temperature of continuous operation is 270°C. The reactor is cooled down with the forced airflow.

a)   b)   c)
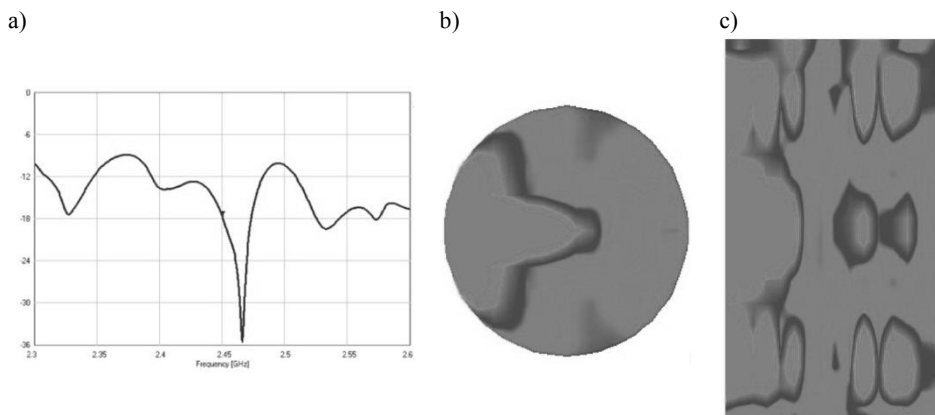
Fig. 2. Results of the analyses of the distribution of the electromagnetic field for the MSS2 reactor: a) frequency characteristics for reflection coefficient |*S11*|; b) distribution of average bulk density of power losses in the *xy* plane; c) distribution of average bulk density of power losses in the xy plane; scale 5 µW/mm^2, medium in the chamber – water

The dimensions of the chamber were set with the use of computer simulations (QWED) so that the best adjustment of the chamber to the microwave generation path could be achieved, no leakage of microwaves at the ends of the plungers prevented, and a homogenous arrangement of the electromagnetic field ensured (Fig. 2).

The microwave track of the device includes a generator with the 3 kW magnetron and a proper feeder (ERTEC Poland). The track is also equipped with two reeds located in the waveguide connecting the circulator with the process chamber, which together with reflected power measurement system allows for the system to be adjusted at the time of the process.

2. Process control

The main tasks realised in the process control system include:
− Regulation of process parameters;
− Superior control of processes;
− Monitoring and record of processes;
− Security and emergency states maintenance.

For the regulation of pressure (Fig. 3), due to maximum speed of temperature rise and high delay caused by the microwave magnetron feeder, a two-phase regulator with hysteresis was applied.

The dynamics of the object can be determined with the use of the balance of power supplied to the reaction chamber. Power of the microwave generator P_0 is partly reflected and the power that is actually supplied to the chamber is power P_e:

$$P_e = \eta P_0 \tag{1}$$

where: η – power supply efficiency coefficient.

The power absorbed by the substrate is defined with the following:

$$P_e = 2\pi f \varepsilon_0 \varepsilon'' E^2 V \tag{2}$$

where:

f – microwave radiation frequency,
ε_0 – electric permittivity of vacuum, ε_0 = 8.85 10–12 F/m,
ε'' – dielectric dissipation,
E – electric field intensity with frequency f,
V – batch volume, V_{max} = 400 ml.
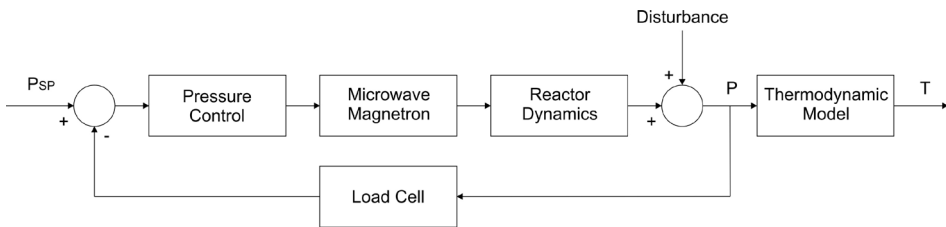
Fig. 3. Block diagram of pressure P regulation system and process temperature T determination

Power Pe is changed into heat P_t and by means of convection (P_c) and radiation (P_r) lost:

$$P_e = P_t + P_c + P_r \tag{3}$$

$$P_t = mc_w \frac{dT}{dt} \tag{4}$$

$$P_c = \alpha S(T - T_a) \tag{5}$$

$$P_r = \varepsilon \sigma S T^4 \tag{6}$$

where:

m – batch weight,
c_w – actual heat of batch,

T – temperature in re action chamber,
t – time of temperature rise,
α – convection coefficient,
S – field of external surface of chamber,
T_a – temperature of the surrounding,
ε – emissivity,
σ – Stefan-Boltzmann's constant, $\sigma = 5.67 \times 10^{-8}$ W/(m^{2}K^4).

Transforming equations (2) –(6) the following formula for the determination of the speed of temperature increase can be obtained:

$$\frac{dT}{dt} = \frac{2\pi f \varepsilon_0 \varepsilon'' E^2 V - \alpha S (T - T_a) - \varepsilon \sigma S T^4}{m c_w} \tag{7}$$

Solution to this equation for real synthesis process poses a lot of difficulties. The water dielectric dissipation coefficient is a non-linear temperature function. Additional problems occur in the case of mixtures that also contain non-polar ingredients [17]. Nonlinearity of the object is also visible in the case of work of the pressure regulator (Fig. 4).
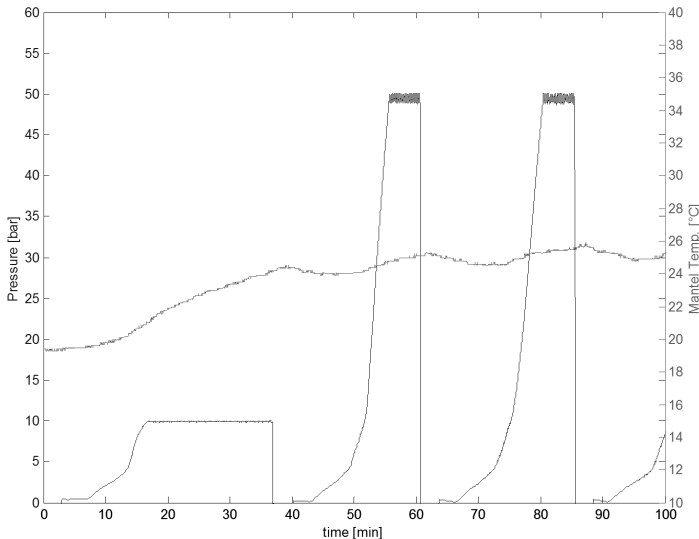
Fig. 4. Pressure and temperature course in the chamber: Psp1 = 10 bar, Psp2 = 50 bar, batch – deionised water 350 ml

Temperature T is measured according to the following water thermodynamic model [18]:

$$P = A10^{\left(\frac{mT}{T+T_n}\right)} \tag{8}$$

where: A, m, T_n – coefficients depending on temperature changes.

Maximum error occurs in the range of 200–350°C and it amounts to 0.59%. The measurement of the steam saturation temperature in the control system has an informational character and is not applied in the control process.

3. Batch control of the process

Superior process control is realised according to the PN-EN 61512 norm for the control of batch processes. In this control the realization of the process takes place automatically with the use of a procedure (technological recipe) which contains single phases of the process.

The process is divided into phases of (Fig. 5a): chamber load, process, chamber unload, chamber overflow, with the following parameters: *Load (V)*, Process (p_p, P, t_p), *Unload* (p_u, t_u), *Overflow* (V, t_u),

where:
- V – batch volume,
- p_p – pressure in the process chamber,
- P – power of microwave generator,
- t_p – pressure regulation time,
- p_u – level of pressure at which process chamber is opened, $p_u = 0$ stands for immediate opening of the chamber,
- t_u – process chamber scavenge time.

Consecutive realisation of the stages is equivalent with the realisation of the process with the aforementioned parameters set (Fig. 5c). The realisation of the process may also take place in the phase control mode in which each of the phases is realised as a single task, or in the manual control mode , in which each unit of the reactor can be switched on individually with the parameters set.

In automatic control the cyclical repetition of the programmed technological recipe is possible (Fig. 5b), which leads to the automatic processing of the prepared volume of the substrate.

The system controls suitability of phase conditions (i.e. no pressure in the process chamber for the load phase, or presence of substrates in the process chamber for the process phase). Realisation of each of the phases can be paused manually at any time and the process can be resumed once a new sequence of procedural control is programmed or the paused process stopped by the

realisation of appropriate phases in phase control and the procedural control with the current technological recipe resumed.

a)

b)

c)
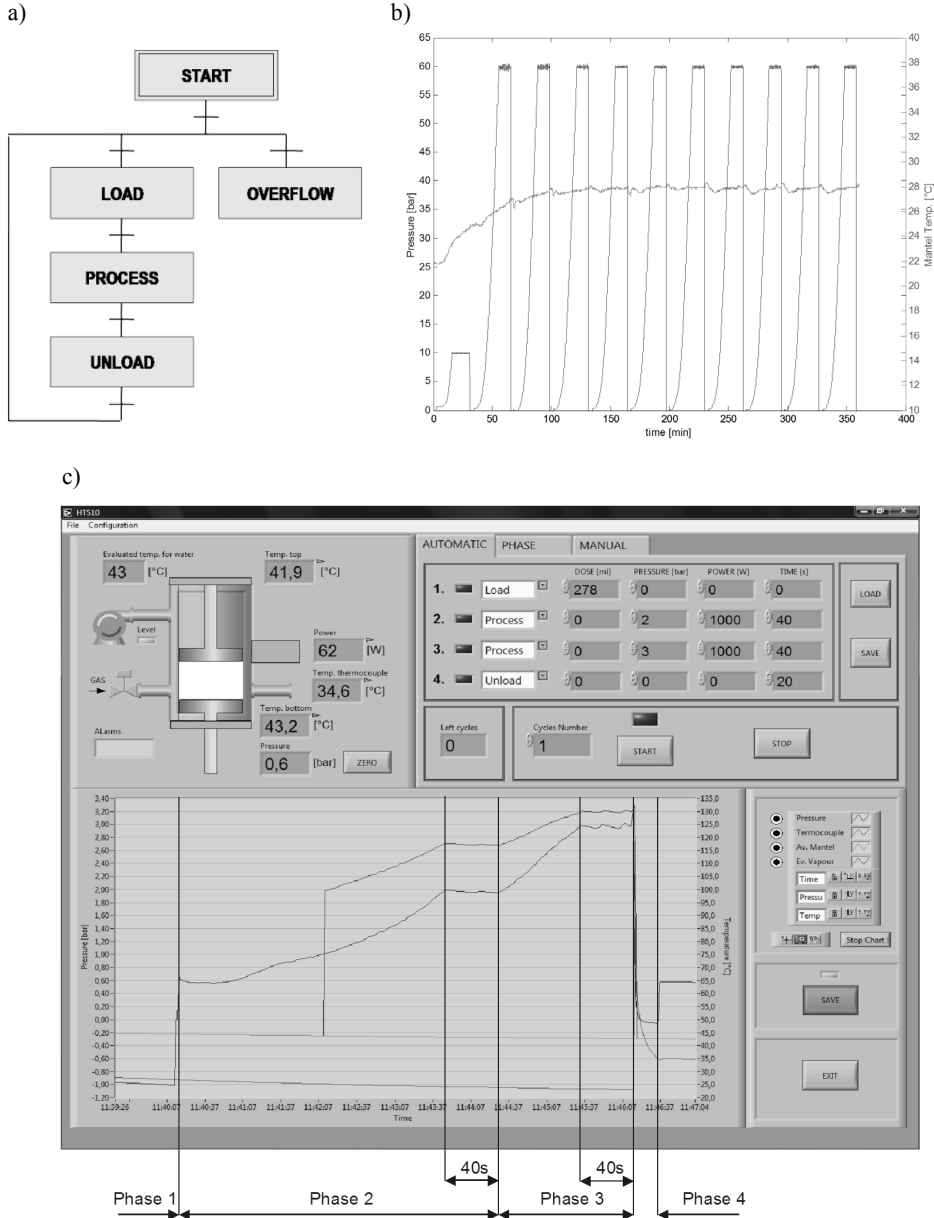
Fig. 5. Batch process control: a) process phases; b) course of process variables for cyclical recurrence of technological recipe realisation; c) image of the window of the control programme after realisation of a single recipe: Phase 1 – Load (278 ml), Phase 2 – Process (2 bar, 1 kW, 40 s), Phase 3 – Process (3 bar, 1 kW, 40 s), Phase 4 – Unload (0, 20 s)

Technological recipes are stored in text sets. The software allows for the use of formerly programmed recipes and their design in form of text sets in different environments than the main programme of the device.

Alarm and security procedures implemented in the control system constitute a supplement to hardware security. Emergencies are divided into levels connected with:
− condition of the device,
− setting of process parameters,
− initial conditions of process realisation phases,
− real values of process parameters.

Condition of the device is measured in the real time mode with the frequency of reading, in the control computer, of 1 Hz. This includes the following discrete stages: four side panels (removed, installed), state of the magnetron feeder (preparation to operation, readiness), pressure of air supplying pneumatic systems (too low, proper), activation of the explosion system, jamming of the plungers of the process chamber, level of fluid in the dosing pump container. The incorrect value of the state signal blocks the possibility for the realisation of processes.

Parameter setting is limited to nominal ranges. This concerns parameters of functions realised in manual, phase and procedural control modes.

Initial conditions for the realization of process phases are also checked in each of the control modes. All possible collisions are specified as follows:
− shift of plungers of the process chamber to the top position at the chamber pressure value above zero. This causes dosing pump damage or the rupture of the line through which substrates are fed,
− ignition of microwave heating when the process chamber is totally empty or filled in 10% only. This leads to the damage to the microwave track (circula-tor, magnetron) or overheating of chamber Teflon batch.

In the case of the above listed situations, the programme informs the user and prevents the realization of collision likely control procedures.

Real values of process parameters concern analogue signals, particularly pressure in the process chamber of the reactor, which is measured at the frequency of ca. 0.5 kHz and controlled by the PLC controller in the device.

Protection against microwave radiation constitutes an important safety aspect. Measured according to the PN-EN 55011 norm ("Industrial, medical and scientific devices with radio frequency") average values of electromagnetic disturbances do not exceed 70 dB (μV/m). The measurements were taken with the use of the FSH 8 electromagnetic field meter (by Rohde & Schwarz) with the HE 300 aerial (by Rohde & Schwarz) in the place where the reactor was installed. The device is also equipped with WPM-1 radiation indicator (ERTEC Poland) for constant monitoring of the level of microwave radiation emission.

The reactor was applied for the production of nano-crystal zinc oxide (ZnO--NPs) and nanocrystal zinc oxide mixed with cobalt (ZnO:Co-NPs) [19–22].

Summary

The original architecture of the reactor presented allows for full automation of the process and the procurement of nanopowders in a significantly greater scale than in the case of the application of laboratory equipment. It radically speeds up the realization of the process and enables to obtain products measured in litres, not as in the case of laboratory apparatus, millilitres.

The size of the process chamber does not influence excessive disturbances in the homogeneity of the distribution of the electromagnetic field and the existing heterogeneity of this distribution causes spontaneous mixing of the batch and prevents the creation of points with increased temperature.

A significant advantage of the reactor consists in the maintenance, thanks to the application of chemically neutral materials, of high cleanliness of reaction and low sensitivity to substrates of high density, suspensions with sedimentation tendencies included.

The control system enables automatic realization of processes with consideration of operator and environment safety aspects and allows for the device to be easily included in a complex technological line.

Nanopowders obtained in the device are characterized by low distribution of grain size, high purity, and high production recurrence, which confirms the usefulness of the device in chemical, pharmaceutical and cosmetic industries.

References

1. Somiya S., Roy R.: Hydrothermal synthesis of fine oxide powders. Bulletin of Materials Science, Vol. 23, No. 6, 2000, pp. 453–460.
2. Somiya S., Roy R., Komarneni S.: Hydrothermal Synthesis of Ceramic Oxide Powders. In Lee B., Chemical Processing of Ceramics, Second Edition. Taylor & Francis Group, 2005, pp. 4–20.
3. Masashi I.: Solvothermal Synthesis. Chemical Processing of Ceramics, Second Edition. Taylor & Francis Group, 2005, pp. 22–63.
4. Kappe C.O., Dallinger D.: Controlled microwave heating in modern organic synthesis: highlights from the 2004–2008 literature. Molecular Diversity, 13, 2009, pp. 71–193.

5. Polshettiwar V., Mallikarjuna M.N., Varma R.S.: Microwave-Assisted Chemistry: a Rapid and Sustainable Route to Synthesis of Organics and Nanomaterials. Australian Journal of Chemistry 62(1), 2009, pp. 16–26.
6. Hayes B.L.: Microwave Synthesis: Chemistry at the Speed of Light. CEM Publishing: Matthews, NC, 2002.
7. Barnhardt E.K.: Microwave ring expansion reactions performed at sub-ambient temperatures. ACS National Meeting, 2004.
8. Lonelli C., Łojkowski W.: Main development directions in the application of microwave irradiation to the synthesis of nanopowders. Chemistry Today 25 (2007) 34, pp. 36–38.
9. Lidstrom P., Tierney J., Wathey B., Westman J.: Microwave assisted organic synthesis – a review. Tetrahedron 51, 2001, pp. 9225–9283.
10. Dallinger D., Kappe O.: Microwave-Assisted Synthesis in Water as Solvent. Chemical Reviews 2007, 107, pp. 2563–2591.
11. Strauss R.C.: On scale up of organic reactions in closed vessel microwave systems. Organic Process Research & Development 2009, 13, pp. 915–923.
12. Lehman H., LaVecchia L.: Evaluation of microwave reactors for prep-scale synthesis in a kilolab. JALA Journal of Laboratory Automation 2005, 10, 412–417.
13. Bowman M.D., Holcomb J.L., Kormos C.M., Leadbeather N.E., Williams V.A.: Approaches for scale-up of microwave-promoted reactions. Organic Process Research & Development 2008, 12, pp. 41–57.
14. Moseley J.D., Leden P., Lockwood M., Rudna K., Sherlock J-P., Thomson A.D., Gilday J.P.: A comparison of commercial microwave reactors for scale-up within process chemistry. Organic Process Research & Development 2008, 12, pp. 30–40.
15. Narendra G.P. at al: Effect of load size on the efficiency of microwave heating under stop flow and continuous flow conditions. Journal of Microwave Power and Electromagnetic Energy, 46(2), 2012, pp. 83–92.
16. Wiesbrock F., Hoogenboom R., Schubert U.S.: Microwave-Assisted Polymer Synthesis: State-of-the-Art and Future Perspectives. Macromolecular Rapid Communications 2004, 25, pp. 1739–1764.
17. Kennedy A., Reznik A., Tadesse S., Nunes J.: Time dependence of component temperatures in microwave heated immiscible liquid mixture. Journal of Microwave Power and Electromagnetic Energy, 43(2), 2009, pp. 52–62.
18. Wagner W., Pruss A.: The IAPWS Formulation 1995 for the thermodynamic properties of ordinary water substance for general and scientific use. Journal of Physical and Chemical Reference Data, Vol. 31, No. 2, 2002, pp. 387–535.
19. Wojnarowicz J., Opalińska A., Smoleń D., Kuśnieruk S., Chudoba T., Łojkowski W.: Solvothermal synthesis of doped zinc oxide nanopowder for NanFATE. Nano-Biotechnologia PL, (2012), Warszawa.

20. Majcher A., Wiejak J., Przybylski J., Chudoba T., Wojnarowicz J.: A novel reactor for microwave hydrothermal scale-up nanopowder synthesis. International Journal of Chemical Reactor Engineering. Volume 11, Issue 1, 2013, pp. 1–8.
21. Majcher A.: Automation of the process of microwave hydrothermal synthesis of nanopowders. Pomiary Automatyka Robotyka PAR, 2/2013, pp. 208–212.
22. Łojkowski W., Leonelli C., Chudoba T., Wojnarowicz J, Majcher A., Mazurkiewicz A.: High-energy-low-temperature technologies for the synthesis of nanoparticles: microwaves and high pressure. Inorganics 2014, 2(4), pp. 606–619.

Wsadowa realizacja procesów hydrotermalnej syntezy nanoproszków

Słowa kluczowe

Sterowanie wsadowe, mikrofalowa synteza hydrotermalna, tryb pracy stop-flow, nanoproszki.

Streszczenie

Mikrofalowe hydrotermalne procesy syntezy pozwalają na uzyskiwanie nanoproszków o wyjątkowo wysokiej jakości. Natomiast ich wadą w aspekcie zastosowań przemysłowych jest niska wydajność. W artykule przedstawiono system technologiczny, który przełamuje tę barierę. Opracowano nowy typ reaktora, posiadającego unikatową konstrukcję komory procesowej, co w połączeniu z zastosowanym systemem sterowania wsadowego pozwala na uzyskiwanie dużej wydajności produkcji nanoproszków. Opisano konstrukcję reaktora z uwzględnieniem nowej zasady działania, materiałów konstrukcyjnych, rozkładu pola elektromagnetycznego. Przedstawiono system sterowania urządzeniem, który zapewnia automatyczną realizację procesów, regulację ciśnienia procesu, ciągłe monitorowanie parametrów procesów oraz zachowanie bezpieczeństwa obsługi urządzenia.

Jacek WOJUTYŃSKI

Institute for Sustainable Technologies – National Research Institute, Radom
jacek.wojutynski@itee.radom.pl

A METHOD FOR THE CONSTRUCTION OF SOFTWARE AND A CONTROL SYSTEM FOR TESTING AND CERTIFICATION DEVICES IN THE FURNITURE INDUSTRY

Key words

Certification, test, device, furniture, PLC, HMI, impact hammer test.

Abstract

The article presents the problem of designing test equipment for testing and certification of furniture and materials used in the furniture industry. One of the main issues is the modularization of equipment and the automation of the tests. A natural consequence of the application of the modular structure of the hardware devices is the modularization of software to provide the synchronization of the operation of individual modules. This paper presents a software design methodology for the measuring and control of test equipment for the testing of furniture. The issues related to the diagnostics of the measurement and control system and the monitoring of the process of testing are discussed. A method was developed for the calibration of measurement circuits and the testing of the accuracy of positioning of products being tested. An example of process automation a functional device for impact test data of furniture is presented. The possibilities of applications of a developed solution for the impact testing of glassware are presented.

Introduction

Selected standards defining the proof tests and certification in the furniture industry [7] were analysed and the constructions of equipment from global manufacturers were reviewed 1–4. From the furniture industry, the standards for testing of chairs, tables, desks and bed frames were selected. The main tests of furniture are conducted for their stability, static strength, and fatigue and impact resistance. By analysing the standards, the construction blocks for testing equipment of furniture were identified. These are modules to exert vertical force and the horizontal force and the realisation of vertical and horizontal impacts.

A separate group constitutes speed control modules generally realised by means of an inverter for the AC motors or a PWM controller for the DC motors. The photographs (Fig. 1) show the completed test apparatus for furniture. The paper presents the following hardware and software modules that were found useful in the construction of the equipment for testing furniture:

- A module for the implementation of vertical and horizontal forces,
- A module for the implementation of the horizontal impacts, and
- A calibration module for measurement channels.

1. Control-measurement system for proof testing and certification equipment for the furniture industry

It was assumed that the control-measurement system would be implemented based on a modular controller PLC[1] with HMI touch operator panel, and a FC5A-type controller was selected with a built-in webserver D12S1E and operator's panel HG1F or HG2G from IDEC. The controller and panel connections to other devices were implemented through a local network and Modbus protocol (RTU TCP) [8], [9]. An example of the implementation of measurement and control system is shown in Fig. 2. Depending on the device, this scheme can be simplified. There are always preferred solutions with galvanic insulation.

The diagnostics of the sensor data were provided by the relevant programming modules for analogue inputs and outputs of the PLC controller and allow easy conversion of measured analogue values into "engineering units" without the programming of special software.

The touch panel allows the operator to set the number of cycles, the duration of force exertion, cycle time or the force value, temperature value, etc. For example, the synchronization of force exerting modules may include (1) the start of the next cycle after returning to the retraction position of actuators, or (2) further exertion of force upon reaching by the all actuators the position of contact of stamp with the surface of the furniture. Software functions of the HMI

---

[1] FC5A-D12S1E controller from IDEC with built-in webserver.

operator panel and PLC controller make the software procedure (module) distributed.

a)

b)

c)

Fig. 1. a) Device for testing the rotary bases of office chairs and for rotation test of chair according to p. 7.3.3 and p. 7.3.5 of the PN-EN 1335-3:2099 standard, type **BK-EN 1335-3**, b) Device for impact testing the furniture, type **MU-M/D**, c) Device for testing the endurance and hardness of bed frames according to PN-EN 1957:2002 standard 5, 6

a)   b)
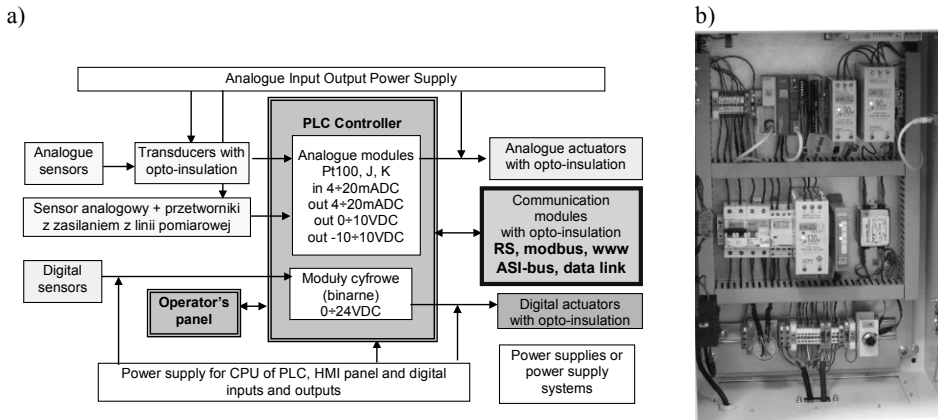
Fig. 2. a) Scheme of measurement circuit with two separate DC power supplies for analogue and
         for digital circuits, CPU and operator's panel; b) Realisation of control and measurement
         system for the device for testing the impact resistance of furniture (Fig. 1b)

RS232/485 output module supplied by the IDEC complete the communication protocol that provides the possibility for communication and programming the devices on a PC. The SCADA software module is implemented in Delphi and works in Windows 98 and Windows 8 environments without the installation of additional libraries and components.

In the controller used, all the software resources (inputs, outputs, registers, internal relays – also called flags, counters, Timers) are global. The controller is programmable in Ladder Logic Diagram Programming. The software has an expanded list of instructions for the ladder diagram. Due to the large reserves of flags, registers, timers, and counters, the "systematic programming rule" [10] was applied: All the flags and registers associated with the actuator are, e.g., in terms of numbers starting with 100–119, the next area is 120–139, etc. The application of regularity in the designation of registers defining the scope of analogue signals and in the designation of the current scope of measured (or computed) signal causes the following:

- Easy creation and modification of the control system software,
- Transparency of software, and
- Simplified commissioning of different software modules.

1.1. Technique for programming with flags

Since the controller programming is done using the LD, the technique of microprocessor systems programming and the creation of complex control software [11] was applied. Flags are understood here as a bit controlling the operation of sub-processes. The idea of programming techniques using the flags is shown in (Fig. 3a). The **FLGn** flag is set to the ON state and starts up the

process. When the process (1) terminates or (2) meets the relevant conditions (e.g. an achieved position) or (3) generates alarm situations (the red line) or (4) has reached a preset control time, the **FLAGn** flag is set to the OFF state. Flag **FLAGn** at any moment can be reset from the main program of the PLC controller. Sometimes resetting makes it necessary to securely terminate the process. The **FLAGn** flag can be used to control the state of the process. This technique allows 'concurrent' operation of processes, where there can be several processes initiated simultaneously (Fig. 3b). Flags from some processes may condition the performance of other processes. The author uses and recommends the use of a separate synchronization process to control the process sequence, e.g. to control several actuators. Each process can run more processes (Fig. 3c). Concurrency is apparent here, since the program in the PLC is executed sequentially every few milliseconds, but from the point of view of the observer it appears to be performing concurrently and performing control tasks at maximum speed.
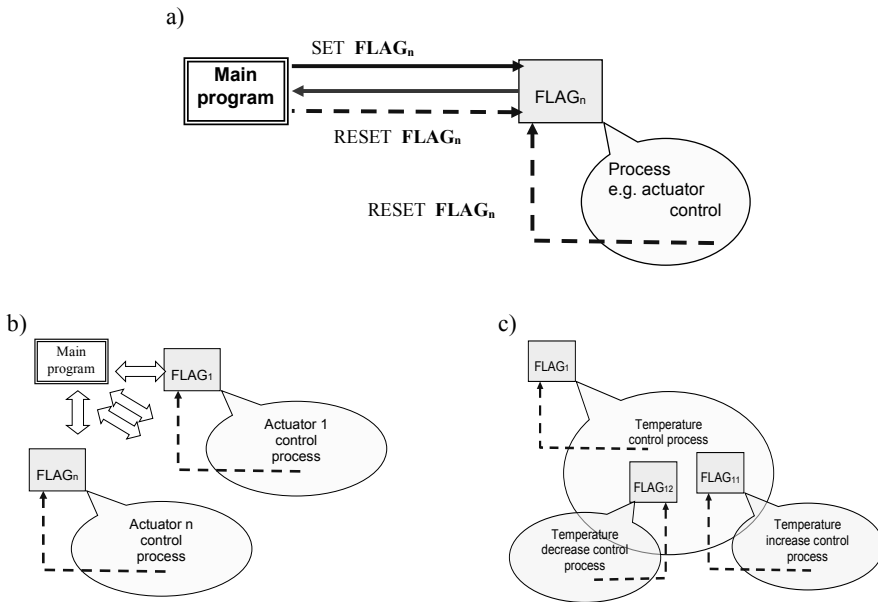
Fig. 3. Technique for programming with flags: a) The principle of control, b) Concurrency of processes, c) Controlling the sub-processes

The processes in Fig. 3 can be related to the operator's panel screens that define and initiate the processes. Then a switch and buttons on the operator panel initiate the beginning of the process.

2. Force exertion module

The method of exerting a vertical (horizontal) force is implemented by means of a pneumatic cylinder (Fig. 4). The air pressure corresponding to set force is supplied to the pneumatic cylinder. Piston position sensors are used for checking the control states. Pressure to force is converted automatically in the controller. The force exerted by pneumatic cylinders is specified by standards with an accuracy of 5% FS. The system shown in Fig. 4 ensures that accuracy.
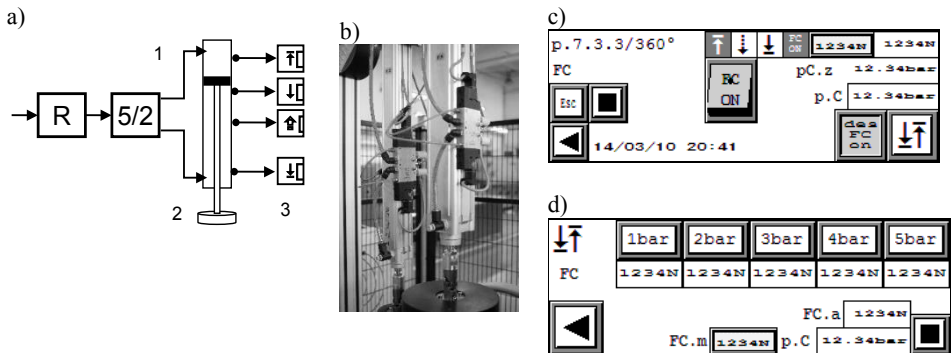
Fig. 4. The system for vertical or horizontal force exertion for the device (Fig. 1a): a) Block diagram, b) Valves fixed on the pneumatic cylinder, c) Manual actuator control screen d) Calibration screen for pressure-force tract for 40mm pneumatic cylinder; 1 – Double-acting pneumatic cylinder with valves, 2 – Holding plate, 3 – Piston position sensors, R – precise manual or electronic pressure regulator, 5/2 – electrical valve. Piston position: ⊤, ⊥ – at limit, ↓ – working, ⇧ – element damage

Screens from Fig. 4c correspond to the sub-processes, where the FC/ON/OFF switch acts as a flag for cylinder action and the exertion of proper force.

The screen from Fig. 4d is used to calibrate the tract of the cylinder. The calibration results are automatically stored in the calibration macro. It is realised by the calibration software. The process is initiated by opening and stopped by closing the screen. Thanks to the software features of operator's panel, part of the operations performed by the controller is performed by the operator's panel.[2]

Emergency situations in the case of this module are defined as follows:
- In the case of setting the FC flag:
  1) A lack of a signal reaching the working position after a certain time,
  2) A lack of signal leaving the limit position after a certain time,
  3) A signal reaching the element damage position;
- In case of resetting the FC flag:
  1) A lack of signal reaching the limit position after a certain time.

---

[2] Mutual locking of buttons, the ranges of input values of forces, the signalling of faulty data, macros for the calculation of values, the handling of different language versions, etc.

Emergency situations are defined for all processes and are processed by a separate process – ERROR.

3. Horizontal impact module

The module for the implementation of the horizontal impacts is composed of (Fig. 5a) the following:

- A DC motor (4) operating in one direction and connected by an Oldham-flex[3] coupling to electrical clutch (3);
- The handle of a hammer (2) connected by bellows coupling[4] of potentiometric angle position transducer (1) is mounted to the armature of the electrical clutch; and,
- The entire structure is designed to be fixed to the frame structure built of ⌀38 mm pipe.
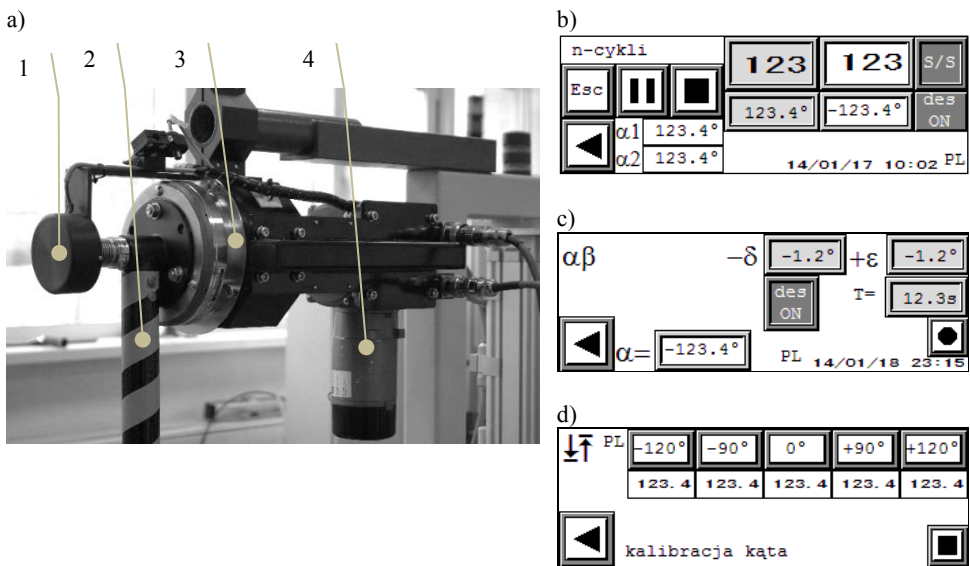
Fig. 5. System for vertical impacts for the device (Fig. 1b): a) Solution of the head for lifting the hammer, b) Screen for test performance, c) Screen for resetting and definition of angles, d) Screen for the calibration of angle transducer; 1 – Potentiometric angle transducer, 2 – hammer, 3 – electrical clutch, 4 – DC motor

The screen from Fig. 5d is used to calibrate the angle transducer tract. The calibration results are automatically stored in the calibration macro. It is realised

---

[3] Oldham coupling allows high absorption of radial displacement, produces no errors in kinematic transmission, and mechanical protection against excessive torque.

[4] Bellows coupling allows high absorption of shifts and high torsional stiffness.

by the calibration software. The process is initiated by opening and stopped by closing the screen. Thanks to the software features of operator's panel, part of the operations performed by the controller is performed by operator's panel.

The screen from Fig. 5c is used to reset and define angles. It is used before starting the process control screen. The screen from Fig. 5b is used to perform the testing procedure. The S/S[5] acts as a flag initiating the test.

Emergency situations in the case of this module are defined as follows:

- Operation of S/S when the hammer is not in the neutral position,
- When electrical clutch is not locked in the neutral position of the hammer.

Summary

Construction and software modules developed by the author of this article are intended for the construction of specialized equipment for testing and certification in the furniture industry. This concept has proven itself in practice.

The method for the construction of the software and the control system for testing and certification equipment in the furniture industry developed by the author of this article are intended for the construction of devices for testing of furniture. This concept of the design of devices from the modules has proven itself in practice.

The concept of measurement and control system in the form of an open distributed system allows flexible configuration of stands and their modifications in the future.

The prototype of the stand for horizontal impacts and the stand for the rotational chair testing was introduced in PUR Remodex Ltd. who specialises in quality and safety tests of furniture, and practical implementations for the furniture industry.

The prototype of the stand for testing bed hardness and wear resistance has been introduced at the Institute of Wood Technology in Poznan, which specialises in quality and safety tests and practical implementations for the furniture industry.

---

[5] Start/Stop.

References

1.   Website of CATAS company www.catas.it access on 20.01.2015.
2.   Website of IDM company http://www.idminstruments.com.au/access on 20.01.2015.
3.   Website of Texo Aplication AB company http://www.texoapplication.se/access on 20.01.2015.
4.   Website of Hegewald & Peschke company http://www.hegewald-peschke.de/access on 20.01.2015.
5.   Stand for testing sleeping surfaces http://katalog.itee.radom.pl/images/stories/karty/46.stanowisko_ang.pdf access on 20.02.2015.
6.   Wojutyński J., Dobrodziej J., Matecki K., Gospodarczyk A., Rogoziński M.: Maszyna testowa do badania trwałości i twardości leżysk mebli, Problemy Eksploatacji, 2006.
7.   Raport końcowy z realizacji zadania badawczego nr III.3.3/PS „Urządzenia do badań testowych i certyfikacyjnych w przemyśle meblarskim i materiałów budowlanych", Radom, lipiec 2013.
8.   User's Manual. Web Server CPU Module. Dokumentacja FC9Y-1278.pdf firmy IDEC.
9.   FC5A SERIES. Micro Programmable Logic Controller. User's Manual. Dokumentacja FC5A(B927).pdf firmy IDEC.
10. Wirth N.: Wstęp do programowania systematycznego. WNT, Warszawa 1987 (wyd. 2).
11. Wojutyński J.: Rodzina języków JSM. Problemy Eksploatacji 4'95, s. 17–32.

Metoda konstruowania oprogramowania i systemu sterowania urządzeń do badań testowych i certyfikacyjnych w przemyśle meblarskim

Słowa kluczowe

Certyfikacja, test, urządzenia, meble, PLC, HMI, impact hammer test.

Streszczenie

W artykule przedstawiono problematykę projektowania urządzeń do badań testowych i certyfikacyjnych dla mebli oraz materiałów stosowanych w przemyśle meblarskim. Jednym z podstawowych zagadnień jest modularyzacja urządzeń oraz automatyzacja prowadzonych testów. Naturalną konsekwencją zastosowania modułowej struktury sprzętowej urządzeń jest modularyzacja oprogramowania zapewniającego synchronizację działania poszczególnych modułów.

W artykule przedstawiono metodykę projektowania oprogramowania systemu pomiarowo-sterującego urządzeń testowych do badań mebli. Omówiono zagadnienia dotyczące diagnostyki systemu pomiarowo-sterującego oraz monitorowania procesu wykonywania testów. Zaprezentowano metodę kalibracji torów pomiarowych oraz kontroli dokładności pozycjonowania wyrobów poddawanych testom. Na przykładzie automatyzacji procesu badań udarnościowych mebli zaprezentowano funkcjonalne walory urządzenia. Przedstawiono możliwości zastosowań opracowanego rozwiązana w badaniach testowych udarności wyrobów szklanych.

Sławomir PAWŁOWSKI, Grzegorz DOBIŃSKI, Marek SMOLNY
University of Łódź, Faculty of Physics and Applied Informatics, Łódź
slpawlowski@gmail.com, gdobinski@mvii.uni.lodz.pl,
msmolny@mvii.uni.lodz.pl
Andrzej MAJCHER, Mirosław MROZEK
Institute for Sustainable Technologies – National Research Institute, Radom
andrzej.majcher@itee.radom.pl, miroslaw.mrozek@itee.radom.pl

IMAGING SYSTEM USING HIGHER-HARMONIC IN THE TAPPING MODE OF THE "TERRA AFM" MICROSCOPE

Key words

Atomic force microscope, tapping mode, synchronous detection, phase imaging.

Abstract

Terra AFM is the atomic force microscope designed and built by the authors as a device for research applications in advanced technologies in industry and in teaching. In tapping-mode, in atomic force microscopy, the interaction between the tip and the sample is, in fact, non-linear and consequently higher harmonics of the fundamental resonance frequency of the oscillating cantilever are generated. In this paper, we present the Terra AFM system using the method of synchronous detection that allows simultaneously recording the amplitudes and phases of the fundamental resonance frequency and of the higher harmonics. The used detection system, composed of 16 bit 100 mega-samples per second (MSPS) analogue-to-digital converter (ADC) and

field-programmable gate array (FPGA) device, allows measuring the amplitude and phase of the cantilever within one oscillation cycle and with good signal-to--noise ratio. As a result, good-quality images at higher harmonics could be obtained with the use of conventional cantilevers. The obtained results prove that higher-harmonics imaging can be used to distinguish between different materials. High spatial resolution (about 1 nm) of the presented system is also demonstrated.

Introduction

The main criterion for the development of an atomic force microscope AFM Terra was the ease of use while maintaining high measurement parameters [1]. Modular mechanical design, control, and software were used, which allows making changes and modifications to extend the range of applications. Such changes are due to the experience gained with the use of the built microscopes and are focused on their better adaptation to the objects of research.

The use of the AFM microscope for characterization of objects of heterogeneous rheological structure is often done with the use of an imaging phase. Thus, improvement of the microscope "Terra AFM" is an imaging module utilizing advanced measuring amplitude and the phase of harmonics of the signal from the probe operating in tapping mode (intermittent contact mode). The module improves the quality of the measurement properties of visco-elastic structures, such as composite materials and biological objects.

The most widely used mode of operation of AFM is the tapping mode. The main reason is that, in this mode, the lateral interaction forces between the tip and the sample are minimized. In the tapping mode, the cantilever is excited to vibrate (with free amplitude) at or close to the resonant frequency (this resonant frequency is one of its flexural resonances) of the fundamental mode and is brought close to the studied sample surface so that the tip makes intermittent contacts (tapping) with the surface once in every oscillation period. The contact with the surface alters the amplitude and phase of the cantilever vibration. The vibrations are detected with an optical system where a laser beam reflects from the back of the cantilever and then falls onto a position-sensitive photodiode. As the cantilever is scanned across the surface, the vibration amplitude is maintained at a set-point value (below the free amplitude) through a feedback loop that adjusts the height of the cantilever base. Therefore, the feedback signal reflects the topography of the sample surface. The tip-sample interaction is in fact non-linear. As a consequence, this results in the appearance of higher harmonics of the fundamental oscillation (resonance frequency) of the cantilever [2, 3].

The phase shift between excitation and response of the vibrating cantilever depends on the energy dissipation during the tip-sample contact [3, 4, 5]. Balantekin and Atalar [6] showed that the amount of power dissipated in

a sample is related to the mechanical properties of the sample, such as viscosity and elasticity. According to their theoretical considerations, for a given sample, elastic properties one can determine approximately the sample-damping constant by measuring the average power dissipation.

A theoretical analysis carried out by Stark and Heckl [7] showed that information on the elastic properties of the sample surface is contained in the higher harmonics of the fundamental oscillation signal in tapping-mode AFM. In addition, Sahin et al. [8] showed that higher harmonics offer the potential for imaging and sensing material properties at the nanoscale. They pointed out that resonantly enhanced higher harmonics are sensitive to the stiffness of the material under investigation.

The measurement techniques used commonly in commercial AFM allow one to control only the amplitude and phase of the fundamental mode (the first order Fourier component in frequency domain) of the cantilever, and information on the higher-order Fourier components, related to the non-linear interaction between the tip and the sample, is lost. In this paper, we present an AFM system using the method of synchronous detection that allows simultaneously recording the amplitude and phase of the higher harmonics of the fundamental oscillation of the cantilever. As a result, information on the non--linear tip-sample interaction, and, in particular, an insight into the mechanical properties of the sample, can be obtained. Because of the fact that higher harmonics signals obtained with the use of conventional cantilevers and conventional detectors/lock in amplifiers systems have low signal-to-noise ratios, the authors of previous works concerning the analysis of higher harmonics used specially designed harmonic cantilevers that enhanced one of higher harmonics [2], used specially designed torsional harmonic cantilevers [3], or enhanced higher harmonics by driving a conventional cantilever close to a submultiple of its resonant frequency [6]. Only Stark et al. [9] demonstrated that higher-harmonics imaging with the use of a conventional cantilever is possible, although they used the cantilever with a low resonant frequency to obtain higher harmonics within the limited bandwidth of the photodiode preamplifier and recorded higher-harmonics images consecutively.

1. The design of the microscope

The atomic force microscopy, AFM Terra (Fig. 1a), consists of three main parts: the measuring head, electronic control system and software, and an external PC.

The measuring head is a part of the apparatus, which is placed in a test sample, scanner, measuring amplifiers, current converters in four segments photodiode and pre-sample approximation to the probe (Fig. 1b). The measuring unit head comprises the following modules: a photodiode, semiconductor laser,

surveillance cameras and photodiode positioning system, and a laser guidance system.

The measuring head assembly has two degrees of freedom in the horizontal plane in perpendicular directions. The AFM holder remains stationary relative to the sample, and its movement actuators perform the measuring assembly. In order to keep the compact dimensions of the laser, the beam track-measuring unit was devastated using a plane mirror, focusing the laser beam on the edge of the probe (cantilever). Two degrees of freedom allow the measuring unit to guide the laser beam on the cantilever.
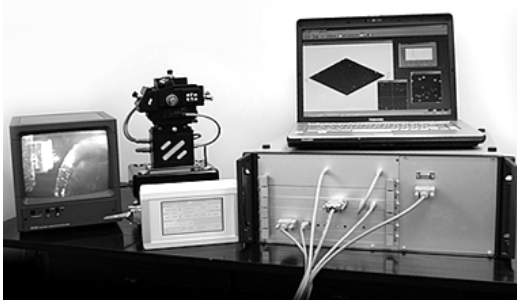
a)   b)
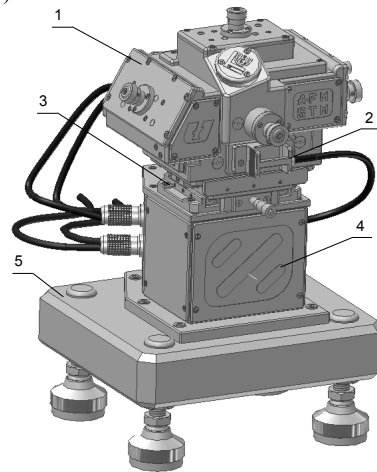
Fig. 1. Atomic force microscope Terra AFM (a) and view of a solid model of the head AFM (b); 1 – measuring unit, 2 – removable module AFM / STM, 3 – XY table, 4 – scanner, 5 – base

The photodiode also has two, independent of the measuring unit, degrees of freedom, enabling guidance of the photosensitive element reflected from the cantilever beam of laser light. The mixing head and a photodiode were implemented by using miniature micrometre screws.

The closure of the positioning mechanisms was implemented by using tension springs. The precise handling "wheelchair head" (the fitting cantilever) is provided by the use of miniature, backlash-free linear roller bearings. To avoid the effect of air movement, the measurement space was built inside the head, without the possibility of direct viewing of the sample and tip scanning. In order to observe the process of scanning and execute precise movements, preview actuators using two miniature CCD cameras were applied.

The measuring unit is placed on scanner unit (Fig. 2b). The structure of the scanner consists of exchangeable piezoelectric tube system, moto reducer, and the traverse. The arrangement of the piezoelectric tube is used for precise

positioning of the test sample material. The tube is built on a base inside the sleeve serving as mechanical guards. The piezotube is finished with a magnetic table to fix the samples. The bracket system allows the use of interchangeable piezoelectric tubes of different lengths.

a)   b)
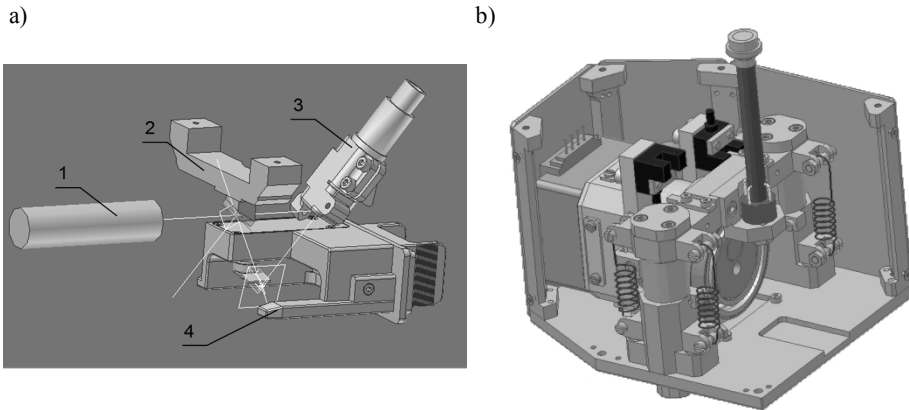
Fig. 2. View of the elements inside the measuring unit of the microscope (a) and scanner unit with the module of piezo tube (b); 1 – laser, 2 – handle with mirror, 3 – arm photodiode, 4 – truck head of the cantilever

The scanner system is used for the approximation of the initial pusher eccentric mechanism, in which the conversion of the rotational movement to the progressive movement of the eccentric tappet occurs. The components of the scanner were attached to a torsion box enclosure that provides adequate rigidity and mechanical protection of the precision scanner. As a part of the drive, a stepper motor cooperating with a miniature transmission wave and eccentric was used.

Modules placed in a cassette with the VME bus communication and operator panel create the electronic control system microscope. The operator panel is designed to facilitate the process of adjustment of the microscope optics for the user. Imaging parameters of this process is done with the touch screen LCD, working independently from the PC.

The modules of the control unit perform the following functions and devises:

− Proportional-integral controller ensuring the maintenance of a distance probe – sample (atomic scale) during the scanning process;
− The master controller and a communication system comprising a programmable FPGA, and a 32-bit microprocessor with peripherals; and,
− Providing a high voltage amplifier control voltages piezo-ceramic tube scanner ±225 V (for each, the four segments of the inner tube and its surface responsible for the shift in the direction of the axis Z).

In the loop proportional-integral regulator, due to the cooperation of electronic circuits to the mechanics, such as the scanning tube, measuring bar, and "optical lever", the feedback system was used with the parameters controlled in a wide range of gain and time constants. The loop uses a 12-bit resistive ladder (AD7547), which is able to increase the dynamics of the gain control at the level of 72 dB and adjust the time constant in the range from 10 s to 400 ms.

The controller also includes systems of differential amplifier input signals, the system pre-setting the initial scan based on the D/A converter (AD669), and a detection system that exceeded the threshold current for process control and automatic approximation of switching circuits and memorizing (AD7512 and AD585).

Terra AFM microscope software, implemented in an external PC, is primarily used for the analysis and presentation of the measurement data obtained. In addition, the software includes a virtual model of the microscope with a set of variables describing the current status of the device and the scanning process control algorithms.

2. Imaging system using harmonic vibration probe

For Terra AFM microscope working in tapping mode, a method of enabling simultaneous, synchronous measurement of both amplitude and phase of harmonics of the oscillating signal from the probe was developed (Fig. 3).

An algorithm for a Discrete Fourier Transform (DFT) is implemented in FPGA circuits. It calculates the amplitude value of the first (or the any) harmonic, which is fed to the feedback loop circuit in order to stabilize the operating point of the microscope. The computational complexity of the conventional DFT algorithm is $O(N^2)$. To reduce the computational time, most frequently the fast Fourier transform (FFT) algorithm is used for which the computational complexity is $O[N \log_2(N)]$. This algorithm is also used by us. To further reduce the computational time, one can use the recursive DFT algorithm, also called "the sliding DFT (SDFT) technique," which performs an N-point DFT on time samples within a sliding window. The SDFT initially computes the DFT of the N time samples. Then, the time window is advanced one sample, and a new N-point DFT is calculated. The large advantage of this process is that each new DFT is efficiently computed directly from the results of the previous DFT. The SDFT process can be described as follows:

$$S_m(n) = \left[S_m(n-1) + x(n) - x(n-N) \right] \left[\cos\left(\frac{2\pi n}{N} \right) + j \sin\left(\frac{2\pi n}{N} \right) \right]$$

where $S_m(n)$ is the new spectral component and $S_m(n-1)$ is the previous spectral component. The subscript m denotes that the spectra are related to the m-th DFT

bin. The computational complexity of each successive N-point output for the SDFT algorithm is O(N) [10].
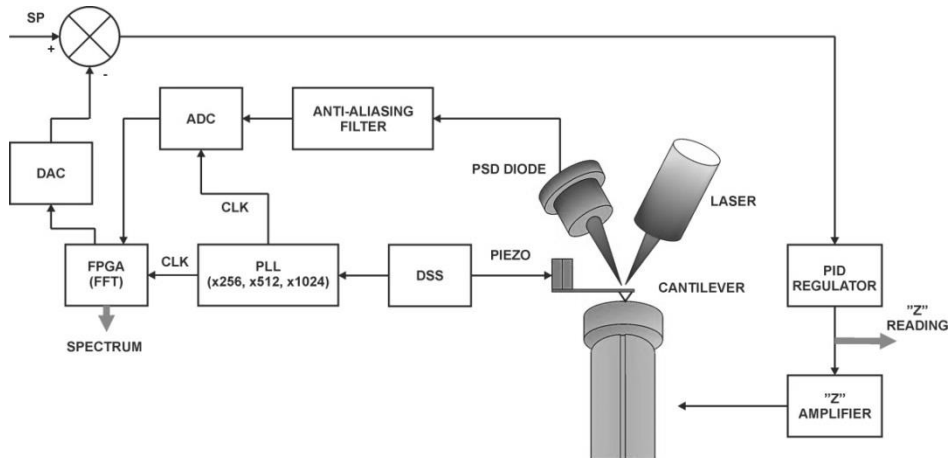
Fig. 3. Block diagram of the excitation and detection of digital vibration amplitude of the probe using the discrete Fourier transformation

Excitation of the probe vibration signal is generated by the digital direct synthesis circuit DDS, and it is also a programmable reference signal to a Phase Locked Loop (PLL), which is used to reproduce the clock signal frequency by a factor of *2n* (e.g., 64, 128, 256). The clock pulses produced in this way are used, in turn, for the timing of operating at speeds up to 100 MHz analogue-to-digital converters, as well as parts of FPGA logic resources that are responsible for reading the data and calculate the amplitude and phase of vibration probe. Since the sampling frequency is an integer multiple of the fundamental frequency of vibration of the measuring probe, the calculated frequency spectrum components using the DFT correspond to the actual harmonic amplitudes of the signal from the probe. This sampling method eliminates spectral leakage phenomenon known in digital signal processing and, in this case, there is no need to use windowing and, consequently, the introduction of correction factors to the calculated amplitudes of the signal components.

3. Imaging system verification

The proper operation of the system has been tested using a reference sample (HP-LDPE, Veeco). This sample consists of a mixture of polystyrene and polyolefin forming a thin layer applied to a silicon substrate. We used a Bruker RTESPA cantilever with a resonance frequency of 303.9 kHz and a spring constant 40 N/m. For convenience, the PLL chip was set to multiply the

excitation frequency 256 times. As a result, the ADC and FPGA chip were working with a 77.8 MHz clock. The analogue PID controller was fed with an error signal proportional to the magnitude of the first harmonic of the fundamental oscillation signal determined by 256-point DFT. No additional averaging/post-processing algorithms were used. Sample images are shown in Fig. 4.

It is very well known that the image quality depends on the signal-to-noise performance and that the minimum acceptable signal-to-noise ratio is necessary to detect a given contrast level. The obtained images of the surface topography were of good quality. They possessed relatively high contrast and a low level of noise. This means that good signal-to-noise ratio was achieved. In comparison with other detection methods, good signal-to-noise ratios in connection with a high detection speed are specific and large advantages of the applied method of synchronous detection. As a consequence, this method is found to be very useful and well suited to applications in which oscillation modes are used. It is also worth noting that the application of advanced digital data filtration algorithms to the data obtained from the detection system will lead to further improvement of the signal-to-noise ratio.

a)   b)
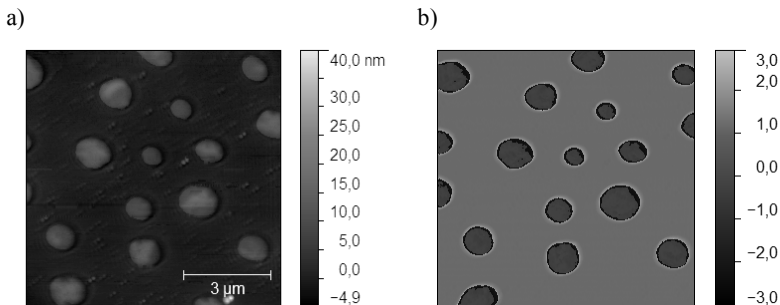
Fig. 4. The amplitude feedback – topographic image (a) and the phase feedback – phase contrast image (b) of reference sample

To test usability of the applied method of synchronous detection to simultaneously detect higher harmonics of the fundamental oscillation signal, we used the same reference sample. We used a Bruker V shaped silicon cantilever (type SNL 10) with a spring constant 0.12 N/m. The cantilever was driven at a fixed frequency close to the fundamental flexural resonance frequency 66.9 kHz.

The set-point amplitude was adjusted to 12.7% of the free amplitude. The second and third flexural resonance frequencies of the cantilever were measured to be 337.6 kHz and 920.7 kHz, respectively; that is, they are equal to 5.05 and 13.76 times the fundamental flexural resonance frequency of the cantilever, respectively. It is also to be noted that there was no measurable higher-harmonic

content in the cantilever deflection signal when the cantilever was away from the sample.
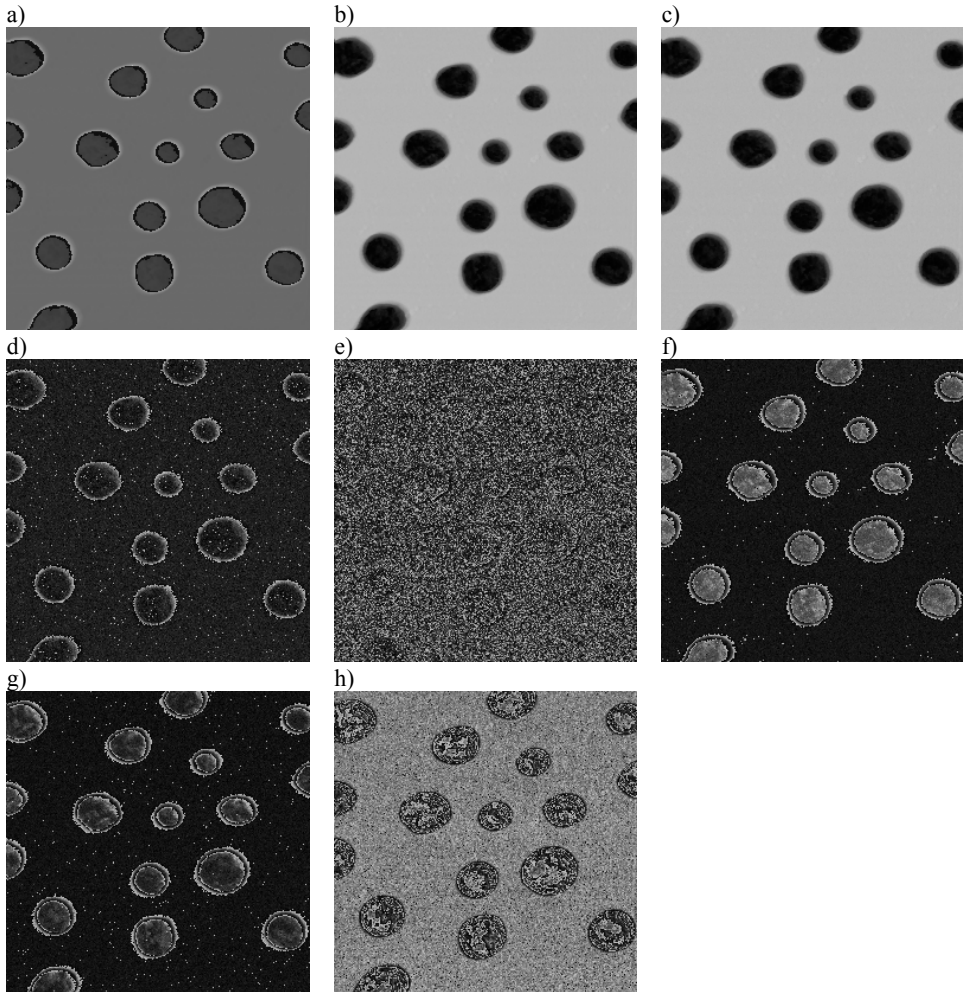
Fig. 5. The phase shift images of the same sample obtained with the reference system with detection module amplitude and phase of harmonics respectively: the first (a), a second (b), a third (c), fourth (d), fifth (e), sixth (f), the seventh (g), the eighth (h) harmonic

Fig. 5 present images of the same surface area of the PS–LDPE sample, recorded using the phases of the first 8 harmonics of the fundamental oscillation signal. In all these images, the PS and LDPE regions can be distinguished. Of all images in Fig. 5, those at the 1st (Fig. 5a), 4th (Fig. 5d), and 6th (Fig. 5f) harmonics are characterized by best signal-to-noise ratio and contrast. The images prove that the phase imaging at higher harmonics can be used to

distinguish between different materials, even when a conventional cantilever is used. Note also, that for eight of them (Figs. 5d, f, g), the phase differences between the PS and LDPE regions are larger than that for the traditionally used phase image of the first harmonic (Fig. 5a), which shows the usefulness of the higher harmonics imaging for revealing mechanically heterogeneous regions of the sample. In the context of phase imaging at higher harmonic, it is worth noting that recently, in investigations of biological objects, Dulebo et al. [11] presented second-harmonic phase images revealing additional features at the nanometre scale that were not present in the first-harmonic phase images.

Imaging using the higher harmonics in the feedback control sample position Z allows one to carry out further work to clarify the correlation between those obtained images of the phase and mechanical properties of the tested structures.

Conclusions

The design of the Terra AFM microscope follows the changes and developments in the wider area of nanotechnology. Many measurement sessions performed by both authors and other researchers in scanning microscopy techniques allowed sampling to predict the most useful solution in the existing applications of the microscope.

The presented method using harmonic imaging allows simultaneous, synchronous measurement of both the amplitude and phase of harmonic signal from the oscillating probe. The used detection system, composed of 16-bit MSPS ADC and FPGA device, allows one to measure the amplitude and phase of the cantilever within one oscillation cycle and with good signal-to-noise ratio. As a result, good-quality images at higher harmonics could be obtained with the use of conventional cantilevers. In comparison with other detection methods, good signal-to-noise ratios in connection with high detection speeds are specific and large advantages of the applied method of synchronous detection.

Interpreting the nature of the contrast in phase images is difficult because of the multiple contributions to the energy dissipation [3]. Phase images at the 4th and 6th harmonics were characterized by the best signal-to-noise ratio and contrast.

The microscope with the analysis of harmonic imaging allows sensitive, real-world structures, without interfering in their construction and minimizing the impact of the gauge on the test object, and allows for deeper analysis of the mechanical properties of the test material.

References

1. Majcher A., Mrozek M., Zbrowski A., Olejniczak W., Pawłowski S., Piskorski M.: STM/AFM microscope for application in industrial advanced technologies and the high schools education. Maintenance Problems 3/2011, pp. 177–188.
2. Sahin O., Yaralioglu G., Grow R., Zappe S.F., Atalar A., Quate C., Solgaard O.: High-resolution imaging of elastic properties using harmonic cantilevers. Sens. Actuators A 114 (2004), pp. 183–190.
3. Sahin O., Erina N.: High resolution and large dynamic range nanomechanical mapping in tapping-mode atomic force microscopy" Nanotechnology, 19, 445717 (2008), p. 9.
4. Cleveland J.P., Anczykowski B., Schmid A.E., Elings V.B.: Energy dissipation in tapping-mode atomic force microscopy. Appl. Phys. Lett. 72 (1998), pp. 2613– 2615.
5. Martínez N.F., García R.: Measuring phase shifts and energy dissipation with amplitude modulation atomic force microscopy. Nanotechnology 17 (2006), pp. 167–172.
6. Balantekin M., Atalar A.: Power dissipation analysis in tapping-mode atomic force microscopy. Phys. Rev. B 67, (2003), pp. 193–404.
7. Stark R.W., Heckl W.M.: Fourier transformed atomic force microscopy: tapping mode atomic force microscopy beyond the Hookian approximation. Surface Science 457 (2000), pp. 219–228.
8. Sahin O., Quate C.F., Solgaard O., Atalar A.: Resonant harmonic response in tapping-mode atomic force microscopy. Phys. Rev. B 69 (2004), pp. 165–416.
9. Stark R.W., Heckl W.M.: Higher harmonics imaging in tapping-mode atomic-force microscopy. Rev. Sci. Instrum. 74 (2003), 5111.
10. Lyons R.G. (Ed.): Streamlining Digital Signal Processing, IEEE Press, Wiley, New Jersey, 2007.
11. Dulebo A., Preiner J., Kienberger F., Kada G., Rankl C., Chtcheglova L., Lamprecht C., Kaftan D., Hinterdorfer P.: Second harmonic atomic force microscopy imaging of live and fixed mammalian cells. Ultramicroscopy 109 (2009), pp. 1056–1060.

System obrazowania wykorzystujący wyższe harmoniczne w trybie kontaktu przerywanego mikroskopu „Terra AFM"

Słowa kluczowe

Mikroskop sił atomowych, tryb kontaktu przerywanego, detekcja synchroniczna, obrazowanie fazowe.

Streszczenie

Mirroskop Terra AFM jest mikroskopem sił atomowych opracowanym i zbudowanym przez autorów jako urządzenie do zastosowań badawczych, przemysłowych i edukacyjnych w obszarze zaawansowanych technologii. W każdym mikroskopie sił atomowych pracującym w trybie kontaktu przerywanego oddziaływanie pomiędzy sondą i próbką ma charakter nieliniowy, co powoduje powstawanie wyższych harmonicznych częstotliwości podstawowej drgań sondy. W artykule przedstawiono system mikroskopu Terra AFM wykorzystujący metodę detekcji synchronicznej umożliwiającą jednoczesne wyznaczanie amplitudy i fazy wyższych harmonicznych przebiegu podstawowego. Głównymi elementami opracowanego systemu detekcji są przetwornik analogowo-cyfrowy o rozdzielczości 16 bitów i szybkości próbkowania 100 MSPS oraz układ programowalny FPGA pozwalający na pomiar amplitudy i fazy w okresu przebiegu podstawowego drgań sondy z dobrą wartością stosunku sygnału do szumu. Prowadzi to do otrzymywania dobrej jakości obrazów przy wyższych harmonicznych z użyciem typowej sondy mikroskopu AFM. Przedstawiono przykłady uzyskiwanych obrazów, które wskazują na przydatność systemu do rozróżniania obszarów próbek zbudowanych z różnych materiałów. Potwierdzają one również wysoką rozdzielczość przestrzenną (około 1 nm) opracowanego systemu.

Anita BEDNARSKA, Edyta OSUCH-SŁOMKA, Marian GRĄDKOWSKI
Institute for Sustainable Technologies – National Research Institute, Radom
anita.bednarska@itee.radom.pl, edyta.slomka@itee.radom.pl,
marian.gradkowski@itee.radom.pl

A METHODOLOGY FOR IDENTIFYING THE CHEMICAL COMPOSITION OF THE SURFACE OF SOLIDS USING THE XPS AND SEM/EDS TECHNIQUES

Key words

SEM/EDS, XPS/ESCA, sputtering, vertical profile.

Abstract

In many fields of science and technology, it is necessary to apply non-destructive methods of analysis. Such non-destructive methods include scanning electron microscopy coupled with energy-dispersive X-ray spectroscopy (SEM/EDS) and X-ray photoelectron spectroscopy (XPS), and the results obtained with this set are often regarded as complementary. These methods were used in this study to research the chemical composition of the top layer of a model made with gold on a ceramic coating produced by the PVD technique on the surface of steel. The gold layer was ion sputtered until its complete removal and was studied by means of X-ray photoelectron spectroscopy and X-ray micro-analysis. It was found that the analytical data for an identical specimen obtained by SEM/EDS and XPS might differ significantly. This necessitates very careful consideration in treating these techniques as

complementary, and during the interpretation of the results, one should take into account the physical essence of each method.

Introduction

In materials engineering and in many other areas of technology, the knowledge of the physical and chemical structure of the material is important. In some cases, the data on the outer layers of the material alone is of critical importance, since they determine its functional properties. In surface engineering, the data properties that are important concern the coating and the surface layer of solids on the nanometric and even molecular level. Moreover, it is important that the testing is non-destructive and the specimen properties are not changed. Particularly useful in this regard are spectroscopic techniques. In materials testing, the application of scanning electron microscopy coupled with energy-dispersive X-ray spectroscopy (SEM/EDS) and X-ray photoelectron spectroscopy (XPS) has become widespread. The basic data describing techniques are shown in Table 1. These data show the boundary capabilities of each individual technique resulting from the laws of physics and the development of technology. The actual parameters of a particular device depend on its design and are often lower than those given in Table 1.

Table 1. Comparison of parameter and detection limits of used analytical techniques [2]

Technique	Parameter limits						
	Range of elements	Detection limits	Quantitative accuracy	Analysis area (radius)	Minimum film thickness	Depth of information	The type of data
SEM/EDS	B-U	0.1 atom. %	±10%	>0.5–4 μm	500 nm	500–3000 nm	qualitative and quantitative
XPS/ESCA	Li-U	0.1 atom. %	±10%	>15–500 μm	5 nm	1–10 nm	+ chemical status of elements

The SEM/EDS and XPS techniques are based on an analysis of the electron energy emitted from the specimen. The main difference consists in how the excitation is induced in the specimen: In SEM/EDS, it is an electron beam with an established energy, and in XPS, it is monochromatic X-ray radiation. In the first case, it is a result of an elastic collision of the electrons. In the second case, it is an external photoelectric phenomenon. In consequence, for each technique, there is a characteristic energy of the electron leaving the specimen and the information it carries [1]. There are also important differences in the size of the excitation area and thus in the planar and vertical resolution. SEM/EDS is characterized by a greater planar but a smaller vertical resolution than XPS. The advantage of XPS over the SEM/EDS is the possibility of ion sputtering of the

test specimen (Ar^+) and, thanks to the high vertical resolution, creating depth profiles of the chemical structure of the test material. In summary, both methods provide data with different levels of detail, and in many cases, they can be complementary.

The analytical information from SEM comes from the surface layer, but the thickness of the layer significantly depends on the atomic mass of constituent elements. The depth of the analysis for selected elements is shown in Figure 1, where the larger the atomic mass, the shallower is response of the element.
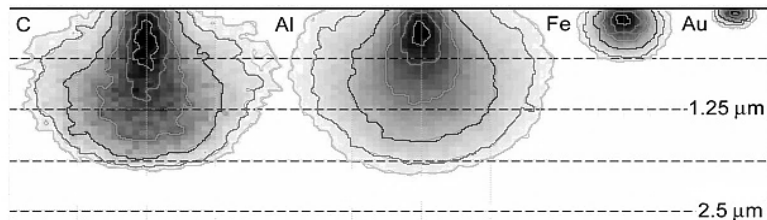

Fig. 1. Monte Carlo simulation of energy distribution in SEM imaging: Energy distribution depends on the material and acceleration voltage, which was 15 kV in this visualisation. Contour lines illustrate the amount of energy: 5% (outside line), 50% (bright line), 90% (centre) **[3]**

The XPS technology exemplifies the wave-particle theory of matter. It applies only to the elements that are located sufficiently shallow in the surface layer, so that it is possible for the electrons excited by monochromatic X radiation to leave freely [4]. The kinetic energy of the electron (KE) is the sum of the binding energy (BE) and energy of the "taken over" X-ray quantum (hv). Thus, by measuring the KE, we can determine the electron energy before its "impact" with the X-ray quantum, which is the binding energy BE in the atom. This energy is dependent on the atomic number and on the position of the electron in the atom (the atomic orbital) [5]. When determining BE, a coefficient should be taken into account that compensates for the difference between the electron exit energy from the specimen and the spectrometer [6]. The KE measurement is obtained using the analyser, which is a part of the XPS apparatus. As a result of the counting of the number of electrons at a specific KE in a unit of time, a photoelectronic spectrum is created [7].

In XPS analysis, it is usually assumed that the test surface is flat and homogeneous. However, in vertical resolution at the level of the single nanometres, the shape of the surface is essential because of the change in the analytical signal to the background signal [8]. This is particularly important in the study of thin layers.

The aim of this study was to develop a methodology of ion sputtering and the identification of the chemical composition of the surface layer using the XPS technique by creating depth profiles, analysing the structure of the functionally

coated materials, and verifying the data obtained by SEM/EDS technique and correlating and comparing the data obtained in each method.

1. Research object

The object of study was a steel disc, 25.4 mm in diameter, with a functional ceramic coating embedded in it by using the PVD method, which was covered in a layer of gold with a nominal thickness of 20 nm, determined based on the sputtering parameters using the BAL-TEC SCD 050 Sputter Coater [9]. Covering the surface of the specimen with a layer of gold with a known thickness makes it possible to link the parameters of ion milling with the characteristics of the specimen layers being uncovered. The specimen was fixed in the holder of the XPS using conductive graphite tape.

2. Research method

The SEM images and the X-ray EDS microanalysis were performed using a scanning electron microscope with a Schottky type thermal field emitter (model SU-70 by Hitachi) in conjunction with an X-ray microanalyser by Thermo Scientific, enabling the detection of elements from beryllium to uranium. The analyses were carried out in a vacuum at 1×10^{-8} Pa, with an accelerating voltage of 15 kV. The angle of the reception of secondary electrons (SE) was 30.4°. During the EDS analysis, spectra were recorded for selected portions of the surface along the selected lines or points of 10 x 10 nm.

The XPS analysis was carried out using a spectroscope by PREVAC. In order to remove from the surface of the specimen the adsorbed foreign substances and products the oxidation, initial surface cleaning of the specimen was conducted using the ion mill Ar^+. To induce excitation in the specimen, an X-ray lamp equipped with the standard achromatic source of X-rays, accompanied by a double anode Al/Mg, were used. The main ion sputtering (for creating depth profiles) was conducted with 5 kV beam, with a current of 10 mA, and current density at 147 µA/cm^2. Survey analyses after each cycle of ion sputtering were conducted using radiation Al Kα energy 1486.6 eV, with a transition energy of 200 eV and an increment of 200 meV. The parameters for creating a detailed spectrum for each element were selected individually, taking into account the power of the X-ray excitation, the element, sampling density, transition energy, and slits of the analyser lenses. These parameters were set in such a way so that the quality of the obtained spectra was the highest. The recorded spectra were subjected to a detailed digital analysis, based on which the quantitative composition of elements in subsequent layers was established.

3. Test results-discussion and conclusions

Figure 2 shows a survey of the XPS spectra of the specimen surface before gold coating (a), after the gold coating (b), and after ion sputtering of the gold (c). As can be seen from the data in Figure 2, after coating the surface with gold, all of the signals of all specimen elements were "covered," except for carbon. The spectrum (b) spectrum was registered after an initial 30-minute cleaning of the surface of a specimen with an argon ion beam. Spectrum analysis showed that, after this operation on the surface of the specimen, carbon remained at about 16%. The gold layer level not containing carbon was reached after up to 50 minutes of further cleaning. It is therefore necessary to monitor the effectiveness of the initial surface cleaning of the specimen and, if necessary, carry it out with greater intensity.
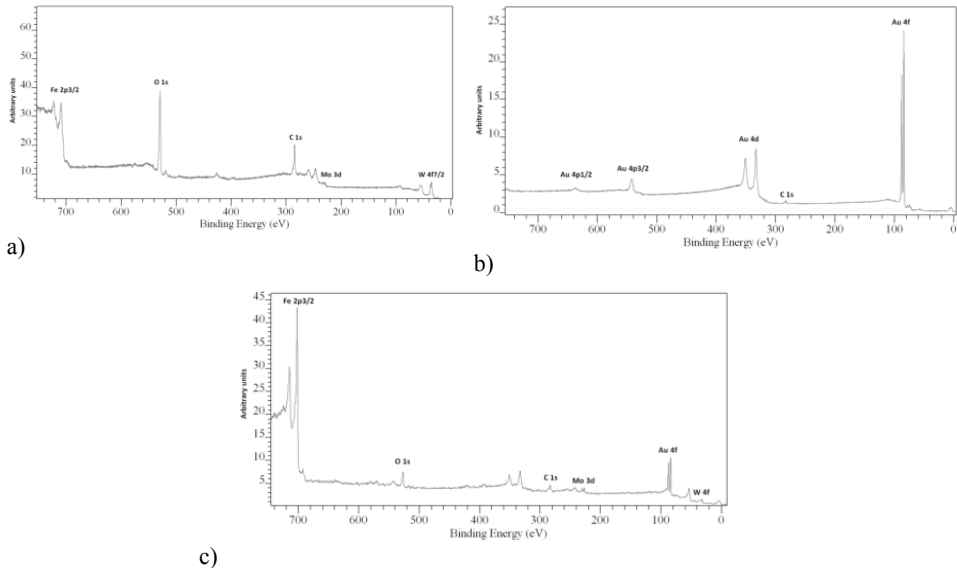
Fig. 2. XPS survey spectra: a) specimen before coating – without gold, b) specimen after gold coating, c) specimen after gold coating and ion sputtering

Figure 3 shows the depth profile of the content of each of the elements in the layers being uncovered after consecutive cycles of ion sputtering, between which XPS data acquisition was carried out. After each test, a detailed analysis of each of the peaks was conducted (Figure 4) in order to determine the atomic concentration of all elements. When quantifying the XPS spectra, in order to adjust the size of the measured area under each peak for each of the elements, the relative sensitivity coefficient RSF was taken into account [10]. In the first 300-minute milling phase with the XPS technique, no elements other than gold were detected. After this time, iron appeared and its content steadily increased,

and then tungsten, carbon, oxygen, and molybdenum. This indicated the gradual revealing of the substrate coated by gold (analysis of the composition of the substrate was not the aim of the testing). The milling was completed after 1,230 minutes, because cycles after 1,110 min did not reduce the participation of gold in the composition of the milled material. Despite the extended time of ion milling, there was gold content in the tested layer. This may be related to the fact that the used XPS spectrometer is not equipped with a monochromator; therefore, concentrating the excitation radiation beam is possible only within the area around 1 mm^2. As a result, the analysis might have included a fragment of the specimen lying outside the milled surface.
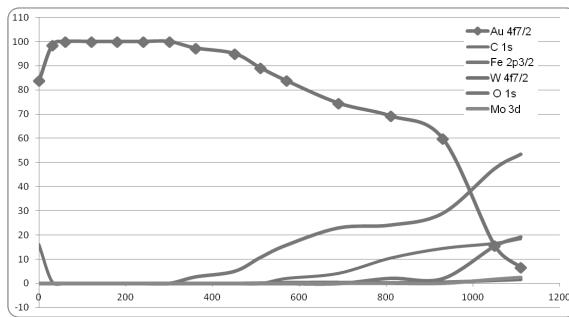
Fig. 3. Depth profiles of elements atomic concentration in gold coated specimen

a)   b)
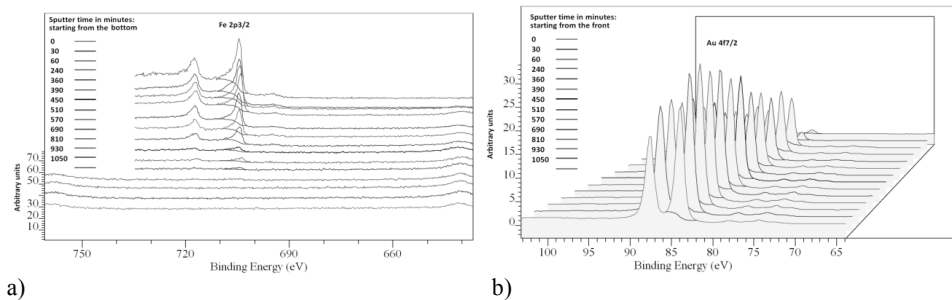
Fig. 4. Detailed spectra of selected elements in consecutive layers of examined specimen: a) 2D XPS spectra compilation of Fe2p3/2 peak before and after ion sputtering; b) 3D XPS spectra compilation of Au 4f7/2 peak before and after ion sputtering

Since optical examination of the specimen showed no presence of gold in the place of sputtering, it was decided to subject it to the SEM/EDS test. The results of SEM observations and EDS analyses of the specimen surface layer after gold coating and after sputtering is shown in Figs. 5 and 6. As can be seen from the SEM image shown in Fig. 5a, the surface of the specimen is not

homogeneous; the same case is for this this material before coating it with gold. This is characteristic of the coating that constituted the substrate. Due to the much greater depth of analysis of the EDS technique (≥500 nm) than XPS (~1 nm), in EDS spectra (Fig. 5b) in addition to gold, there are also elements of the substrate. Local analysis of this surface (Table 1) illustrates the chemical composition of the coating with gold deposition rather than a gold layer (XPS analysis – 100% gold at this point). Figure 7a shows a SEM image of the same specimen after ion sputtering. Characteristic is the "dispersed" of globular structures (Fig. 6a) located on the surface of the specimen, in the opposite direction to the direction of the Ar^+ ion sputtering. As a result of sputtering, there has been a significant change in the surface structure of the specimen. An EDS analysis (Fig. 6b) has not, however, found the presence of gold on the surface, in contrast to the analysis of XPS. Since the planar resolution of the EDS is much greater than of the XPS, the hypothesis is that the results of the XPS analysis were influenced by too large an analytic field can be considered verified. However, one should also bear in mind the potential impact on the outcome of the depth from which the analytical information in both methods is taken and the deformation of spherical structures on the surface of the specimen. However, the most likely option is that the SEM/EDS technique proved insufficiently sensitive for gold under the conditions of the experiment.
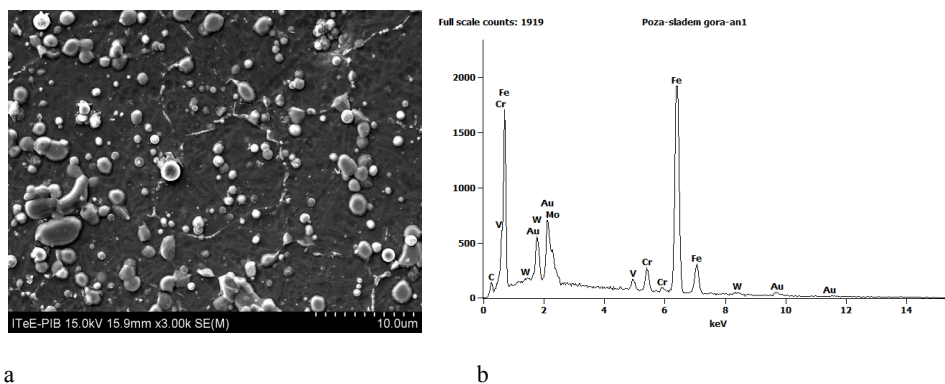
Fig. 5. SEM images (a) and EDS results (b) of the surface of the layer covered with gold

Figure 7 shows the SEM images correlated with the results of the linear gold content analysis used in the EDS technique on the boundary between the sputtered and un-sputtered surface (left). As the data in Fig. 7 indicates, the proportion of gold in the surface layer decreases along the lines of analysis; however, traces of the gold signal disappear entirely after crossing the sputtering boundary, indicating that gold is absent (right).

a   b
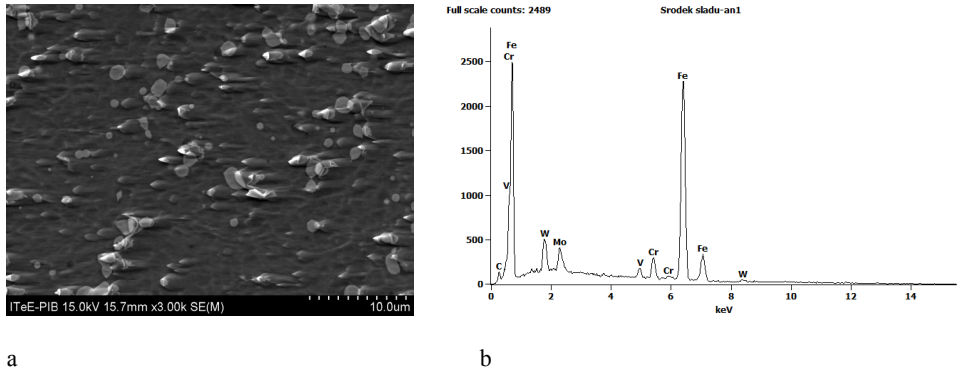
Fig. 6. SEM images (a) and EDS results (b) of the surface of the layer covered with gold after ion sputtering with Ar^+

Table 2. Atomic concentration of main components before and after sputtering (EDS)

Element	Atomic concentration [%]	
	Before sputtering	Middle of the sputter spot
Au	3.4	0.1
C	7.1	5.1
Fe	76.6	83.0
W	2.5	2.4
O	0.7	0.0
Mo	2.8	2.6
V	2.4	2.2
Cr	4.5	4.7
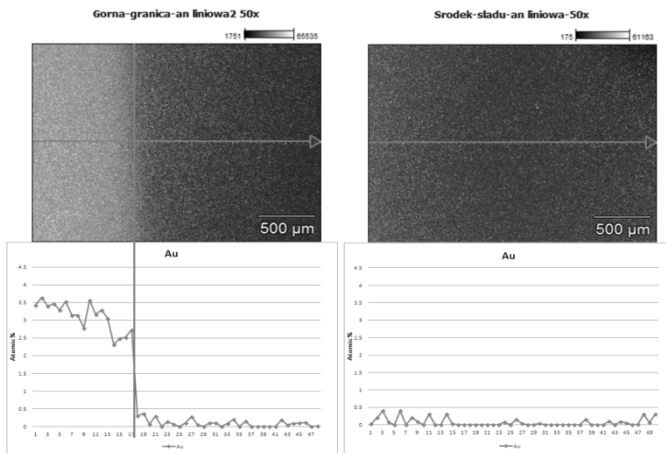
Fig. 7. Linear EDS analysis results correlated with SEM images for the boundary of sputtering spot (left) and for the middle of the spot (right)

The study has shown that quantitative data derived the SEM/EDS and XPS techniques for the same object may vary significantly. It also demonstrated the importance of the surface structure of the specimen to the process of ion sputtering in XPS. These facts should be taken into account, both when planning research, and during the interpretation and correlation of results obtained with these methods. The data presented will facilitate the planning and implementation of research techniques for SEM/EDS and XPS of materials with ceramic coatings, including multilayer coatings.

Summary

This study compared the results of the chemical composition testing of surface layers in the coating material using the SEM/EDS and XPS spectral techniques. Both techniques rely on the properties of electrons "escaping" from the specimen and provide qualitative and quantitative analyses of elements. The XPS technology enables ion sputtering of the surface of the specimen and the creation of depth profiles of the chemical structure of successive layers of material. It was found that the qualitative and quantitative data obtained for the same object of research converge for both methods if the material is homogeneous. In the case of heterogeneous materials, the results of qualitative analysis and particularly the quantitative analysis of the two methods can essentially differ. The key importance lies in the structure of the tested material and, above all, in the ratio of the thickness of the layers of different composition in the vertical structure of the material to the depth of electron output. Therefore, the methods of SEM/EDS and XPS cannot be considered complementary in all cases.

References

1. Friedman R.B., Kessler R.: The Photoelectric Effect & Its Applications, Yerkes Summer Institute, 2005.
2. www.xpsdata.com.
3. http://www4.nau.edu/microanalysis/microprobe-sem/signals.html.
4. Barr T.L.: Modern ESCA – The Principles and Practice of X-Ray Photoelectron Spectroscopy. ISBN: 0-84938653-5; Taylor & Francis Ltd, 1994.
5. Chung Y-W,: Practical Guide to Surface Science and Spectroscopy, ISBN: 0121746100, Academic Press, 2001.

6.   Watts J.F., Wolstenholme J.: An Introduction to Surface Analysis by XPS and AES. Wiley, 2008.
7.   Moulder J.F., Stickle W.F., Sobol P.E., Bomben K.D.: Handbook of X-ray Photoelectron Spectroscopy, A Reference Book of Standard Spectra for Identification and Interpretation of XPS Data. ISBN: 0-9648124-1-X; Physical Electronics, 1995.
8.   ISO/TR 14187:2011(E).
9.   Sputter Coater SCD 050. Blazers Operating Instructions, Edition 5, 1990.
10.   Fairley N., Carrick A.: The Casa Cookbook. Part 1: Recipes for XPS data processing. ISBN-10: 0954953304; Acolyte Science, 2005.

Metodyka identyfikacji składu chemicznego powierzchni ciał stałych technikami XPS i SEM/EDS

Słowa kluczowe

SEM/EDS, XPS/ESCA, sputtering, profil głębokościowy.

Streszczenie

W wielu dziedzinach nauki i techniki niezbędne jest zastosowanie nieniszczących metod analizy. Do takich metod należy skaningowa spektroskopia elektronów sprzężona z mikroanalizą rentgenowską (SEM/EDS) oraz rentgenowska spektroskopia fotoelektronów (XPS), a wyniki uzyskiwane za ich pomocą często są traktowane jako uzupełniające się. W pracy zastosowano te metody do badania składu chemicznego modelowej warstwy wierzchniej, utworzonej ze złota na podłożu powłoki ceramicznej wytworzonej techniką PVD na powierzchni stali. Warstwę złota trawiono jonowo aż do jej całkowitego usunięcia i badano za pomocą rentgenowskiej spektroskopii fotoelektronów oraz mikroanalizy rentgenowskiej. Stwierdzono, że dane analityczne dla identycznej próbki uzyskiwane metodami SEM/EDS oraz XPS mogą dość istotnie różnić się. Oznacza to konieczność dużej ostrożności przy traktowaniu tych technik jako komplementarne, podczas interpretacji wyników należy uwzględniać fizyczną istotę obydwu metod.

Andrzej MAJCHER
Institute for Sustainable Technologies – National Research Institute, Radom
andrzej.majcher@itee.radom.pl

A SYSTEM FOR TESTING MATERIALS IN LONG-TERM MECHANICAL AND THERMAL LOADS

Key words

Creep, creep-testing device, accelerated creep test, low-cycle fatigue.

Abstract

The article presents a system for testing materials used in manufacturing machinery elements operating in high stresses and temperatures. An essential element of the system is a multi-purpose device for performing normative creep tests (PN-EN ISO 204) and dedicated tests for low-cycle loads and various profiles of temperature changes. The device works with two databases: collecting the results of strength tests and collecting data used in predicting time of the damage of materials. The article describes the functionality of the individual system components and gives examples of the conducted strength tests.

Introduction

Creep tests are a well-known type of materials testing. They are usually conducted in the vertical creep-testing devices in which the uniaxial stress on the sample is obtained by gravity and calibrated weights or by electricity using the motor with the appropriate control. Both types of creep-testing devices have a multi-section heating chamber that provides the required temperature of the

sample. However, such devices are not keeping up with trends in the development of materials research. One of them is the development of methodologies for less time-consuming assessments of the creep resistance of the material. Classical creep-testing machines are of little use in conducting this type of research. For the new methods, there are devices being developed that can generate low-cycle thermal-mechanical loads, cyclic creep-to-rupture load types, and creep tests as a function of the indentation depth, which can measure the creep rate [1, 2, 3]. The article presents the author's own solution in the form of a system for long-term strength tests. The main feature of the system is a device that can carry out normative creep tests and user-programmable tests, including the low-cycle loads and stress in variable temperature profiles. An important element of this system is a database of tested materials, where test-run results can be automatically recorded in addition to other useful parameters in the calculation of strength. The system allows researching assessment methods for materials in machinery construction, especially those working in conditions of variable loads and high temperatures.

1. The design of the device

The design of the device (Fig. 1) uses the framework structure for a stable resistance to constant loads, characteristic for long-term creep tests, which fall within the range of up to 50 kN. Performance elements constitute a hybrid system containing the following: elements of the modified upper lever with regulated gear ratios and an additional counterweight to balance the lever with different gear ratios, electric synchronous motor, and load creep-tester. In gravitational load, the sample stress comes from the weights placed on a pan connected with a chain connector to the side lever. In a system with a servomotor, the connector is articulately linked with a table that can be moved vertically, and thus can exert the desired load or strain. The motion of the table along the rolling guides is regulated by the signal from the tensometric force transducer mounted in the path of the load or the measuring system of the strain in the sample.

There also is an option of using feedback, which allows free modification of the load characteristics in the course of research. When using gravity load with the moving table constructed with the screw-roll mechanism, it is possible to implement a cyclical loading and unloading of the sample. Additionally, movement of the table following the elongation of the sample secures the load system in case of rupture during the test.

Heating the sample takes place in the two-section oven equipped with heaters G_1-G_4 (Fig. 2). The temperature is measured by two thermocouples (temperature T_g and T_d) placed directly on the sample. An important feature of the heating oven, not common in these types of devices, is the option of opening the lower or the upper outlet (which allows the introduction of additional sensors for monitoring the status of the sample) and the cooling system that uses forced airflow.
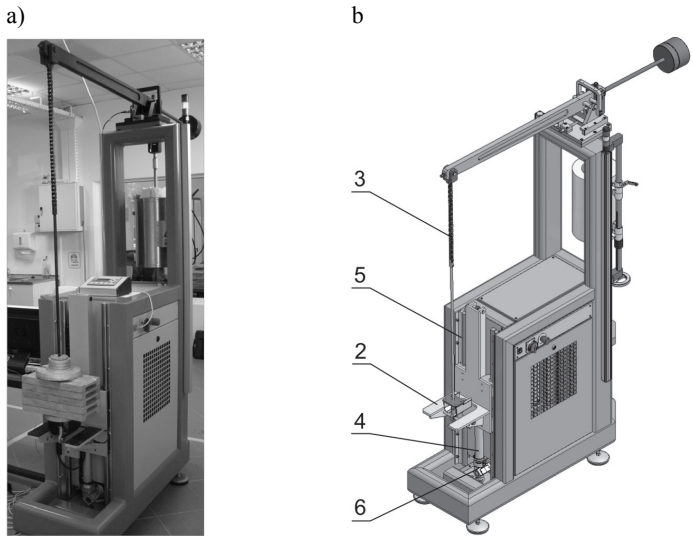
Fig. 1. The view of the device with gravitational load (a) and using the electric motor (b)
        1 – weights, 2 – table, 3 – connector, 4 – screw-rolling mechanism, 5 – rolling guides,
        6 – synchronous motor power supply
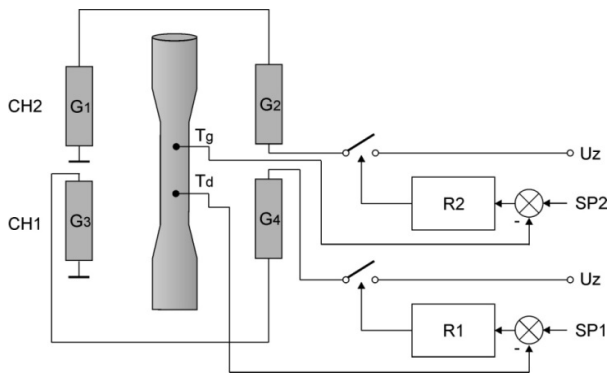
Fig. 2. A diagram of the measurement system and temperature control in the heating chamber

Temperature regulators *R1* and *R2* use a PID control algorithm with variable parameters adjustments (gain scheduling). The alteration in the parameters is automatic for specific temperature ranges. The accuracy in adjustment obtained for normative test is the full-range of 0.2°C up to the maximum temperature of 1,200°C (Fig. 3). The maximum temperature is reached within 1.2 h. Uncontrolled cooling from this level, down to 100°C, takes 9h. When using the cooling system, this time is reduced to about 1h. The turning on of the cooling

system turns off the heater temperature control with resistance heaters H_t, H_b, while maintaining the measuring path and temperature monitoring feed.

a)

b)
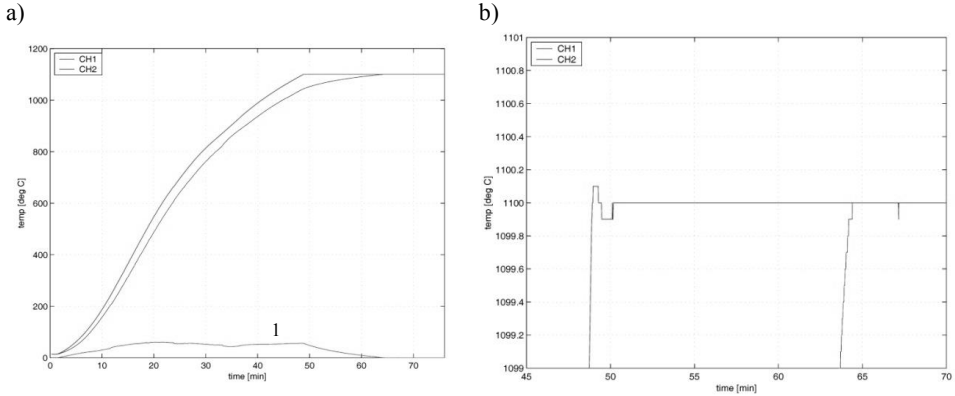
Fig. 3. The process of temperature control of the lower (CH1) and the upper (CH2) part of the sample while approaching the set value of 1,100°C. Line No. 1 on the Fig. 3a – a momentary temperature difference (CH2-CH1)

The power system uses a synchronous motor with a VSD (Variable Speed Driver). Accuracy adjustment has been obtained at the level of 7 N, in the range from 0 to 35,000 N. The force increase rate is set within the non-unit range of $v = 1$ to 6000. The actual values for the constant temperature range are from 3.9 to 500 N/s for a range of 1 kN (Fig. 4a).

a)

b)
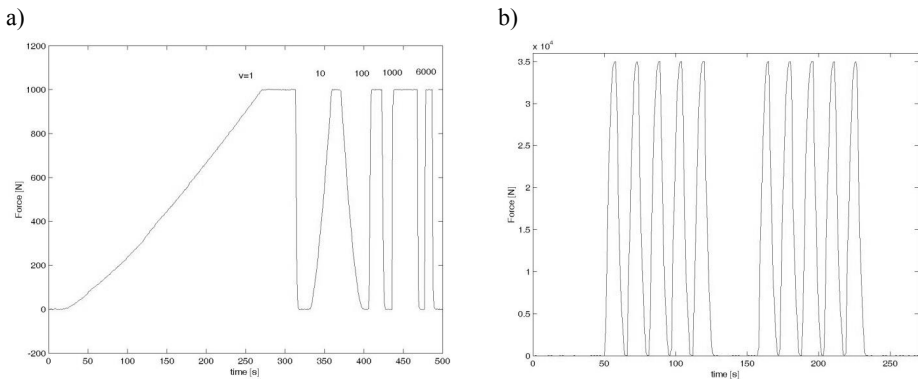
Fig. 4. The chart of the time of the force increase for different velocities of the synchronous motor (a), and cyclical loads for the maximum parameters of force and rotational velocity of the synchronous motor (b)

The obtained durations in force changes allow the estimation of the number of cycles that are possible to perform at reasonable intervals, in low-cycle

fatigue research. For maximum parameters of cyclical loads in the system with a force regulator and maximum velocity v = 6000, the obtained cycle period is T = 15.4 s and force increase rate is 4,545 N/s (Fig. 3b). These parameters give the following durations in flow-cycle fatigue tests: 10^3 – 4.17 h, 10^4 – 41.67 h, 10^5 – 416.67 h, and so on. Due to the durations of tests, the devise is designated to work in low-cycle load testing in the 10^4 – 10^5 cycle range.

Programming for a run of normative tests, in accordance with the PN-EN ISO 204 norm, is done automatically by specifying parameters of the sample, example stress, points of the measurement of stress and strain, the temperature of the sample, a condition for the completion of the creep test, and creep values for which obtained duration values are reported.

Programming for testing with changeable parameters is carried out using the batch control method. The device implements basic commands, whose parameters determine the conditions for the subsequent phases of the test. Sequential execution of the subsequent basic commands ensures the desired course of the test.

2. Software for data collection and analysis

The materials engineering methods and techniques employ metallographic tests and the testing of mechanical properties for the assessment of the working condition of an item in terms of creep and its suitability for further service. The adaptation of the equipment for such an assessment is based on its cooperation with the two databases: the database for measurements that collects the information obtained in the creep tests and the database of materials containing parameters of the test material properties, containing detailed description of the material and has the capabilities to include the description of creep tests performed by the device (Fig. 5). Both databases use standard database streaming (Citadel, Oracle).
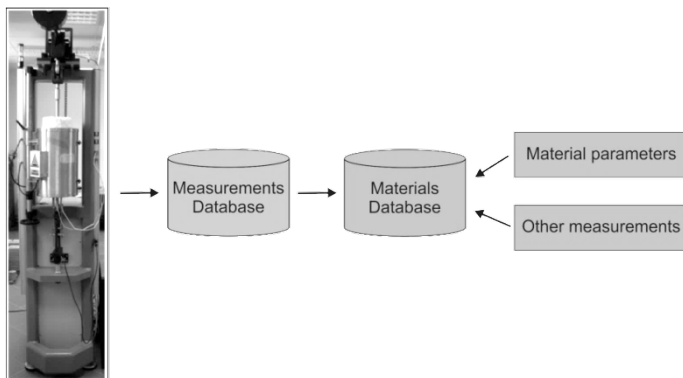
Fig. 5. The structure of the information collection in the software of the device

a)

b)

c)   d)
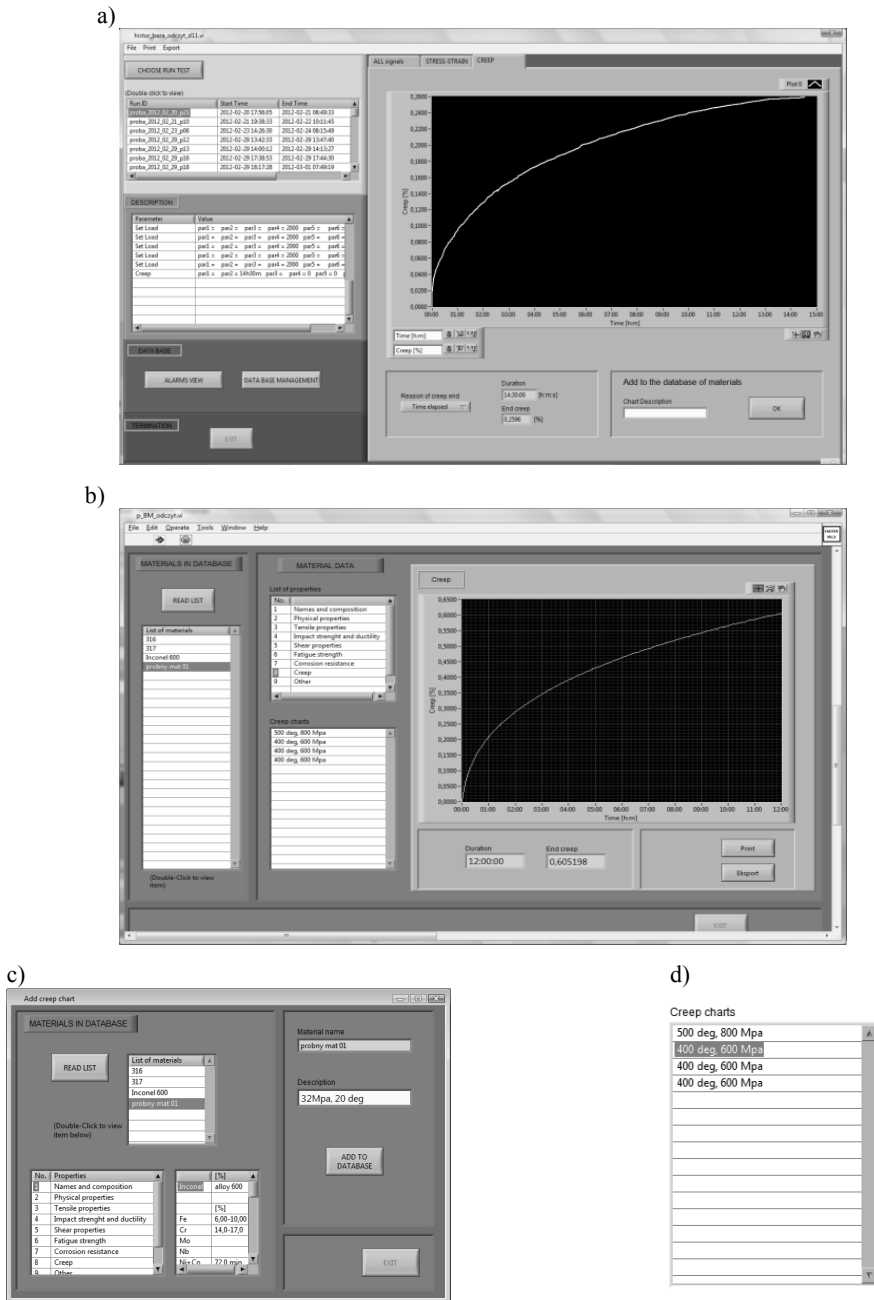
Fig. 6. Screenshots of the software windows for the implementation of creep charts from the measurement database to the materials database: a) the measurement database window); b) the materials database window; c) window for adding a description of the material; d) the window for selecting saved creep charts for a give material

The measurement database contains procedures for saving and retrieving the following objects: all measurement signals, a full test description, alerts, and charts (stress-strain, creep). The features implemented in the software of the measurement database are the following: connecting test runs, printing charts, reporting, test run export, and database management.

The description of the material in the database is divided into the following groups: name and chemical composition, physical properties, tensile test, impact strength and plasticity, shear strength, fatigue strength, corrosion resistance, creep, and other parameters.

The information in the description of "creep" is derived from the database of measurement. Their inclusion in the database occurs in the sub-programme of the measurement data base management (Fig. 6a). The procedure of chart inclusion (Fig. 6c) allows attaching to the designated material any number of creep charts. Reading of the runs (Fig. 6b) takes place by selecting the chart name entered by the user (Fig. 6d).

The group in the material description ("other parameters") allows entering any data (numeric and text) in a two-dimensional array. It can contain graphically designated values of the functions related to the material research, general forms and parameters of the approximating functions for measuring runs, and analysed results of test runs and superposition runs performed with specific parameters.

3. Setting the parameters of strength tests

The programming of the device is done in a "batch" system [5]. Each test, regardless of whether it is done according to the creep norm of uniaxial tension (PN-EN ISO 204) or according to the user settings, is programmed in the device (a computer directly managing the device) or an external spreadsheet. The programming consists in filling in a table with the basic commands. Each command has the appropriate parameters. For example, *Load (V, F)* command means loading the sample with a force of value *F*, with the increase velocity of *V*. The set of commands includes all possible functions arising from the construction of the device and its hardware. An example of the implementation of a normative test programmed in this way is shown in Figure 7.

This way of programming tests also allows an adequate simulation of the actual loads on materials [6].

An example of such a process of simulation (Fig. 8) is a repetition of stress changes (*stress_r*) and temperature (*temp_r*) on a steam boiler element. Other types of tests may include a combination of temperature changes with cyclical loads.

The device can perform automatic hybrid tests, combining normative creep tests, low cycle loads, variable amplitude and frequency loads, and programmable temperature changes.

a)

b)
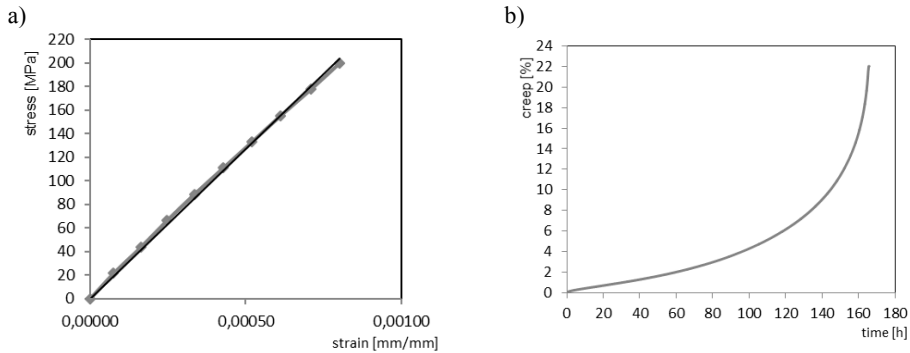
Fig. 7. The results of the normative measurements – characteristics of stress-strain (a) and creep chart (b)
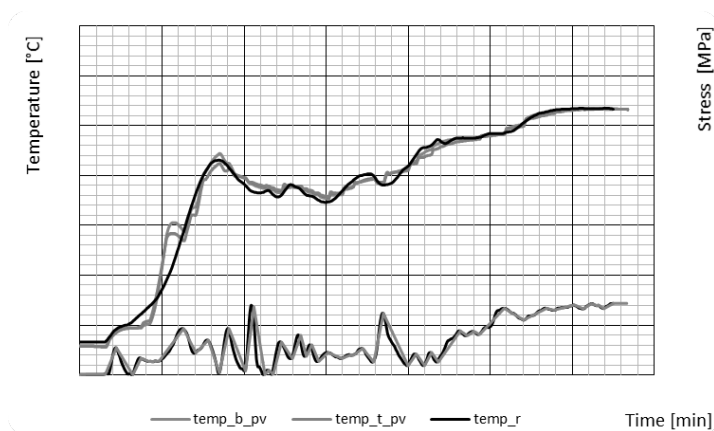
Fig. 8. The simulation of actual operating conditions of the an electric device: temp_b_pv – parameter value of the lower part of the sample, temp_t_pv – parameter value of the upper (CH2) part of the sample, black lines – temp_r, stress_r (temperature and stress from real object)

Conclusions

The designed and manufactured device is an innovative research tool. Its control system uses advanced control algorithms. Consequently, the precision of the temperature control and strength exceeds the requirements of the norm on creep in uniaxial tension. Tests carried out in accordance with this standard are supported by the following: calibration procedures for path measurement, automatic reporting of test results, and procedures for manual and automatic interruption and resuming of testing.

An analysis of the results is facilitated by the cooperation with the two databases. The measurement database collects information about the parameters of the tests carried out. The material database contains selected information from the measurement database and additional data describing the material.

Test programming takes place in the device or in a spreadsheet. This is coupled with the batch test method, which is a selection of commands carried out by the device, and the construction solutions of the heating oven enables the user to generate their own tests with programmable temperature and stress changes, including tests recreating the actual conditions of the machinery functioning in high temperatures and increased pressure.

Adequate simulation of various loads of machine components allows conducting research on new ways to fast-track research of materials and the prediction time of damage to critical machine components.

References

1. Mandziej S.T.: Accelerated creep testing of new steels for power generation and chemical processing. Proceedings of Conference Metal 2010, paper 72.
2. Woodford D.A.: Accelerated Testing for High-Temperature Materials Performance and Remaining Life Assessment (EPRI, Palo Alto, CA: 1999, TR-114045).
3. Izaki T. et al.: A creep life assessment method for boiler pipes using small punch creep test. International Journal of Pressure Vessels and Piping 86 (2009), pp. 637–642.
4. Samborski T., Zbrowski A., Kozioł S., Majcher A.: Mechatroniczne stano-wisko do badań zmęczeniowych. Energetyka, Zeszyt tematyczny nr XXII, listopad 2011, s. 76–79.
5. Majcher A.: Programowanie dedykowanych testów badawczych w urządze-niu do badań pełzania przy jednoosiowym rozciąganiu. Pomiary Automatyka Kontrola PAK vol. 59, nr 4/2013, s. 349–352.
6. Majcher A., Weglowski B., Oclon P.: Multi-function device for creep testing at elevated temperature. Advanced Materials Research, Vols. 875–877 (2014) pp. 462–466.

System do badań materiałów w warunkach długotrwałych obciążeń mechanicznych i termicznych

Słowa kluczowe

Pełzanie, pełzarka, przyśpieszone badania pełzania, zmęczenie niskocyklowe.

Streszczenie

W artykule przedstawiono system do badań materiałów stosowanych do wytwarzania elementów maszyn pracujących w warunkach podwyższonych naprężeń i wysokich temperatur. Podstawowym elementem systemu jest wielofunkcyjne urządzenie umożliwiające wykonywanie normatywnych testów pełzania (PN-EN ISO 204) oraz dedykowanych testów o obciążeniach niskocyklowych oraz różnych profilach zmian temperatury. Urządzenie współpracuje z dwiema bazami danych – do zbierania wyników testów wytrzymałościowych oraz do zbierania danych materiałowych wykorzystywanych w predykcji czasu do uszkodzenia. Opisano funkcjonalność poszczególnych elementów systemu oraz podano przykłady przeprowadzonych testów wytrzymałościowych.

Andrzej PIECZARA, Tadeusz PIOTROWSKI
Gonar Bis sp. z o.o., Katowice
gonar@gonar.com.pl, andrzej@gonar.com.pl, piotrowski@gonar.com.pl
Wojciech LEŚNIEWSKI, Marek WAWRYLAK, Piotr WIELICZKO
Instytut Odlewnictwa, Kraków
iod@iod.krakow.pl, wojciech.lesniewski@iod.krakow.pl,
marek.wawrylak@iod.krakow.pl, piotr.wieliczko@iod.krakow.pl

THE IMPACT OF BRAZING PARAMETERS ON THE STRENGTH OF A WC/Co-FILLER METAL-STEEL JOINT

Key words

Metal-ceramics material, brazing, machining tools.

Abstract

Manufacturing and geotechnical engineering utilise a number of machining tools. In their construction, a significant role is played by brazed joints, thanks to which the machining element can be made of WC/Co materials. The metal-ceramics material is joined with steel or cast steel elements with the use of filler metal, based on copper alloys. The components of filler metals are different depending on technological requirements. These may be the alloys of copper, silver, zinc, nickel, cobalt, and manganese. The article presents various techniques of brazing 40HM steel and WC/Co material with filler metal not containing zinc Cu87Mn10Co3. The experimental joints were made with the use of distance rods, steel mesh, and nickel mesh. The impact of the material that provides repeatability of the geometry of the brazing process was tested on the strength of a joint that is subjected to shear stress. The impact of distance elements is mostly positively assessed; however, in some data from publications,

the impact of steel mesh is assessed negatively. In order to assess the correctness of joints, x-ray computer tomography was conducted.

Introduction

During the production of tools designated for applications in geotechnical engineering, the working machining element, mostly manufactured as a WC/Co profile, is joined with a steel mandrel of the tool most often by brazing. Other techniques like gluing, pressure welding, or welding, including laser welding, are also used [1–3]. The durability and reliability of tools depend on the quality of the joint. In brazed joints, the selection of filler metal is key, because it directly impacts the strength of the resulting joint. Filler metals based on copper alloys are the most common. Alloying additions aim at both increasing strength parameters and improving the conditions for producing the joint. Take the example of cobalt, whose presence in filler metal facilitates the process of wetting WC/Co material. A few percent content of manganese in filler metal allows wetting cemented carbides in which there exist phases which are difficult to wet (TiC or elemental carbon) [4]. Commercial filler metals that contain silver are characteristic of low melting temperature (600–800°C) [5] and are used for joining materials in tools in which exceeding the temperature of phase transformation is unwelcome.

The process of brazing determines the quality of the joint, during which special attention is paid to achieving proper gap. The filler metal joins both elements and compensates stresses that occur during the cooling of a brazed joint, resulting from different expandability coefficients of cemented carbide and steel [6]. In turn, it is significant for the joint to correctly carry the stress, which occurs during the work of the tool. Due to this fact, the thickness of the gap cannot be too small and the maximum strength parameters of the joint are usually achieved for a certain width of the gap. Introducing additional filling elements (reinforcing) between the carbide and steel, for example fibres or meshes, facilitates the control over the thickness of the gap and generally improves the strength parameters of the joint [7]. It is important for the reinforcing elements to be characteristic of higher melting temperatures than the filler metal itself.

1. The aim and research methodology

The conducted research was aimed at defining the impact of brazing parameters (temperature and the applied distance element) on the quality of achieved brazed joints. The quality of the joint was verified by conducting a shear stress test.

2. Materials

Experimental brazed joints were manufactured according to the following scheme: steel base–filler metal sample–distance element–WC/Co profile ("sandwich"). The samples were brazed with the use of the following three different distance elements:

1) A pair of parallel steel wires 0.2 mm in thickness 4 mm apart,
2) Stainless steel mesh 0.3 mm in thickness in a shape of a circle 10 mm in diameter, and
3) Nickel mesh 0.2 mm in thickness in a shape of a circle 10 mm in diameter.

The base in all cases constituted discs 17.4 mm in diameter and 4.5 mm in height made of 40HM steel. In the discs, holes were made 1 mm in diameter and 4 mm in depth, which allow placing a measuring thermo-element. Cuboidal WC/Co profiles with dimensions $7 \times 7 \times 5$ mm made of B30 grade were brazed to the base. The joints were made with Cu87Mn10Co3 filler metal in a form of cylinders 3 mm in diameter and height selected for the applied distance elements. The height of the filler metal cylinders was selected experimentally, providing complete filling of the gap. Examples of sets before brazing are presented in Figure 1.
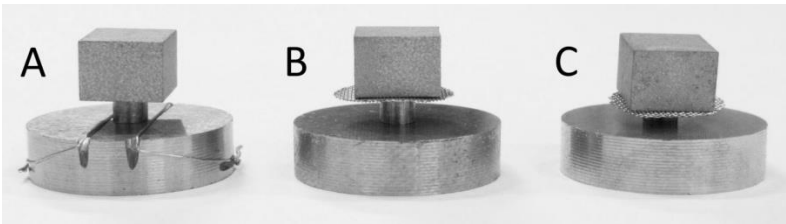
Fig. 1. The set before brazing: A – with steel wires, B – with steel mesh, C – with nickel mesh

3. Producing experimental brazed joints

Samples of experimental joints were manufactured in a working coil of an induction generator, placing the set on the upper surface of a porous ceramic cylinder with a centrally placed measuring thermos-element. The samples were heated inductively in the coil 35 mm in diameter using approx. 25% of 10 kW generator power. Three series of measurements were conducted, heating the sets to three selected values of temperature: 1040°C, 1080°C and 1120°C. The selection of temperature value was made based on the double equilibrium diagram of copper and nickel. At 1080°C, the process of nickel dissolving is initiated in pure copper. Producing joints at this temperature was complemented by joints at temperatures higher by 40°C and lower by 40°C. Overheating the

filler metal by 40°C in a short time above 1080°C should not cause dissolving of nickel mesh in liquid filler metal.

Samples were heated to the selected temperature, after reaching this temperature, the induction coil was manually turned off. The joints were made in a protective atmosphere. Nine series of samples were made – three distance elements, three different temperature values, and three samples in each of the series.

4. Testing the quality of manufactured joints

Samples underwent shear stress tests. The achieved maximum value of shearing force was calculated into the value of average shear stress according to the following formula (1):

$$\tau = \frac{F}{A} \tag{1}$$

where:

τ – average shear stress,
F – shearing force destroying the joint,
A – surface area of the joint (A = 49 mm^2).

The achieved results of measurements are presented in Figure 2.
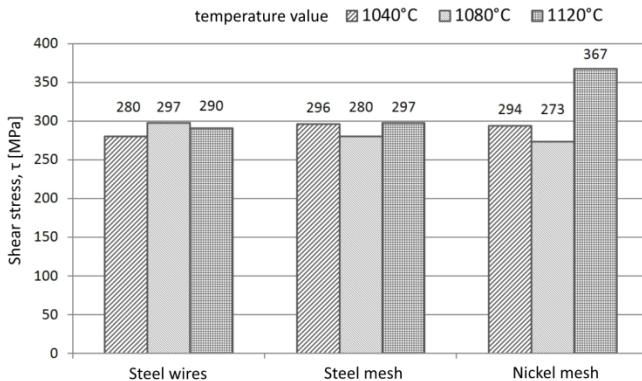

Fig. 2. The results of measuring shear stress in relation to the value of temperature at which the joint was made and the applied distance element

In order to define the quality of joints at an angle of the presence of brazing effects, non-destructive tests were conducted with the use of a V|tome|x L-450

computer tomography machine. The obtained series of photographs allow the assessment of a tested sample at an angle of porosity presence both in the produced joint and in the material of WC/Co profile. Figure 3A presents a tomography photograph taken in the plane of a brazed joint. Mesh and slight porosity in the joint are clearly visible. Figure 3B presents the view of a destructed joint. The shear of the joint took place between mesh and a WC/Co profile, visible is the structure of mesh and sections of a destructed joint at the level of the surface profile-filler metal.
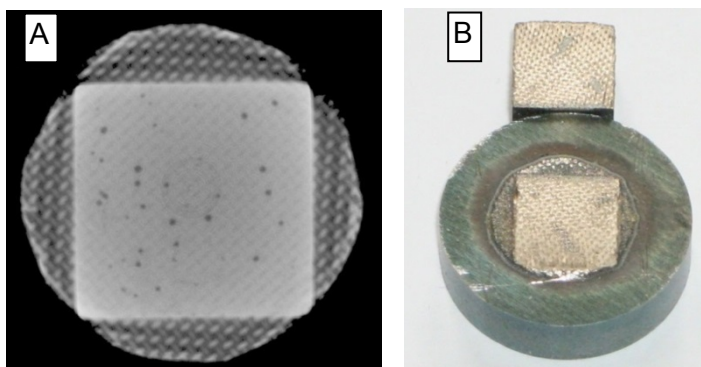
Fig. 3. A – A photograph taken in the plane of the joint with the use of a computer tomography machine, B – A photograph of a destructed joint after conducting shear stress test

Summary

    All manufactured samples were characteristic of slight porosity, which lowered the strength of tested joints. The achieved results, after measuring the shear stresses of samples, indicate practically equal strength. The expected differences of the joint strength in relation to the type of applied distance material were not observed. Joints made with the use of nickel mesh at 1120°C were characteristic of the highest strength. The increase in strength is related to the change of filler metal composition caused by partial dissolving of mesh into the filler metal. The samples in which steel wires were used as a distance element do not have visible porosity in the joint.

References

1. Northop I.T.: The joining of tungsten carbide hardmetal to steel, J.S. Afr. Inst. Min. Metall, 87, no. 5 (1987), pp. 125–135.
2. Czechowski K., Kurleto A., Poselska-Filip I., Wszołek J.: Klejenie części roboczych narzędzi jako technologia alternatywna dla lutowania, Przegląd Spawalnictwa, nr 9 (2007), s. 142–145.

3. Barbatti C., Garcia J., Liedl G., Pyzalla A.: Joining of cemented carbides to steel by laser beam welding, Mat.-wiss. u. Werkstofftech. 38, No.11 (2007) pp. 907–914.
4. Willingham J.: Filler metals and fluxes, Johnson Matthey Metal Joining, http://www.jm-metaljoining.com/pdfs/2747%20Tungsten%20Carbide.pdf.
5. Mirski Z.: Spajanie węglików spiekanych ze stalą, Oficyna Wyd. Politechniki Wrocławskiej, Wrocław (2011).
6. Mirski Z.: Sterowanie szerokością szczeliny lutowniczej w procesach spajania materiałów różnoimiennych, Praca Naukowa Instytutu Technologii Maszyn i Automatyzacji Politechniki Wrocławskiej nr 73, Monografie nr 22, Oficyna Wyd. Politechniki Wrocławskiej, Wrocław (2000).
7. Sawashima T., Sugawara H.: Cemented carbides for increased braze spreading and its manufacturing method, Japanese Patent, 125206 (1978).

Wpływ parametrów lutowania na wytrzymałość połączenia WC/Co–lutowie–stal

Słowa kluczowe

Materiały metalowo-ceramiczne, lutowanie, narzędzia skrawające.

Streszczenie

Przemysł przetwórczy oraz geotechnika wykorzystują w swojej działalności olbrzymie ilości narzędzi skrawających. W ich konstrukcji znaczącą rolę odgrywa połączenie lutowane, dzięki któremu element skrawający może być wykonywany z materiałów typu WC/Co. Materiał metalowo-ceramiczny łączony jest z elementami stalowymi lub staliwnymi przy wykorzystaniu lutowi wysokotemperaturowych, bazujących na stopach miedzi. Składniki lutowi są różne i, w zależności od wymagań technologicznych, mogą to być stopy: miedzi, srebra, cynku, niklu, kobaltu oraz manganu. W artykule przedstawiono różne techniki wykonania połączenia lutowanego stali 40HM i materiału WC/Co lutowiem bezcynkowym Cu87Mn10Co3. Doświadczalne połączenia wykonywano z wykorzystaniem dystansowych drutów stalowych, siatek lutowniczych stalowych oraz niklowych. Zbadano wpływ materiału zapewniającego powtarzalność geometrii procesu lutowniczego na wytrzymałość połączenia poddanemu naprężeniu ścinającemu. Wpływ elementów dystansujących jest przeważnie oceniany pozytywnie, jednak w niektórych danych literaturowych [5] wpływ siatki stalowej oceniany jest negatywnie. Do określenia poprawności wykonanych spoin wykorzystano rentgenowski tomograf komputerowy.

Jacek WOJUTYŃSKI

Institute for Sustainable Technologies – National Research Institute, Radom
jacek.wojutynski@itee.radom.pl

THE METHOD FOR STABILISATION
OF TEMPERATURE AND HUMIDITY
IN VOC CHAMBERS

Key words

VOC, humidity, temperature, fuzzy logic.

Abstract

   This paper presents selected issues of the design of precise control devices for the characteristics of the process environment in the VOC (Volatile Organic Compounds) chambers, in which non-standard validation tests are performed. The main parameters defining the environmental conditions are temperature and humidity. Particular attention was paid to the elimination of pollution generating sources in the background of the chamber. The module designed to control the temperature and humidity is presented. The results of the recording of temperature and humidity in several-month-long test cycles are presented. The developed modules have been used in chambers for testing the emissions of volatile organic compounds and formaldehyde.

Introduction

   In the process environment (Fig. 1), usually implemented by the validation chamber, in which the test piece is placed, we distinguish an environmental

parameter maintenance subsystem, a subsystem to generate excitations on the test object, and a subsystem for control and measuring environmental parameters (climate) and the reaction to the test object to excitations. The division of these systems depends on the test procedure, e.g., the force exerted on the test object in the chamber either may be the environmental parameter or generated excitation.
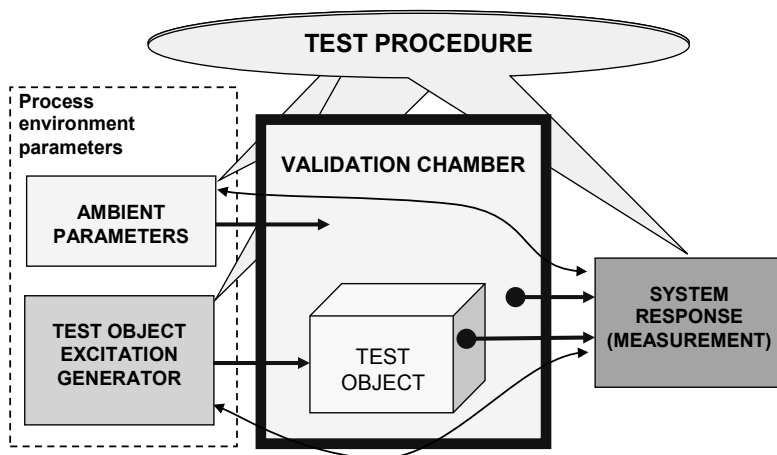
Fig. 1. Validation chamber as a system with controlled characteristics of process environment

Within the task "Specialized equipment for validation testing with controlled characteristics of the process" realised within Strategic Programme of the chambers for testing VOC emissions and carbonation of concrete were selected as examples. The VOC chamber can also be used to test formaldehyde emission with a chamber method.

The idea of VOC emissions test is as follows:

- The chamber in which the sample is placed is made of glass or stainless steel. The seals are Teflon. The study of emissions of volatile organic compounds is carried out at a temperature $23°C±0.5°C$ and a relative humidity 45% RH±3.0% for the European standards, and at $25°C±1.0°C$ and a humidity of 50% RH±4.0% for the United States requirements.
- The chamber pressure is maintained at 1000–2000 Pa.
- A service unit supplies air at a suitable temperature, humidity, and cleanliness.
- The analysis of samples is carried out using a chromatograph.

The paper discusses the temperature and humidity control for VOC chambers, in which, because of the method of the test, there is no need to lower the humidity and temperature.

As a result of the analysis of standards [2] to [6], it was assumed that the construction of the chamber should be as follows:

- Air supply – air intake with filter: Air intake is from the outside, from a zero air generator, or from a lubricant-free compressor.
- Service unit: It functions to ensure the temperature, humidity, and the mass volume control of air flow (in the standard [2] conditioning system, airflow regulator).
- The VOC chamber: It consists in an internal fan with a motor located on the outside of the chamber to ensure the airflow rate around the sample in the range of 0.1–0.3 m/s.
- Sample acquisition system air from the chamber.
- A data acquisition system: This is a standard system for monitoring temperature and humidity.

A block diagram of the test chamber for VOC emissions is shown in (Fig. 2).
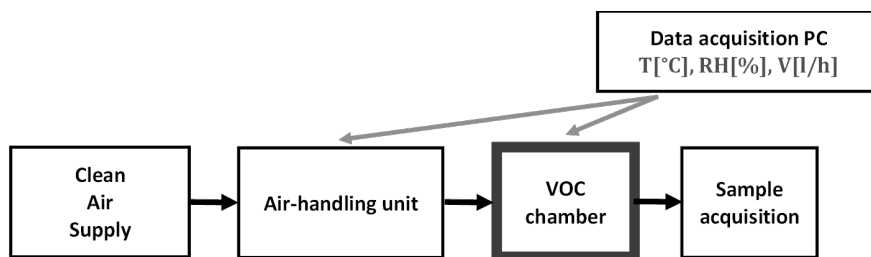
Fig. 2. Schematic diagram of a chamber for testing the VOC emissions

Since the chambers are made of glass or stainless steel and have no insulation, it is required that the VOC chamber is placed in an air-conditioned room [1]. Since the standard air conditioning does not provide a good stabilisation of the temperature in the room, the use of reheated air introduced into the chamber is required.

An important problem is the purity of the background of the chamber, tested by chromatographic methods, which should be <20 g/m^3, the total concentration of volatile organic compounds (TVOC), and the concentration of a single intentional VOC should be <2 $\mu g/m^3$.

1. Air humidity control module

The standard PN-EN 717-1:2004 [2] shows a sample device for RH stabilisation of the controlled air flow with a relative humidity 45% (Fig. 3).

According to the standard, the idea of preparation of air of the desired relative humidity is mixing dry air stream, which is the upper tract, with the air humidified in the washers, which is the lower tract [2]. This method of

conditioning the relative humidity of air (gas) is used in other applications developed at ITeE-PIB. After analysis, the construction of an air-handling unit was proposed according to the diagram (Fig. 4). What is new is the use of two mass flow regulators controlled by an electric signal of 4–20 mA and an automatic water filling system.
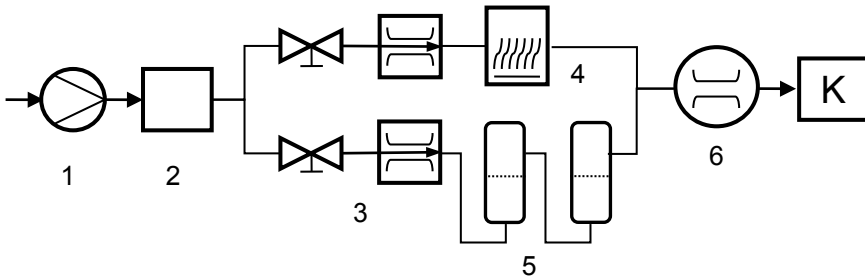
Fig. 3. Sample structure of an air preparation system according to PN-EN 717-1:2004 [2]: 1) Gas pump, 2) Charcoal filter, 3) Flow meter and flow control for air, 4) Silica gel filter, 5) Water washer (humidification), 6) Flow control or gas-meter; K) Validation chamber
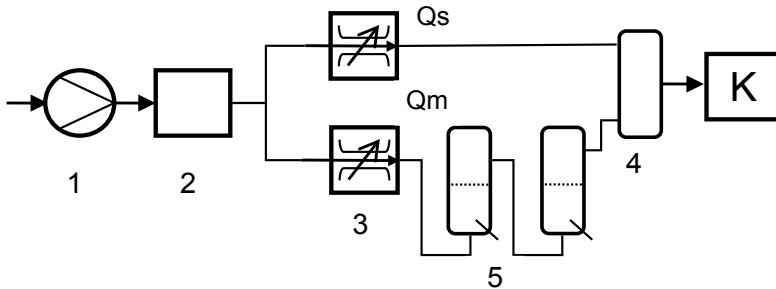
Fig. 4. The structure of the service unit with two flow regulators: 1) Lubricant-free compressor, 2) Air filters, 3) Air flow regulator, 4) Mixing tank with heaters, 5) Washers with automated water filling system, 6) Regulated dumping valve, F) Air filters, K) Validation chamber

Given air flow Q_Z [l/h] calculated according to the standard is divided for two flow regulators – dry air tract Q_s and moist air tract Q_m according to the following equations:

$$Q_Z = Q_s + Q_m \quad Q_s = k_s \cdot Q_Z \ \text{ and } \ Q_m = k_m \cdot Q_Z \qquad (1)$$

where

$$k_s + k_m = 1 \ \text{ and } k_s, k_m \geq 0.02 \ \ Q_s \geq Q_{min} \text{ and } Q_m \geq Q_{min} \qquad (2)$$

Q_{min} is a minimal value possible to obtain and resulting from the "regulation depth" of the regulator. For the applied mass flow regulators, the regulation depth is 50:1. So when the regulator with a maximum flow of 250 [l/h] is used, the minimal flow is 5 [l/h] for dry air and moist air, so the total minimal flow is 10 [l/h]. Then, $k_s = k_m = 0.5$. The user sets the required value of air humidity and the PLC based measurement-control system calculates and regulates proper coefficients k_s and k_m. Fig. 5 shows the developed air preparation system [7].
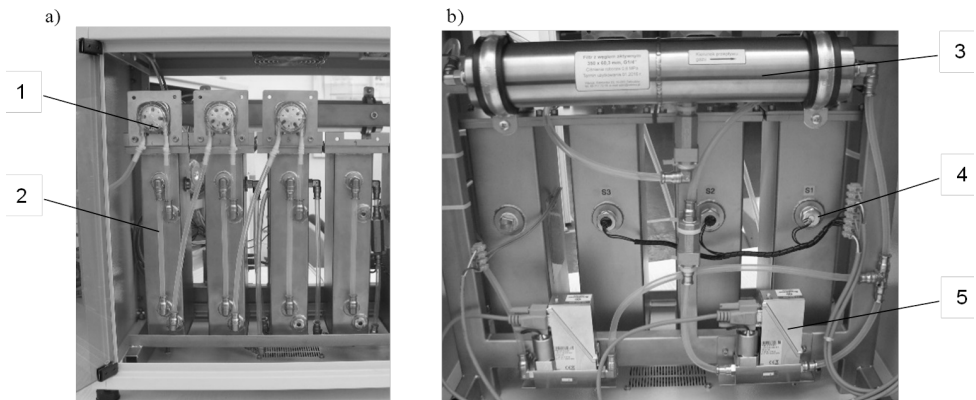
Fig. 5. Air preparation unit with steel washers with automated water filling and two flow regulators: a) washer with peristaltic pumps – front, b) mass flow meters – back of the unit; 1) peristaltic pump, 2) Washer units with level gauges, 3) Carbon filter, 4) The water level sensor, 5) Air mass flow regulator
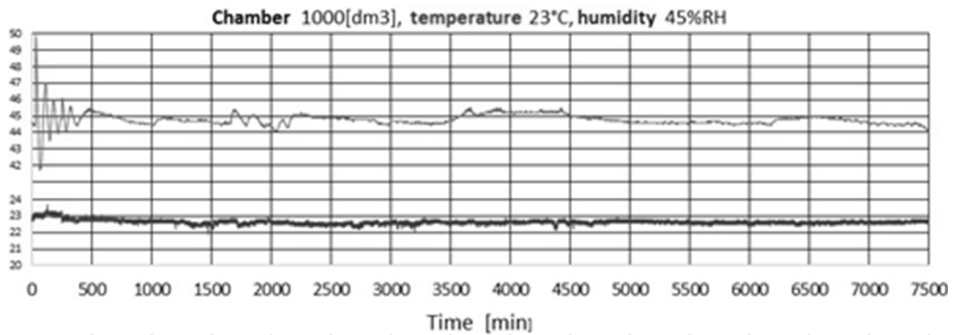
Fig. 6. Long-term test of the glass chamber of volume of 1000 dm^3 – without heater inside of the chamber and with two mass flow regulators according to diagram (Fig. 4). Record time approx. 125 days, sampling period 5 seconds

The developed service unit has been subjected to long-term tests. The results of the regulation of temperature and humidity are shown in (Fig. 6) [7]. For the tests, a chamber with a volume of 1000 dm^3 was selected, which is more

difficult to stabilise due to its size. At the beginning of the test, the experiments with the airflow regulator were conducted, including starting and stopping the airflow. Later, the airflow was set at 1195 [l/h], which allows the exchange of air in the chamber within approx. 1 hour.

The developed service unit has also been tested for air purity. The chromatograms of "zero" air samples taken from the cylinder, zero air generator, and after passing through the air handling system were compared. The results are shown in (Fig. 7). All samples were collected under a pressure of about 0.01 bar, at the airflow of 200 [l/h]. The amount of air was approximately 10 [l] (18 l/h for 30 min). Each sample was acquired 2 times on two different Tanax TA absorption tubes, and the results are consistent.
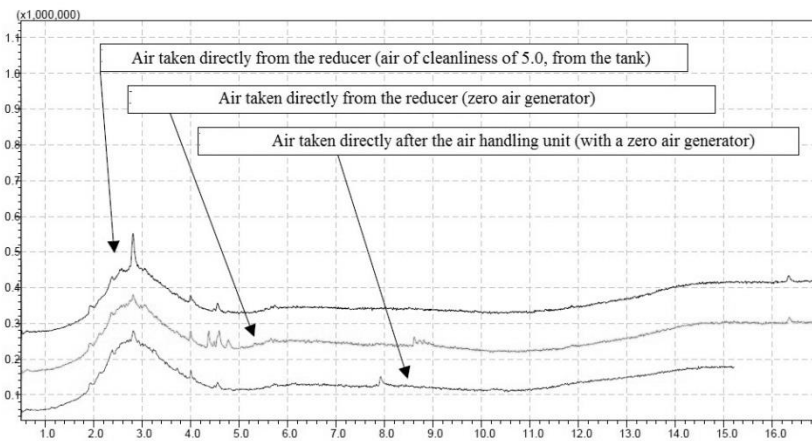
Fig. 7. Chromatographic tests of the zero air from the container, from the zero air generator and after passing through the air preparation system

The tests documented very good air quality obtained from an air-handling unit.

2. Air temperature control module

As mentioned in the introduction, due to the use of glass and metal chambers without external insulation, the chambers were placed in an air-conditioned room. Therefore, the temperature control system only regulates the air temperature within the chamber to a small extent, i.e. a few degrees and a few percent relative humidity.

Air density is dependent on pressure, temperature and composition, for example, the density of dry air, at atmospheric pressure at sea level at a temperature of 20°C is about $\rho = 1.2$ kg/m^3. The specific heat of the air is

c = 1005 J/kg/K. Therefore, to heat V = 1 m^3 of air (the volume of one of the typical chambers) by Δt = 1 K the energy needed is

$$Q = \rho*V*c*\Delta t = 1206 \text{ J} \qquad (3)$$

With the heater power of P = 24 W, the required time is approx. Q/P≈50 s (at 100% efficiency and in the absence of airflow through the chamber). This is an acceptable time, given the time of tests in VOC chambers (up to several hundred hours).

The method for heating the chamber uses an external heater with a temperature sensor installed in the bottom of the chamber and the external heaters of mixing tank (Fig. 4).

3. Algorithms for air temperature and humidity control

The control and measurement system for the air-handling unit is realised by means of a PLC equipped with touch screen HMI operator panel. To adjust the humidity and temperature, the fuzzy controller is used with the consequent fuzzy singleton according to the model used in the PLC controllers [8]. The presented algorithm and its implementation is the author's solution, since the applied PLC does not provide the implemented fuzzy controller. For analogue signals measured (e.g. humidity, temperature) and calculated (e.g. the rate of change), a method was designed for determining the scope of these signals using the deltas and the lower and upper limits. δ – is used to determine the parameters of the desired range of stabilisation, Δ – defines the scope of the need to change the control-stabilised variable. The developed structure of limit values is helpful for determining fuzzy sets (Fig. 8), boundary fuzzy sets are of the type Z and S, while the middle are of the Λ type. Similarly, fuzzy sets are designed for temperature; we substitute RH with T. Fuzzy sets that are defined with the parametrised conversion macros. The calculations are simplified with a floating--point arithmetic implemented in the controller.
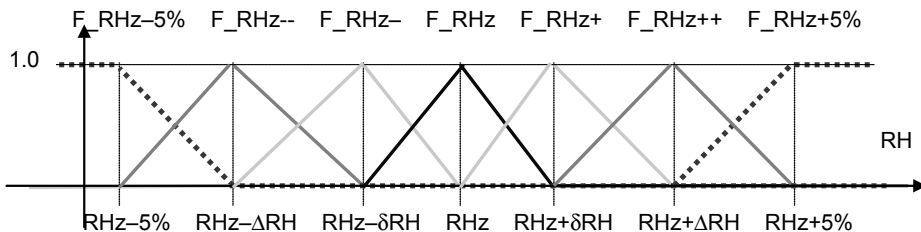

Fig. 8. Definition of fuzzy sets for air humidity

The ratio of airflow is adjusted immediately, and it takes several tens of milliseconds to settle. In contrast, the effect of changes in humidity after changing of the flow ratio is deferred over time. Therefore, the process of adjusting the humidity has long time constants and long delays. To control it, additional mechanisms were introduced to facilitate the implementation of control as follows:

- Generating of a flow control at a control period has the time resulting from the time constants of thermohygrometer and time constants of the system. This is the time, followed by the correction coefficients $k_s + k_m = 1$ in the discussed method for adjusting the humidity.
- Information about the direction of changes in humidity (RH$\downarrow$, RH=, RH$\uparrow$) are updated at the control period.

Sample temperature and humidity rules have the following forms:

$$\textbf{IF}\ \ \text{RH}\ \textbf{is}\ \text{F\_RHz--}\ \ \textbf{and}\ \ \text{RH}\uparrow\ \ \ \textbf{THEN}\ \ \text{Flow}(k_s := k_s + 0.005) \qquad (5)$$

$$\textbf{IF}\ \ \text{RH}\ \textbf{is}\ \text{F\_RHz}\ \ \textbf{and}\ \ \text{RH}=\ \ \ \textbf{THEN}\ \ \text{Flow}(k_s := k_s) \qquad (6)$$

$$\textbf{IF}\ \ \text{T}\ \textbf{is}\ \text{F\_Tz--}\ \ \textbf{THEN}\ \ \text{Heater=PWM\%80} \qquad (7)$$

$$\textbf{IF}\ \ \text{T}\ \textbf{is}\ \text{F\_Tz+}\ \ \textbf{THEN}\ \ \text{Heater=PWM\%off} \qquad (8)$$

Since the temperature adjustment process is slow, there is no need to take into account the rate of change in temperature, since the VOC chamber is not thermally insulated, and the temperature in the air-conditioned room is near the set-point temperature. Long-term tests of the regulation confirm the assumed concept of the temperature and humidity controller (Fig. 6).

Summary

The module for humidity and temperature regulation developed by the author of this article is intended to construct specialised chambers for testing VOC emissions. This method, with two mass flow controllers to regulate the humidity, has proven itself in practice and ensures the desired air quality. Presently, 21 of VOC chambers in different versions have been constructed.

The author's control algorithm for humidity and temperature of the object in which there are long delays and large time constants was developed. The thermohygrometer reaction time is 30 seconds. The algorithm is independent of the size of the VOC chamber, and the same is applied to the chamber with

a capacity of 225 dm^3 and 1000 dm^3. Long-term tests confirm the good stabilization of the temperature and humidity in the VOC chamber.

The measurement and control software takes the form of the distinguished procedures with separate memory spaces, which can be used for software development for other chambers. In case of VOC chambers, there is no need for intensive drying of the chamber space.

The concept of measurement and control system in the form of an open distributed system allows flexible configuration of VOC chambers and their modifications in the future.

References

1. Test chambers for volatile organic compounds (VOC) emission testing, http://katalog.itee.radom.pl/images/stories/karty/10.komora_ang.pdf access 20.02.2015.
2. PN-EN 717-1:2006. Płyty drewnopochodne – Oznaczanie emisji formalde-hydu – Część 1: Emisja formaldehydu metodą komorową.
3. PN-EN 717-2:1999. Płyty drewnopochodne – Oznaczanie emisji formalde-hydu – Emisja formaldehydu metodą analizy gazowej.
4. PN-EN ISO 16000-1:2006. Powietrze wnętrz – Część 1: Główne aspekty strategii pobierania próbek. English version.
5. PN-EN ISO 16000-5:2007. Powietrze wnętrz – Część 5: Strategia pobierania próbek lotnych związków organicznych (VOC). English version.
6. PN-EN ISO 16000-9:2009. Powietrze wnętrz – Część 9: Oznaczanie emisji lotnych związków organicznych z wyrobów budowlanych i wyposażenia – Badanie emisji metodą komorową.
7. Raport końcowy z realizacji zadania badawczego nr III.3.3/PS „Urządzenia do badań testowych i certyfikacyjnych w przemyśle meblarskim i materia-łów budowlanych", Radom, lipiec 2013.
8. PN-EN 61131-7:2004, Sterowniki programowalne – Część 7: Programowa-nie rozmyte.

Metoda stabilizacji temperatury i wilgotności w komorach VOC

Słowa kluczowe

VOC, wilgotność, temperatura, logika rozmyta.

Streszczenie

W artykule przedstawiono wybrane zagadnienia projektowania urządzeń do precyzyjnego sterowania charakterystykami środowiska procesowego w komorach VOC (*Volatile Organic Compounds*), w których prowadzone są niestandardowe badania atestacyjne. Głównymi parametrami określającymi warunki środowiska jest temperatura i wilgotność. Szczególną uwagę zwrócono na eliminację źródeł generowania zanieczyszczeń w tle komory. Zaprezentowano opracowany moduł do regulacji temperatury i wilgotności. Przedstawiono wyniki rejestracji temperatury i wilgotności w kilkumiesięcznych cyklach badawczych. Opracowane moduły zostały zastosowane w komorach do badania emisji lotnych związków organicznych oraz formaldehydu.

Piotr DUDEK, Paweł DARŁAK, Piotr DŁUGOSZ, Aleksander FAJKIEL
Foundry Research Institute, Kraków, Poland
piotr.dudek@iod.krakow.pl, pawel.darlak@iod.krakow.pl,
piotr.dlugosz@iod.krakow.pl, aleksander.fajkiel@iod.krakow.pl

POROUS CERAMIC PREFORMS DEDICATED FOR LOCAL REINFORCEMENT SUBJECTED TO THE SQUEEZE CASTING INFILTRATION PROCESS

Key words

Metal matrix composites, squeeze casting.

Abstract

An attempt was made to obtain ceramic preforms with different contributions of porosity. Compressive strength tests were carried out to estimate the ability of ceramic preforms to be utilised in the process of squeeze casting for the fabricating of metal matrix composites. The achieved ceramic preforms were subjected to the squeeze infiltration process, and materials with much higher mechanical properties relative to monolithic materials were obtained.

Introduction

Metal matrix composites are widely used in many branches of the industry due to an interesting set of features that better or different in relation to monolithic materials. It allows the application of metal matrix composites where other materials do not meet the assumed parameters, e.g., high strength, abrasion resistance, creep resistance, etc., in the whole volume of a casting or its fragment [1–2]. A few basic methods used for fabricating metal matrix composites can be distinguished, although casting methods are most widely applied.

Depending on the type or the reinforcing phase and liquid metal, the following variations of the squeeze casting process can be distinguished [3]:

1. Squeeze infiltration (compression impregnation, high-pressure infiltration casting) of a porous ceramic preform (fibrous, skeletal, or dispersive) which results in a ready casting, a preshaped product, or semi-finished composite material (reinforcement insert);
2. The fabrication of a casting with local reinforcement – by a composite semi-finished product or a porous ceramic preform with its simultaneous high-pressure infiltration;
3. The fabrication of a dispersion particulate reinforced casting, (the reinforcing phase is present in the form of particles, whiskers, or short fibres); or,
4. The fabrication of a hybrid composite casting, reinforced by a preform (sometimes with simultaneous infiltration), and a dispersion phase.

From the utilitarian point of view, the method of high-pressure infiltration is the most useful, which is presently one of the most perspective ways of fabricating particular materials. With the use of this process, a wide scope of materials can be achieved with relatively low outlays [4]. The short time for the solidification of the metal matrix limits its reactiveness with the reinforcing phase, and the high pressure of infiltration guarantees both adequate quality of fabricated heterogeneous materials – practically without participation of porosity, and considerably improves wettability of the reinforcing phase by the liquid matrix. The short time for the solidification of the matrix also limits unfavourable reactions on the boundary of the matrix-reinforcement.

The final properties of metal matrix composites are mainly determined by a proper distribution of the reinforcing phase in the structure of the heterogeneous material. That is why a favourable solution is the introduction of porous preforms to liquid metal that include particles or fibres with a given spatial distribution (homogeneous) of the reinforcing phase [5].

The article describes methods for the fabrication of ceramic preforms designated for local reinforcement of castings achieved with the high-pressure infiltration process. The produced material must be characteristic of the high participation of open porosity and adequately high compressive strength.

The fabrication of a ceramic preform is a very difficult task due to a number of problems that occur. The most important problems are the following [6]:

− Difficulties in obtaining a homogeneous distribution of porosity and sizes of pores, and
− The low repeatability of the process.

1. The course of the research

In the initial stage of research, the input materials were selected for the fabrication of ceramic preforms, of which sample mixtures of ceramic powders with different contributions of pore-creating factors were prepared. Then

mixtures of powders were pressed and sintered at different parameters of processes. The obtained preforms were tested for total and open porosity, as well as compressive strength. Preforms with satisfactory parameters underwent scanning microscopy tests in order to reveal their internal structure. After that, a series of sample composite castings were made infiltrating preforms with liquid 7075 aluminium alloy.

2. The selection of reinforcing materials

A proper selection of ceramic materials for the process of squeeze infiltration constitutes a highly important stage, since physical-chemical properties of the reinforcing phase have a significant impact on the final properties of the heterogeneous material. Based on the analysis of topics in the literature on reinforcing materials and technical possibilities of their later processing, the following reinforcing phases were selected for further tests (attempts to fabricate porous preforms):
− Saffil® continuous fibres
− α – aluminium oxide particles with two diameters of grain (NABOND 0.1 μm + ALCOA 23–48 μm).

3. Fabrication of porous preforms

In order to fabricate preforms with a high participation of open porosity, the following methods were applied:
− Introducing different sizes of particles,
− The addition of organic substances, and
− The addition of removable additions.

Mixtures of powders of aluminium oxide with different sizes of grain (submicron and approx. 35 μm) 1:1 ratio and cut Saffil® fibres were mixed in a high-energy ball mill for 5 minutes with an addition of distilled water and polyvinyl alcohol as a separator, which prevents lumping of ceramic material at 1% by weight. Next, colloidal silica (LUDOX® AS 40) was added to the aforementioned mixture – binding at approx. 5% by weight and the following substances that increase porosity (5–40% by weight):
− Metacellulose (cz.),
− Sawdust,
− Triethanolamine (POCH, Ph.Eur.), and
− Polyvinyl alcohol (POCH).

The material prepared in this manner was mixed once again in the ball mill for 5 minutes. Dried mixtures were introduced into the casting mould installed in a hydraulic press, after which, with the use of a punch, they obtained the final shape (squeeze casting at different pressures 30, 50 and 100 MPa). A cylindrical

mould was used with a diameter of 48 mm. Preforms underwent the process of sintering at changeable temperatures: 900, 1100 and 1300°C for 2 hours in order to give them proper mechanical properties.

4. Results and discussion

Preforms with the range of porosity from 0% (solid ceramics) to 75% (sawdust) as the pore-creating agents were obtained. The participation of porosity achieved in given variants was measured in three ceramic samples. Significant scatter of porosity was observed in the examined material.

Table 1 presents process parameters for the fabrication of ceramic preforms and the obtained total and open porosity.

Table 1. Porosity of sintered ceramic preforms in relation to ceramic mixtures

No.	Initial material	Pore-creating agent	Content [% by weight]	Squeeze pressure [MPa]	Sintering temperature [°C]	Porosity [%]	Open porosity [%]
1.1	Al_2O_3 (0.1 +35 μ)	-	-	30	1100	18.3	7.5
1.2		-	-	50	1100	5.9	0
1.3		-	-	100	1100	2.1	0
2.1		methylocellulose	10	30	1100	31.2	28.6
2.2		methylocellulose	20	30	1100	47.7	43.9
2.3		methylocellulose	40	30	1100	57.3	55.9
3.1		sawdust	10	30	1100	26.2	24.3
3.2		sawdust	30	30	1100	63.5	62.5
3.3		sawdust	40	30	1100	76.1	75.8
4.1		triethanolamine	5	30	1100	23.7	20.9
4.2		triethanolamine	10	30	1100	29.5	25.2
4.3		triethanolamine	20	30	1100	Spalling	
5.1		polyvinyl alcohol	10	30	1100	After removing from the furnace preforms disintegrated	
5.2		polyvinyl alcohol	20	30	1100		
5.3		polyvinyl alcohol	40	30	1100		
6	Saffil®			30	1100	69.3	69.1
7	Al_2O_3 + Saffil®			30	1100	47.4	46.8

The highest quality of preforms was obtained with the application of sawdust as the addition (variation No. 3). The result is surprising, because burning sawdust produces gases and releases contamination, which may cause the degradation of the structure of preforms. Due to this fact, it was believed that methylocellulose, which is a purer material, would be better in the role of a pore-creating agent. Ceramic preforms in variation No. 3 were characteristic of open porosity contribution within the range from 24 to 75%. Figure 1 presents selected examples of achieved ceramic preforms. Both variation No. 1 (solid structure – porosity 0%), and variation No. 2 (big, lumped Al_2O_3 particles) disqualify the fabricated material to be infiltrated with liquid metal.
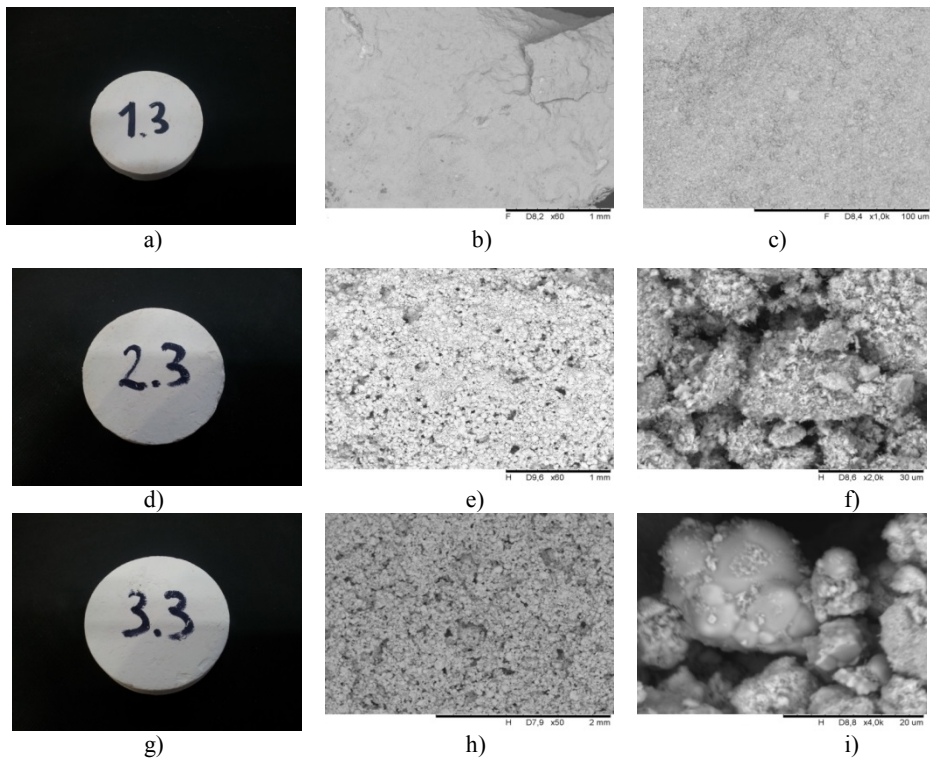
Fig. 1. Selected examples of fabricated ceramic preforms: a) preform made of solid ceramics, b) macrostructure, c) preform's microstructure, d) preform with 56% porosity contribution together with its: e) macro- and f) microstructure, g) variation 3.3 with 75% porosity contribution, h) macrostructure, i) preform's microstructure

Excellent effects were obtained with the use of continuous Saffil® fibres as ceramic material, which were cut and ground in the ball mill in order to reduce

their dimensions. The photograph of the preform, its macro- and microstructure is presented in Fig. 2.

Fabricated ceramic preforms in variation No. 6 are characteristic of an open porosity of 70%, with insignificant closed porosity (0.2%), which predestines them for squeeze infiltration attempts. Compressive strength tests were carried out for the fabricated preforms. The achieved results are presented in Table 2.

a)   b)   c)
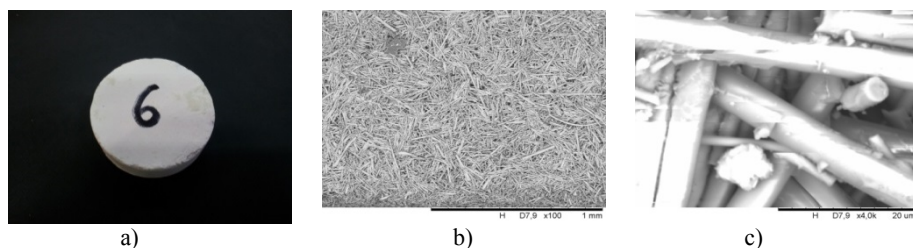
Fig. 2. A research variation of a fabricated ceramic preform made of cut Saffil®: a) a photograph of a solid ceramic preform, b) macrostructure, c) preform microstructure

Table 2. Comparison of compressive strength of selected ceramic preforms

Initial material	Pore-creating agent	Content [% by weight]	Open porosity [%]	Compressive strength [MPa]
Al_2O_3 (0.1 +35 μm)	methylocellulose	20	43.9	55
	methylocellulose	40	55.9	7.5
	sawdust	30	62.5	13.5
Saffil®	–	–	69.1	8.2
Al_2O_3 (0.1 +35 μm)	sawdust	40	75.8	2.4

5. Squeeze infiltration of fabricated ceramic preforms

For infiltration attempts preforms were selected with an open porosity contribution above 50%. The selected preforms underwent infiltration with liquid 7075 aluminium alloy. The preheated preforms were infiltrated with liquid metal with the use of "bottom" infiltration. The tests were made in a UBE VSC 500 hydraulic press. The external pressure was imposed directly on the liquid metal surface (*direct squeeze casting*) with the use of a piston. The pressure equalled 150 MPa, and time was 60 seconds. Figure 3 presents the microstructure of a composite casting fabricated with the use of the squeeze infiltration method of Saffil® fibres with aluminium alloy (7075) for mechanical working.
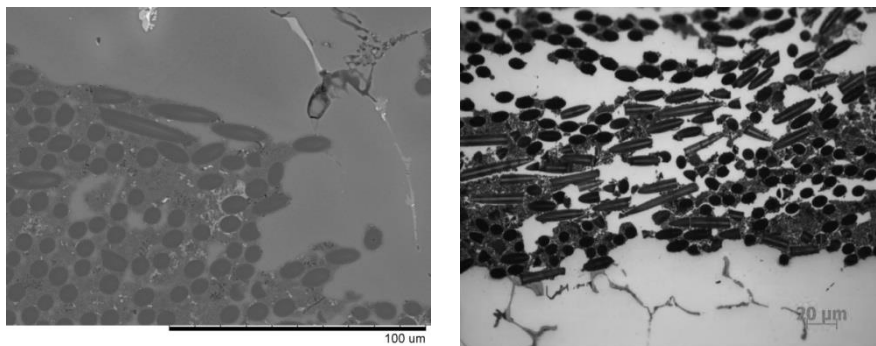
Fig. 3. Composite made of 7075 alloy infiltrated with continuous Saffil® fibre

Conclusions

1. Preforms made of powder ceramics (Al_2O_3) and Saffil® fibres were fabricated.
2. The achieved preforms were characteristic of open porosity within the range from 0 to 75%.
3. A significant impact of additions of pore-creating substances on the content of ceramic preforms was observed.
4. The best effects (the highest porosity and compressive strength) were achieved with the application of sawdust as the pore-creating substance.
5. The fabricated ceramic preforms are characteristic of differentiated compressive strength (from 2.4 to 55 MPa in variations with open porosity above 50%).
6. For the attempts of squeeze infiltration, preforms were used fabricated from Al_2O_3 powders with an addition of sawdust and methylocellulose (open porosity > 50%) and Saffil® fibres (70%).
7. The high efficiency of infiltrating preforms with liquid metal was proved.

References

1. Bai Y., Zhao H.: Tensile properties and fracture behavior of partial squeeze added slow shot die-cast A356 aluminum alloy. Materials and Design, 2010, Vol. 31, No. 9, pp. 4237–4243.

2. Abou El-khair M.T.: Microstructure characterization and tensile properties of squeeze-cast AlSiMg alloys. Materials Letters, 2005, Vol. 59, Nos. 8–9, pp. 894–900.
3. Sobczak J.: Theoretical and practical backgrounds of squeeze casting of non-ferrous metals, Transactions of the Foundry Research Institute, Special Issue 41, Krakow, 1993.
4. Reguła T., Dudek P.: Changes in the microstructure of PA9 alloy under the effect of squeeze pressure, Transactions of Foundry Research Institute, volume LII, Year 2012, number 4, doi: 10.7356/iod.2012.21.
5. Dudek P., Fajkiel A., Reguła T., Sobczak J.J.: Effect of applied pressure on the quality of squeeze cast parts made from AlSi9Mg alloy, Archives of Foundry Engineering, Katowice-Gliwice, tom 11, nr 12/3, s. 55–60.
6. Reguła T., Tchórz A., Darłak P., Sobczak J.J., Purgert R.M.: Computed tomography for quality assessment of composite castings made by pressure infiltration of porous performs. High-Resolution X-ray CT Symposium, Dresden 2010.

Porowate kształtki ceramiczne przeznaczone do lokalnego zbrojenia odlewów sposobem infiltracji ciśnieniowej

Słowa kluczowe

Kompozyty metalowo-ceramiczne, prasowanie w stanie ciekłym.

Streszczenie

Podjęto próbę uzyskania preform ceramicznych o różnym stopniu porowatości.

Przeprowadzono badania ich wytrzymałości na ściskanie w celu określenia możliwości ich zastosowania w procesie otrzymywania kompozytów metalowo--ceramicznych technologią prasowania w stanie ciekłym. Otrzymane preformy poddano infiltracji ciśnieniowej i otrzymano kompozyty o znacząco wyższych właściwościach wytrzymałościowych w stosunku do odlewów monolitycznych.

Zbigniew PAWELEC
Institute for Sustainable Technologies – National Research Institute, Radom
zbigniew.pawelec@itee.radom.pl
Mohammed BAKAR, Marcin KOSTRZEWA
University of Technology and Humanities, Radom
mbakar@wp.pl, m.kostrzewa@pr.radom.pl

SPECIALIZED POLYMER COMPOSITES INTENDED FOR THE REGENERATION OF MACHINE COMPONENTS

Key words

Epoxy resin, polyurethane, interpenetrating polymer networks, polymer composites, polymeric – regeneration, mechanical properties, wear, friction coefficient, guide systems for tool machines.

Abstract

Modern equipment and industrial machinery are characterized by advanced design that allows the implementation of complex manufacturing processes. The complexity of the machine construction results in the high cost of spare element replacements, and in many cases, their condition qualifies them for regeneration with the use of modern composite materials, which guarantee obtaining the required performance parameters of the regenerated element. This article presents the results of a study on the development of special, chemically cured, polymer composite, intended for the regeneration of items of machinery and equipment. The composites' matrix was a modified epoxy resin. Polyester resins and polyurethane were used as polymeric modifiers, which form penetrating

epoxy polymer networks with the matrix (IPN-Interpenetrating Polymer Network). Basic fillers of the composites were metallic powders with a specific chemical composition and granular size, and lubricants with anisotropic consistency. Performance characteristics were examined of the designed composites using modern testing apparatus. These polymer composites were applied for the regeneration of the surfaces of used elements. It was found that they ensure relevant performance features of the regenerated elements. Sample applications are also presented.

Introduction

Intensive use of machine parts causes the wear of involved components and is usually manifested by a change in geometric dimensions and damage to the surface. One of the solutions to the problem of refurbishing surface layers is using special composite materials that combine high wear resistance with a simplicity of the technological process of their application. In the recent years in particular, an important role has been played by composites based on a polymer matrix [1, 2, 3]. Performance requirements for modern composites have led to the dynamic development of research on the chemical modification of polymer matrix materials and to the development of innovative formulas for materials with high performance parameters, while ensuring low-cost repair of machinery elements resulting, in particular, from the maximum simplification of the regeneration technology. Such requirements are fulfilled by metal-polymer composites based on the matrix of epoxy resins, which have carefully selected powder and fibre fillers, as well as the modifiers of specified performance features. Epoxy resins are among the most versatile chemically cured polymer products with good performance and simple and convenient processing technology. However, after the cross-linking, they are stiff and brittle, which causes most of their major drawbacks: low resistance to impact and low strain at rupture. Low flexibility and rigid materials very easily produce internal stresses; therefore, the articles made of epoxy resin are prone to cracking during prolonged stress action. Improving these properties is the most common reason for the modification of epoxy materials with other polymers [4, 5, 6].

The modification of epoxy resin with polymers capable of creating spatial networks is an innovative way to improve its properties. The cross-linked polymer mixes are generally divided into physical and chemical. In the case of chemical mixtures, the polymers – as a result of cross-linking – form a common spatial network that is bound chemically. When the interaction between separate, but mutually penetrating polymer networks is only physical in nature, and there are no bindings across the network and these are interpenetrating polymer networks (IPN). Included in this category are also such systems in which only one component creates a spatial network and the other – of a linear structure – is woven among the cross-linked structure. These are called semi-IPN [7–10].

Interpenetrating polymer networks formed from two or more polymers are relatively new engineering materials, which can also be used as the polymer matrices for composite materials in special applications.

The aim of this study is to examine the effects of polymeric modifiers – polyurethane and polyester resin – on the properties of epoxy matrix and to develop specialized polymer composites for the regeneration of machine components, which should have good performance properties in a variety of technical applications.

1. The subject matter and research methods

The subject of this research was the compositions of epoxy resin Epidian 5 with polymer modifiers Polymeric Polimal 109 and 165, which are polyester resins. As a curing agent for unsaturated polyester resins, Luperox was applied, and the reaction accelerator was cobalt naphthenate. The second polymer modifier was Desmokap 12 polyurethane. The contents of the polymeric modifiers in epoxy matrix constituted 5, 10, and 15% of the weight. Samples for testing their mechanical properties were taken from the resulting compositions. The obtained compositions containing different amounts of modifiers were cross-linked using aliphatic polyamine (triethylenetetramine-Z-1) at room temperature for 24 hours, and then further cross-linked at a temperature of 80°C for three hours. After cross-linking, impact resistance was measured using the Charpy method and Zwick 5012 device according to PN-81/89 C-029 norm, and the 3-point flexural strength was measured using the Instron 5566 strength machine, according to PN-EN ISO 178: 2006 norm.

2. Test results

The testing results for the mechanical properties of the produced compositions are presented in Table 1. The obtained results indicate a strong influence of the type and weight participation of modifiers on the mechanical properties of polymeric epoxy resin.

The results indicate that the applied polymeric modifier significantly improves the mechanical properties of chemically cured epoxy resin. For the majority of tested compositions (with the exception of Polimal 109) which contain 10% of the polymeric impact resistance modifiers, the resistance to dynamic impact (impact strength) increased by about double compared to the unmodified resin. There was also far greater resistance to strain and strain in bending. The distinct increase in strength parameters, considering the lack of chemical bonds between epoxy resin and the applied polymer modifiers, may be due to the creation of the structure of interpenetrating polymer networks (IPN) with increased strength. To confirm this thesis and to examine the chemical composition of the obtained compositions, their infrared (FTIR) spectrum was

created. Comparing the FTIR spectrum of the compositions containing polymeric modifiers with an unmodified epoxy resin spectrum is shown in Fig. 1.

Table 1. The properties of epoxy resin composition with polymer modifiers (IPN)

No.	Composition symbol	Impact resistance [kJ/m2]	Stress [MPa]	Strain
		Unmodified Epidian 5 resin		
1	EPZ/0/0	1.4	53	0.020
		Epidian 5 – polymer modifier – Polimal 109		
2	EPZ/P109/5	1.3	89	0.033
3	EPZ/P109/10	2.7	93	0.037
4	EPZ/P109/15	1.8	98	0.033
		Epidian 5 – polymer modifier: Desmocap 12		
5	EPZ/D12/5	2.4	70	0.030
6	EPZ/D12/10	2.9	74	0.034
7	EPZ/D12/15	4.0	63	0.035
		Epidian 5 – polymer modifier, Polimal 150		
8	EPZ/P150/5	2.8	116	0.037
9	EPZ/P150/10	3.3	66	0.031
10	EPZ/P150/15	3.2	98	0.032
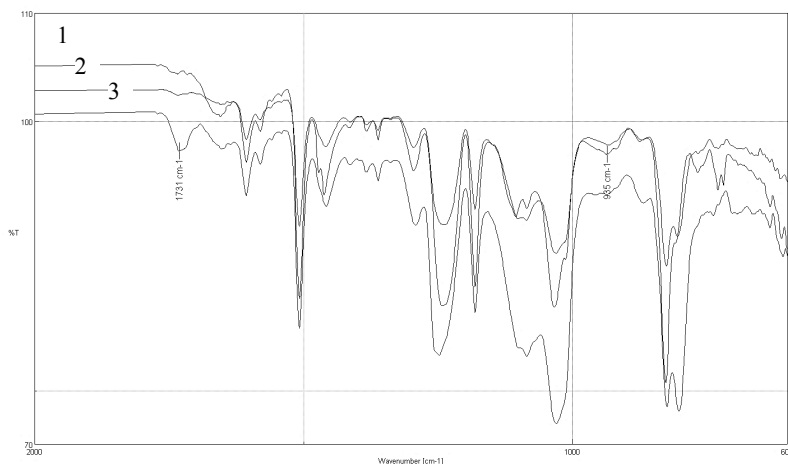
Fig. 1. FTIR spectra of epoxy resin (1), composition containing Desmokap 12 (2) and Polimal 109 (3)

Based on the FTIR spectra, it cannot be unequivocally concluded whether there are chemical reactions between the introduced modifiers and a matrix of epoxy resin. The comparable intensity of the peak characteristic for epoxy groups (935 cm^{-1}) for resin with Desmocap 12 and unmodified resin indicates that it does not affect the cross-linking process, and the composition is a mixture

of polymers with interpenetrating spatial networks without inter-network bonds. The lower intensity of the band for the epoxy group with the composition of Polimal (characteristic peaks for ester groups 1730 cm^{-1}) may be a confirmation of the creation of the IPN structure with cross-network bindings. Having adopted as criteria an improvement in resistance to dynamic impact, an increase in flexibility, larger contraction of polyester resins, and no need to use two types of curing agents and the accelerator, the epoxy composite polyurethane resin was selected as the matrix modified with Desmocap 12 in the amount of 10%. Above this value, there is a decrease in bending stress and a significant increase in viscosity of the composition, which prevented the introduction of optimum quantity of metallic fillers and solid lubricants during the process of developing a regenerative polymer composite.

3. Developing a polymer composite

The possibility of using polymer composite as regenerative materials is determined by appropriate strength, thermal, and tribological parameters, which depend on the fillers with a significant quantitative participation in the mass of the manufactured composite. Since the composite is designed to regenerate steel machinery, iron powders were selected with a specific chemical composition and granule size: iron Fe (type NC 100.24), Fe-Mn alloy, and Fe iron (type MT-212). Based on the images from electron microscope scanning (Fig. 2), it can be observed that they are diverse in terms of geometry. They are mostly irregular polyhedral shapes, showing differences in the size of the total contact surface of the filler with the polymer matrix, which can significantly affect the resultant effect of the mechanical strength of the final-result composite.

As a lubricant for reducing motion resistance and wear, flake graphite M15-99 has been used, and its microscopic image is presented in Figure 2d. The primary fibre filler for the composite is organic polyaramid fibre (Kevlar pulp type 1F651) shown in Fig. 2e.

Preliminary tests, experiments, and publication data formed the basis for setting the weight participation for basic metallic fillers at 300 parts by weight (pbw), for polyaramid fibres at 2 pbw, and lubricant additives at 10 pbw, for 100 parts by weight of the modified epoxy matrix. The production the composites consisted in exact mixing of the liquid matrix the fillers using a laboratory Z homogeniser. Since these composites are intended for regeneration layers in friction connections, it was necessary to examine other strength properties such as hardness, compressive strength affecting wear, pressure limits transferred in the friction node, and a very important parameter – the peel strength, which indirectly indicates layer adhesion of the regenerating polymer composite to metal substrate. These properties were studied based on the norms for plastics (PN-EN ISO 2039-1: 2004, PN-EN ISO 179-1: 2004, PN-EN ISO 604: 2004).

Table 2 shows the influence of metallic fillers on mechanical properties of regenerating polymeric composites.

a)   b)   c)

d)   e)
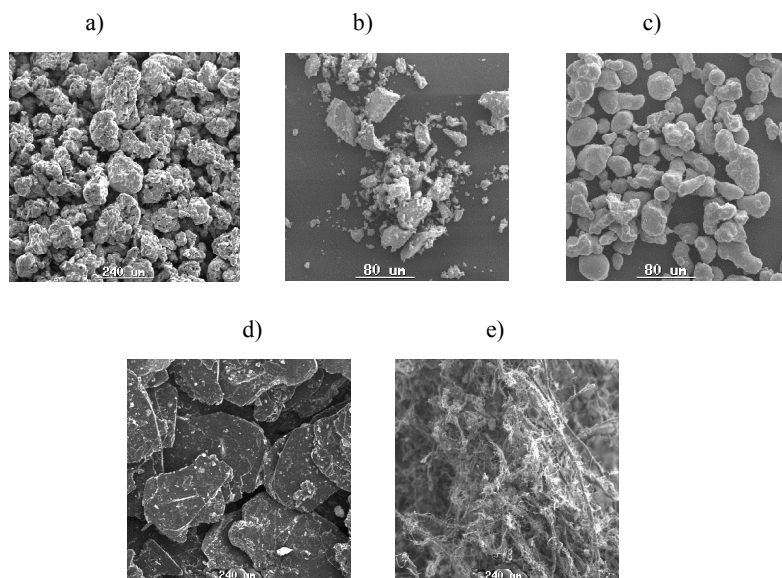
Fig. 2. Microscopic images of polymer composite fillers: a) iron powder Fe NC 100.24, b) powder iron-manganese Fe-Mn, c) iron powder Mt 212, d) graphite, e) aramid fibres

Table 2. Strength properties of polymeric composites

Type of metallic filler	Impact strength [kJ/m²]	Stress [MPa]	Strain	Hardness [MPa]	Compressive strength [MPa]	Peel strength [MPa]
Iron powder NC 100.24	4.2	78.6	0.022	254	105	19.2
Iron powder MT 212	3.1	62.2	0.016	222	89	18.4
Iron-manganese powder	3.2	63.5	0.016	239	100	22.0

The data presented in Table 2 indicates that the type of the applied metallic filler affects mechanical properties of composites. This effect is caused by filler morphology and its surface properties. The best results were obtained for the composite with iron powder NC 100.24, which it is characterized by the highest hardness, resistance to dynamic impact, high resistance to compression, and adhesion to a steel substrate. A comparison of microscopic images of fillers indicates that iron powder NC 100.24 has more irregular shapes and thus provides greater surface area than the other fillers. This makes it easier to

dampen the filler with the liquid matrix, and it increases the adhesion effects between the matrix and the filler.

Apart from mechanical properties, the key properties of polymer composites that determine their applicability in regeneration of worn machine components as a result of friction are tribological properties. The composite selected for the wear and friction in depth testing was the composite with a modified epoxy resin matrix and with metallic iron powder filler – NC 100.24. To determine the tribological characteristics, the T-05 tester was used with roll--and-block in staggered contact. A model friction node of this device is a representation of a sliding bearing. Figure 3 shows an example of a temperature change process and a friction coefficient of composite contact: polymer – bearing alloy (bronze).
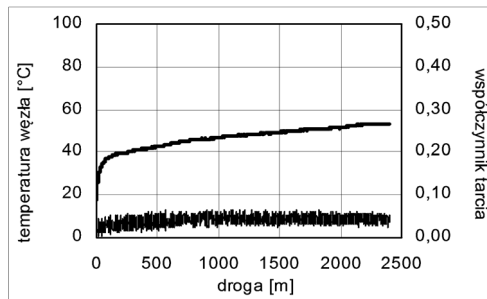

Fig. 3. An example of temperature change process and the friction coefficient of the polymer – bearing alloy (p = 3 MPa, v = 0.3 m/s) contact
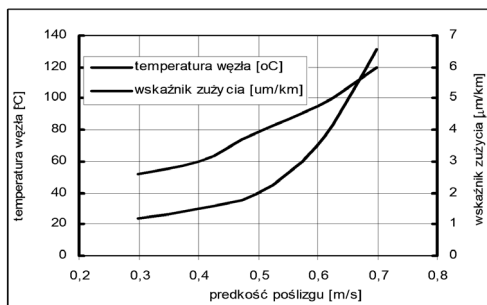

Fig. 4. The relationship between wear indicator and the temperature of the node on the one hand, and the sliding velocity on the other, for the composite – bearing alloy contact, for pressure 3 MPa

The obtained results in the friction coefficient and temperature changes in the friction node for the polymer composite-bronze contact show a monotonic process throughout the entire range of the friction path. This shows stable friction cooperation and a low motion resistance in the developed polymer

composite with the bearing alloy. Figure 4 shows the influence of rubbing velocity on the wear and the temperature indicator of the polymer composite-bronze contact. This indicates that with a rubbing velocity of up to 0.5 m/s, the wear indicator changes are small. A noticeable increase of this parameter can be observed for velocities above 0.5 m/s, and the increase of rubbing velocity by about 0.2 m/s doubles the increase of this parameter. It is related to a significant increase in the temperature in the contact area and the thermal destruction of the polymer composite.

4. Examples of applications

Due to the ease of forming and coating the surfaces of different configurations, high strength characteristics and adhesion to metal substrates, the specialised polymeric composites have been used in many technical applications. They are used, for example, for the regeneration of the roller bearing pins and slide bearing pins (Fig. 5a) while maintaining certain restrictions on the values of load and rubbing velocity.

a)

b)

c)

d)
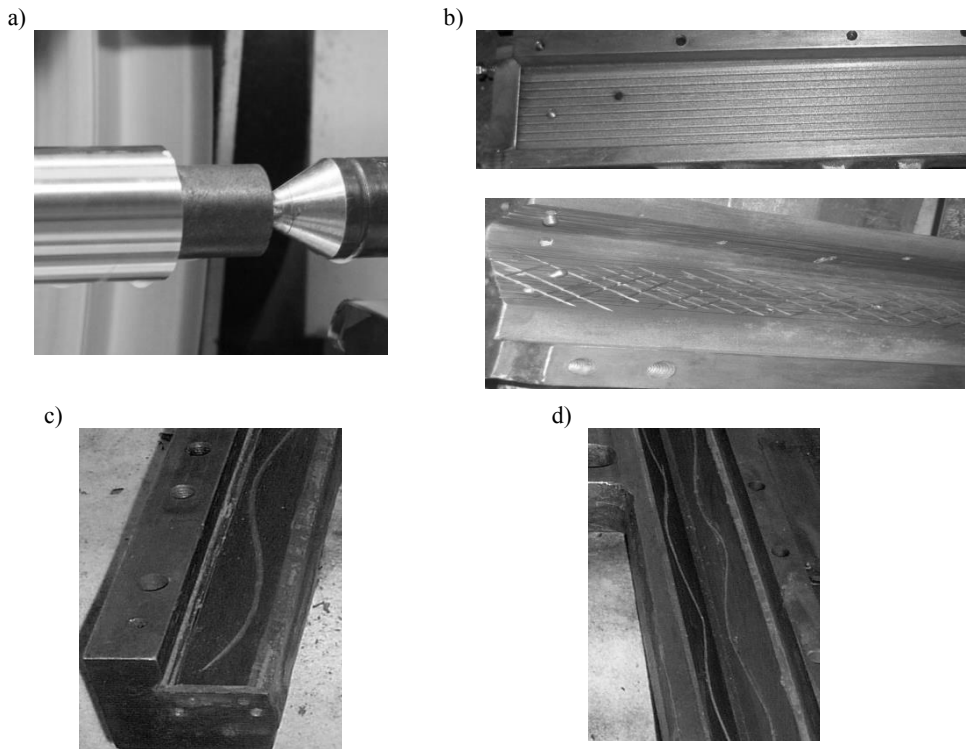
Fig. 5. Finishing machining slide bearing pin (a), machine tool guide with lengthwise and crosswise scoring prepared for regeneration of (b), composite polymer regenerated flat guides (c), triangular guides (d) with lubrication grooves

Due to a lower static friction coefficient in comparison to steel and a minimum tendency for the stick-slip effect (self-excited frictional oscillation), the composite-steel contact is widely used for the regeneration of guide systems for cutting machines (Figs. 5 b, c, d). A valuable advantage of this regeneration process is its uncomplicated technology, using an imaging method independent of the geometric accuracy of the guides. The final stage of the regeneration process is making lubrication grooves.

Summary

The interpenetrating polymer networks (IPN) composed of two polymers – epoxy resin and polyurethane – used as a matrix have made it possible to create a specialized polymer composite with satisfactory performance parameters. This polymer composite may act as a surface layer for different types of friction contacts. It is characterized by good mechanical, heat, and tribological properties. The universal properties of the specialised polymer composite are such that it can be used to regenerate not only the lubrication elements of slide bearings, but also used in friction contacts of different materials working in the conditions of boundary friction (machine tool guides). Moreover, another positive feature of this method is the ease of the process of regeneration and the possibility to carry it out without the need for a complicated and energy-consuming apparatus, as is the case in galvanising or welding.

References

1. Mazurkiewicz A.: Technological innovations for sustainable development. ITeE – PIB, Radom 2009.
2. Fomin V.N., Malyukova E.B., Berlin A.A.: Criteria for optimalization of processing and fabrication of polymer composite materials. Doklady Chemistry, 2004, 394, 2, pp. 39–41.
3. Kozlov H.V., Burya O.I., Aloev V.Z.: Application of fractal fracture mechanics to polymer and polymeric composites. Materials Sci., 2004, 40, 4, pp. 491–496.
4. Ping-Hua Wang, Yuen-Zhu Wu, Qing-Ren Zhu: Polymer metal composite particles: polymer core and metal shell. J. Mater. Sci., 2002, 21, pp. 1825–1828.
5. Czub P., Bończa-Tomaszewski Z., Penczek P., Pielichowski J.: Chemia i technologia żywic epoksydowych, WNT, Warszawa 2002.
6. Pokropski T., Balas A.: Żywice epoksydowe i poliuretany – wzajemne oddziaływanie modyfikujące. Polimery, 2003, 48, s. 591–597.

7.   Anzlovar A., Zigon M.: Semi-interpenetrating polymer networks with varying mass ratios of functional urethane and methacrylate prepolymers. Acta Chim. Slov. 2005, 52, s. 230–237.

8.   Park S.J., Jin J.S.: Energetic studies on epoxy–polyurethane interpenetrating polymer networks. Journal of Applied Polymer Science 2001, 82, pp. 775–780.

9.   Ong S., Ismail J., Abu Bakar M., Rahman I.A., Sipaut C.S., Chee C.K.: Polyurethane-modified epoxy resin: Solventless preparation and properties. Journal of Applied Polymer Science 2009, 111, pp. 3094–3103.

10.   Harani H., Fellahi S., Bakar M.: Toughening of epoxy resins using synthesized polyurethane prepolymer based on hydroxyl terminated polyesters. Journal of Applied Polymer Science, 1998, 70, pp. 2603–2618.

Specjalistyczne kompozyty polimerowe przeznaczone do regeneracji elementów maszyn

Słowa kluczowe

Żywica epoksydowa, poliuretan, przenikające sieci polimerowe, kompozyty polimerowe, regeneracja, właściwości mechaniczne, zużycie, współczynnik tarcia, układy prowadnicowe obrabiarek.

Streszczenie

Współczesne urządzenia i maszyny przemysłowe charakteryzują się zaawansowaną konstrukcją, która pozwala na realizację skomplikowanych procesów wytwórczych. Złożoność konstrukcyjna maszyn powoduje wysokie koszty wymiany zużytych elementów, jednak w wielu przypadkach ich stan pozwala na regenerację z wykorzystaniem nowoczesnych materiałów kompozytowych gwarantujących uzyskanie odpowiednich parametrów użytkowych zregenerowanego elementu. W artykule przedstawiono wyniki prac nad opracowaniem specjalnych chemoutwardzalnych kompozytów polimerowych przeznaczonych do regeneracji elementów maszyn i urządzeń. Osnowę kompozytów stanowiła modyfikowana żywica epoksydowa. Jako modyfikatory polimeryczne zastosowano żywice poliestrowe oraz poliuretan, które tworzą z osnową epoksydową przenikające sieci polimerowe (IPN – *Interpenetrating Polymer Network*). Podstawowymi napełniaczami kompozytów były proszki metaliczne o określonym składzie chemicznym i granulometrycznym oraz smary stałe o spójności anizotropowej. Zbadano właściwości eksploatacyjne opracowanych kompozytów z wykorzystaniem nowoczesnej aparatury badawczej. Opracowane kompozyty polimerowe zastosowano do regeneracji warstw wierzchnich zużytych elementów. Stwierdzono, że gwarantują one uzyskanie odpowiednich właściwości użytkowych zregenerowanych elementów. Omówiono przykładowe aplikacje.

Jacek WOJUTYŃSKI

Institute for Sustainable Technologies – National Research Institute, Radom
jacek.wojutynski@itee.radom.pl

MONITORING THE CONSUMPTION OF ENERGY MEDIA IN TECHNICAL DEVICES

Key words

Electricity, gas flow controller, water consumption.

Abstract

The knowledge about and optimisation of the consumption of energy and technical media is an important issue in the maintenance of technical objects and technical plants. In ITeE – PIB, newly designed devices are equipped with systems for monitoring the consumption of electricity and other media. Applied measurement systems allow the assessment of the cost of research or the conducted process. In the case of a three-phase power supply, the devices that operate alternately can be used equally. The article presents the developed subsystems for monitoring the electricity consumption as well as water and compressed air consumption for nitriding, server room operation, a device for cooling water in a closed circuit, compressor room operation, and a fumigation chamber. Information from the measurement systems can also be used to diagnose the condition of the equipment.

Introduction

Monitoring energy and technology media consumption in devices have been developed in ITeE – PIB. The first operation for which the monitoring equipment has been installed for the consumption of the media was for gas nitriding [1]. In process for gas nitriding the following devices were installed:

- Electricity meters for single and triple phase were installed for the nitriding furnace, neutralisator, dissociator, and water cooling system. The applied electricity meters had mechanical counter and pulse output (1000 pulses/ /1 kWh of electricity), which is connected to the counters in the PLC program. With this approach, we are able to determine the consumption of electricity, from the beginning of the operation of the device or for a given period, e.g. a month or week, or during a process.
- Gas mass flow controllers (N_2, NH_3 i NH_3^+) provide the actual flow of gas in dm^3/h. The controller has an input signal representing the set value (SV) and the output representing the resulting flow (PV) – 4–20 mA standard. Software implemented in the PLC used a totalizer with a reading of flow every 30 seconds. We have precise information on the amount of nitrogen and ammonia consumed in the process. In addition, if the resulting flow is not equal to the set value with the desired accuracy, it generates diagnostic information, e.g., a lack of gas supply, damaged valves, or a pressure increase in the output of the regulator.
- Water flow meters were installed with pulse transmitters in the apparatus for cooling the water in a closed circuit, which supplies water to cool the cover of the retort of the nitriding furnace [2]. Encoders are connected to the inputs of the PLC. Software counters implemented in the controller determine the amount of water used in the process. In addition, when the pump is switched on and there is no pulse from the water meter at a specified time, a signal is generated to indicate a leak in the duct, blocking of flow, etc.

As shown on the example of the nitriding furnace, monitoring the media consumption in devices also provides valuable diagnostic information. Currently, for monitoring the power and technological media consumption, newer technical devices are used as follows:

- Measurement of electricity: The counters with pulse output were still used in cheaper and simpler solutions. The new solutions are N43 meters for the 3-phase network parameter measurements or the 1-phase type N27P from Lumel [4]. A meter with Modbus RTU protocol is usually selected. This simplifies the inclusion of meters into the media monitoring system. The information obtained from these analysers greatly exceed the needs for diagnosing the technical equipment (phase voltage, phase-to-phase voltage, phase current, powers: active, reactive, apparent, active power factor, tan φ, the angle φ, active energy fed back and charged, capacitive and inductive reactive energy, apparent energy, frequency, jitter, etc.).

- Measurement of gas flow: Bronkhost's mass regulators were used (there are also versions for selected liquid).
- Compressed air measuring and filter stations were from Festo or SMC, for example.
- Water: We still used water meters with pulse outputs or remote reading.
- As an extension of media monitoring, vibration was measured in the technical devices (vibration sensor with 4–20 mA output and relay output).

The media monitoring system and technological power were connected directly in the control-measurement system of the technical device or monitoring system, which was designed as a standalone system with a PLC included in the control-measurement system via Modbus RTU or a controller with its own network ID – Modbus TCP Client / Server.

1. An apparatus for cooling water in a closed loop

Figure 1 shows the developed CW-1 device for cooling the water in the closed loop [2]. It was constructed for the purpose of cooling the seal of the retort of the nitriding furnace [1]. The device worked flawlessly for a period of approx. 4 years. Throughout the lifetime, there was no need to supplement the water in the tank. The UV lamp used for the disinfection of water has caused the water to be clear and free of odours. The upgraded water-cooling device in a closed loop was made for ELKAT.

The control-measurement system is a stand-alone device, with the external control system for the gas nitriding system working as a Modbus Slave RTU controller. The information provided are the cooling water temperature, operating states of sensors and actuators, states of emergency, and the actual consumption of water and electricity (Fig. 1b). The water level sensor protects the circulation pumps against dry run.

The operation algorithms are as follows:
- The process of maintaining the temperature in a given range is accomplished through the plate heat exchanger of the chiller (AGR). The circulation pump in the duct of the unit also provides mixing of water in the tank (1).
- When the unit is not operating, the circuit with a UV lamp is started in cycles of 45 minutes with a 15-minute exposure to UV.
- Pump circuits (3) and (4) provide cooling of the seals in the nitriding furnace.
- When the pump is turned on and after a certain time there is no change in the encoder of the water meter, an alarm is generated.

The control-measuring system was developed based on a FC5A-D16RS1 controller and HG1F touch screen operator panel.
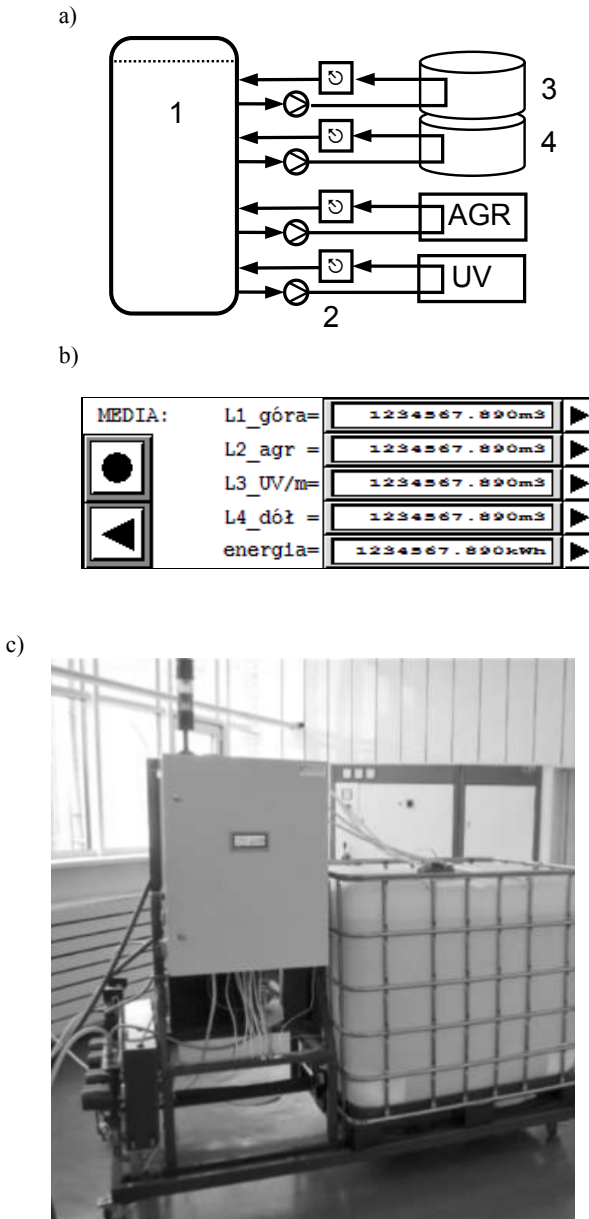
Fig. 1. CW-1 device for cooling the water in a closed system [2]: a) block diagram, b) screen of operator's panel, c) implementation of the device; 1) reservoir with a capacity of 1 m^3 of water with a level sensor and temperature sensor, 2) Circulation pumps with water meter and pulse outputs, 3) retort lid cooling circuit, 4) furnace retort seal cooling circuit, AGR – chiller with plate heat exchanger, UV – circuit with UV lamp for disinfecting water

Additional software counters operating per second report the operation time of the device, the operation time of each pump, the operating time of UV lamp and the chiller, and the number and type of alarms. It is a valuable source of diagnostic information.

2. Monitoring the media in the pressure chamber

The pressure chamber is intended as a fumigation chamber (Fig. 2a) for the preservation of wood, paper, and fabric in anaerobic atmospheres of low oxygen content at a level not exceeding 1%, with a high proportion of non-reactive gas, greater than 99%. The chamber allows the atmosphere to produce high levels of nitrogen and argon, vacuum forming, measuring the oxygen content, and temperature and humidity regulation [3].

Media consumption monitoring fumigation chamber includes the following:

- Monitoring of gas consumption: The selected gases are kept inside the chamber in hyperpressure by the control-measurement system. The chambers are connected to two cylinders of nitrogen and two cylinders of argon, operating in the ramp system (Fig. 2d). When the gas pressure in the first cylinder is low, it is automatically switched to the second cylinder. There is no need to control the amount of gas consumption.
- Measurement of the electricity consumption of the entire chamber is accomplished by a 3-phase meter (Fig. 2b), and the energy consumption of the lubricant-free compressor is measured by a 1-phase meter.
- Measurement of the operation time of vacuum pumps: Software counters count the time of operation of the pumps and after exceeding the time of 2000h and report the need to replace oil.

Just as in the device CW-1, additional software counters report the operation time of the device, the operation time of each pump and solenoid valves, and the number and type of alarms. Diagnostics of the sensors is provided by analogue input and output modules of the PLC controller,[1] and they allow easy conversion of analogue measured values into "engineering units" without writing software. The control-measurement system was developed based on a FC5A-D12S1E controller with built-in webserver and a HG3F multimedia touch screen operator panel. These devices work on an Ethernet network. It is possible to remotely access them through a web interface.


[1] Macro command of ANST controller.

a)
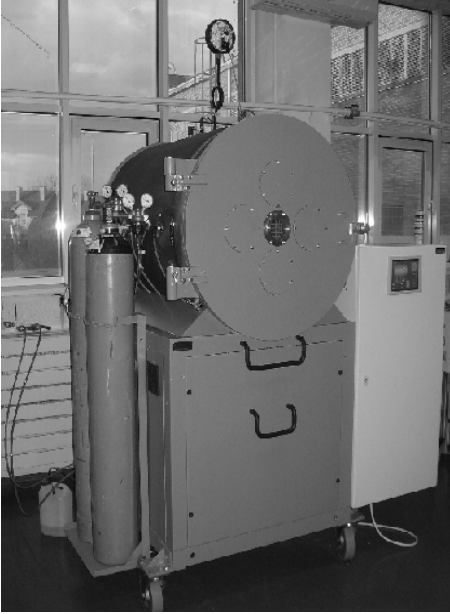
b)
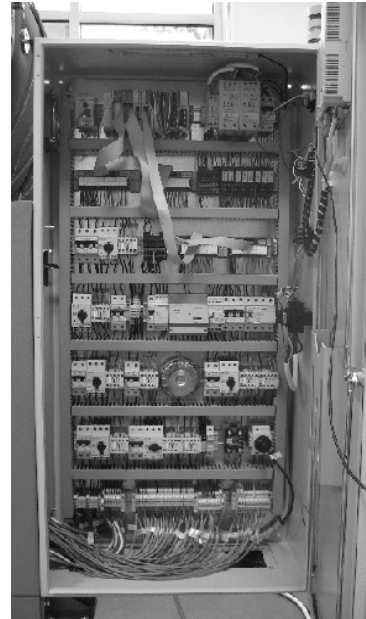
c)

d)
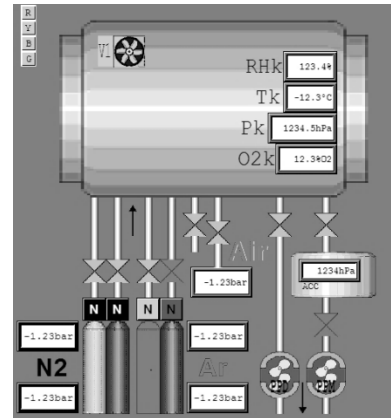
Fig. 2. Fumigation chamber: a) Realized chamber, b) The control-measurement system of the chamber – in the middle the 3-phase electricity meter, c) A view of the touch operator panel, d) Fragment of a monitoring screen for cylinders and vacuum pumps

3. Monitoring the electricity consumption

To monitor the electricity consumption, three, three-phase N43 meters were used that operate on the Modbus RTU with a dedicated RS485 port, where one

measures the electricity consumption of the cabinet with PLC and actuators, and two measure the power consumption of the 47kW furnaces. The N43 meters were used with inputs for direct measurement of current up to 63A (Fig. 3a). The operator panel displays basic information about the voltages, currents, and powers.

a)
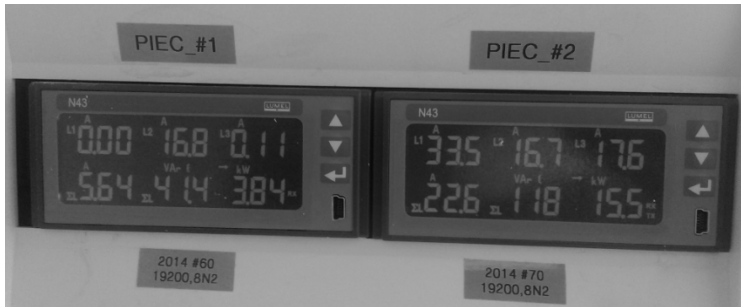
b)   c)

Fig. 3. Measurement of electric energy: a) N43 meters in electric furnaces, b) Operator panel with key data from N43 meters c) Operator panel with details of energy consumption for each phase

The PLC operators' panels operate through a local Ethernet network, and all of them can be accessed remotely in the Institute network or outside. Built-in panel software allows remote control of temperatures as if the operator was physically at the HMI panel. In addition, the PLC has an implemented Modbus TCP Server. This facilitates the development of monitoring software.

Summary

Modern hardware electricity metering devices allow programming the electricity consumption for the various phases. Therefore, by switching, the individual lines can be loaded evenly. Increased energy consumption or no consumption is an information supplied to check the status of the power systems of the device.

Monitoring the energy and technology media consumption in devices and software control of the operation time and the number of events are important information about the status of the unit. Analogue modules of the PLC provide diagnostic information about the status of the analogue circuits – no power supply and tract initialization, exceeding the parameters, breaking the current loop, etc. This information from the measuring systems can also be used to diagnose the condition of the equipment.

Currently, the price of media consumption monitoring devices is a fraction of the cost of the entire device. Information about operation times of components, the number of failures, etc. are valuable information about the operation of technical objects and technological lines. Newly designed devices at ITeE – PIB are, by standard, equipped with monitoring software.

References

1. Control system for gas nitriding processes
   http://katalog.itee.radom.pl/images/stories/karty/51.system_ang.pdf
   accessed 20.02.2015.
2. CW-1 cooling device for closed circuits
   http://katalog.itee.radom.pl/images/stories/karty/72.urzadzenie_ang.pdf
   accessed 20.02.2015.
3. KCF-3 pressure chamber
   http://katalog.itee.radom.pl/images/stories/karty/96.komora_ang.pdf
   accessed 20.02.2015.
4. Katalogue cards for N27P and N43 www.lumel.com.pl accessed 20.02.2015.

Monitorowanie zużycia mediów energetycznych w urządzeniach technicznych

Słowa kluczowe

Energia elektryczna, regulator przepływu gazów, zużycie wody.

Streszczenie

Znajomość i optymalizacja zużycia mediów energetycznych i technologicznych jest ważnym zagadaniem w eksploatacji obiektów technicznych i linii technologicznych. W ITeE – PIB w nowo projektowanych urządzeniach są stosowane urządzenia do monitorowania zużycia energii elektrycznej, a także innych mediów. Zastosowane systemy pomiarowe pozwalają na ocenę kosztu realizowanego badania lub procesu technologicznego. W przypadku zasilania trójfazowego możemy równomiernie wykorzystać urządzenia, które pracują naprzemiennie. W artykule zaprezentowano zrealizowane podsystemy monitorowania zużycia energii elektrycznej, wody i sprężonego powietrza w linii do azotowania, serwerowni, urządzeniu do schładzania wody w obiegu zamkniętym, sprężarce, w komorze fumigacyjnej. Informacje z układów pomiarowych można także wykorzystać do diagnozowania stanu urządzeń.

Robert SOŁTYSIAK
University of Technology and Life Sciences, Faculty of Mechanical Engineering, Bydgoszcz
robert.soltysiak@utp.edu.pl

THE EFFECT OF LASER WELDING PARAMETERS OF DUPLEX STEEL ON FATIGUE LIFE OF JOINTS WITHOUT GEOMETRIC NOTCH IN THE FORM OF FACE AND ROOT

Key words

Laser welding, fatigue life, duplex steel, stainless steel, welding parameters.

Abstract

A geometrical and a structural notch effect have the main influence on the local stress and strain concentration in the welded joints. These factors have a significant influence on the fatigue life of welded joints. This paper presents the results of the fatigue life tests of laser-welded joints of DUPLEX 2205 steel, taking into account the structural notch. The geometric notch in the form of face and root was removed. The Nd-YAG disk laser was used to weld butt joints. The welding process was conducted using two different parameters of welding without using additional material. The parameters were chosen based on previous studies (according to PN-EN ISO 15614-11:2005).

In the study of the fatigue life of laser-welded joints, the geometric notch was ground out. Based on this research, the effect of welding parameters on the fatigue life was not observed. The fatigue cracks initiation and propagation occurred in the base materials in all cases. In addition, the results of the fatigue life of welded joints were related to the fatigue life of the samples taken from the parent material.

Introduction

The progress in materials engineering and welding engineering leads to the creation of new materials and joining techniques [1, 2, 3]. A growing number of new material joining technologies used in practice results in the fatigue life/strength of welds being similar to that of the parent material. The difference in the fatigue life/strength arises from various heterogeneities in the material relating to the geometric and structural notches (caused by, e.g., other temperature processes occurring during the welding), which frequently lead to the local variation of deformations and hence fatigue cracks [4].

One of the relatively new joining methods being more and more frequently used in the industry is laser welding. When compared to the conventional welding methods, the laser welding shows high efficiency and precision. Laser welding allows deep fusion penetration with relatively small dimensions of the weld area (W) and, in particular, the heat-affected zone (HAZ), low heat input, short cycle time, and good cosmetic welds [5, 6]. In addition, a proper selection of welding parameters results in a close-grained structure. Both the narrow HAZ and the close-grained structure have a positive impact on the strength of the weld, particularly in case of time-varying loads [4].

The advantages of the laser welding influence its use in joining various types of structural materials such as corrosion-resistant DUPLEX (DSS) steel. DSS is a dual phase steel of austenitic-ferritic structure. It combines relatively high strength and hardness with good corrosion resistance, being higher than that of the most of the standard austenitic steel grades [7].

DUPLEX steel grades are considered to be readily weldable, e.g. using conventional welding techniques [8, 9] and friction stir welding (FSW) [10]. According to the literature [7, 11], the maintenance of an optimum relation between the corrosion resistance and the strength of welds may be achieved when maintaining the approximate 50/50 ratio between the ferrite and the austenite phases. However, no results have been found for fatigue tests of laser-welded joints in DUPLEX steel.

Based on the previous tests in the selection of DUPLEX 2205 steel welding parameters, sixteen welds were made using various laser-welding parameters. Based on the tests carried out in accordance with the standard [12], two of the best parameters were selected. Then the welded joints made within these parameters were subjected to fatigue tests. This research is a continuation of the studies included in [4]. The study was extended by fatigue tests of welded joints without a geometric notch in the form of face and root. The fatigue tests were related to the fatigue test results of samples taken from the parent material. The results were analysed and the conclusions were drawn.

1. Research object

DUPLEX 2205 steel (X2CrNiMoN22-5-3 according to PN-EN 10027-1:2007) was used for testing. The chemical composition of the material is presented in Table 1. The properties observed during the monotonic tensile test are presented in Table 2.

Table 1. Chemical composition [4]

C [%]	Si [%]	Mn [%]	P [%]	S [%]	Cr [%]	Mo [%]	Ni [%]	Cu [%]	W [%]
0.0222	0.4831	1.5458	0.02096	<0.005	23.946	3.2478	5.3388	0.24302	0.02712

Table 2. Monotonic tensile test properties [4]

R_m [MPa]	$R_{p0.2}$ [MPa]	A_{20} [%]
797	611	35.65

The joints were made by laser welding with no filler, using Trumpf TrueLaser Robot 5020. The welding process and the steel sheet pressing method are presented in Figure 1. Both joints, (P_02 and P_11), were made using the beam of 2 kW. The welding speed used for P_02 joint was 0.1 [m/min] higher than that used for P_11 joint. The laser beam for P_02 joint was focused on the surface of the material being welded while that for P_11 joint was focused in the centre of the sheet. Argon was used as shielding gas, and it was supplied from the top surface of the sheet at the rate of 15 or 20 l/min. The laser welding parameters are listed in Table 3.
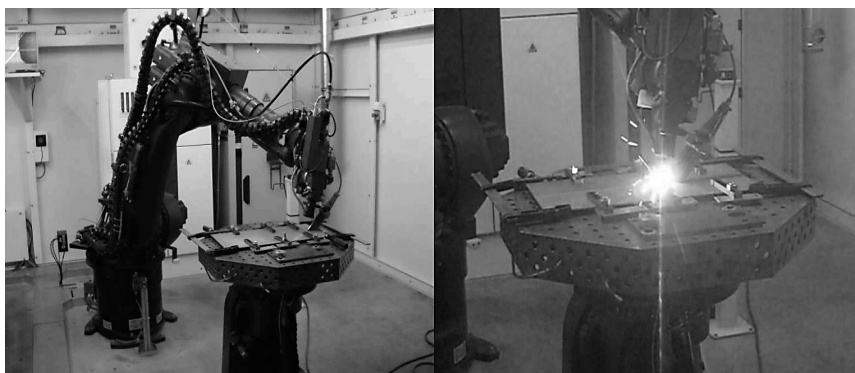

Fig. 1. Laser welding process on Trumpf TrueLaser Robot 5020 including sheet pressing system [4]

Table 3. Laser welding parameters [4]

	Power [kW]	Rate [m/min]	Focus distances of sheet metal surface [mm]	Shielding gas: argon [l/min]
P_02/G_02	2	0.5	0	15
P_11/G_11	2	0.4	-2	20

Despite minor differences in the welding parameters, the macrostructure pictures of the cross-sectional area of the P_02 and the P_11 joints show the differences in the weld shape (Fig. 2). There was observed a clear impact of the laser beam focal distance setting against the sheet surface on the weld shape. The weld width for the P_11 joint is practically constant between the top edge and the central part of the sheet. This is related to the laser beam focus setting in the central part of the sheet.
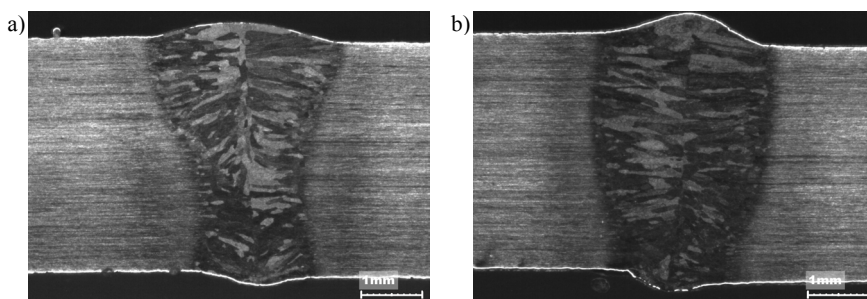

Fig. 2. Macrostructure pictures of joints: a) P_02 and b) P_11 [4]

2. Samples and research program

The tests were conducted at the accredited Institute Laboratory for Material and Structure Testing. The fatigue tests were carried out using an INSTRON 8501 hydraulic machine with controlled stress. Variable sine-wave loads were used with a constant stress amplitude, cycle asymmetry $R = -1$, and a frequency of from 1 to 10 Hz depending on the stress level. The tests were conducted on three stress levels for which the stress amplitude was 488.80, 403.26, and 336.05 MPa, respectively.

Three sample types were prepared for testing. Specimens of the first type were taken from a 4 mm thick sheet before welding (parent material – P_00). The next ones were taken from the welded joints with parameters listed in Table 3. A geometric notch in the form of face and root were ground out after welding. The samples after grinding were marked G_02 and G_11 for welding parameters P_02 and P_11, respectively. The test samples were made according to the dimensions presented in Fig. 3. The samples with the welds were made so that the load direction was perpendicular to the weld bead.
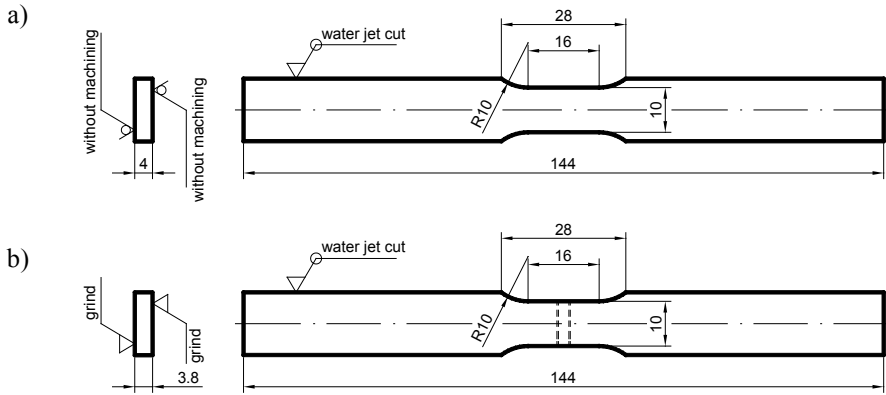
Fig. 3. Fatigue test sample taken from: a) parent material (P_00), b) welded plates after grinding the face and root of the weld (G_02 and G_11)
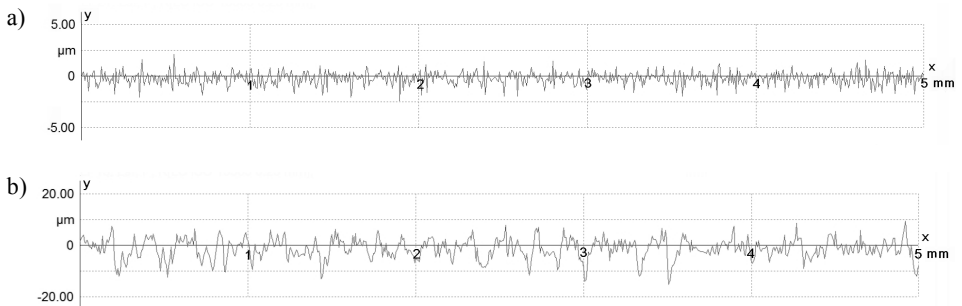

Fig 4.   An exemplary distribution of profile deviation y [m] from average line x for ground (a) and water jet cut (b) surfaces

The roughness measurement was carried out after the grinding and water jet-cutting processes. Measurements have been performed on the MarSurf GD 120 equipment. Among other things, the arithmetic average of the absolute values (R_a) was determined. The R_a parameters were 0.49 μm for ground surface and 2.9 μm for the water jet cut surface. An exemplary distribution of profile deviation y [m] from average line x (for elemental section x = 5 mm) for ground and water jet cut surfaces are shown in Figures 4a and 4b, respectively.

3. Research results

The number of cycles to be destroyed was recorded during the tests. Complete failure of the test sample was adopted as a fatigue failure criterion. The results of the fatigue life for samples taken from the P_00 parent material

and for the grinding samples (G_02 and G_11) taken from the P_02 and P_11 joints are specified in Fig. 5. The crack initiation and propagation occurred in the parent material in all tested samples.
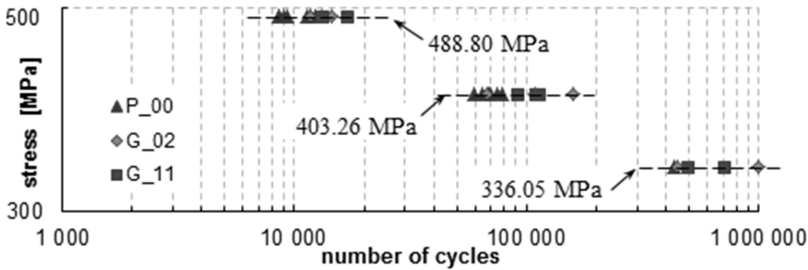

Fig. 5. Fatigue life results for the stress amplitude levels of 488.80, 403.26, and 336.05 MPa

Additionally, the strain and stress amplitudes were recorded during the testing, which made it possible to determine the hysteresis loop for the individual cycles at the respective stress level. Examples of the hysteresis loops for half of the fatigue life are presented in Figure 6. These hysteresis loops were taken from the 488.80 MPa stress amplitude level.
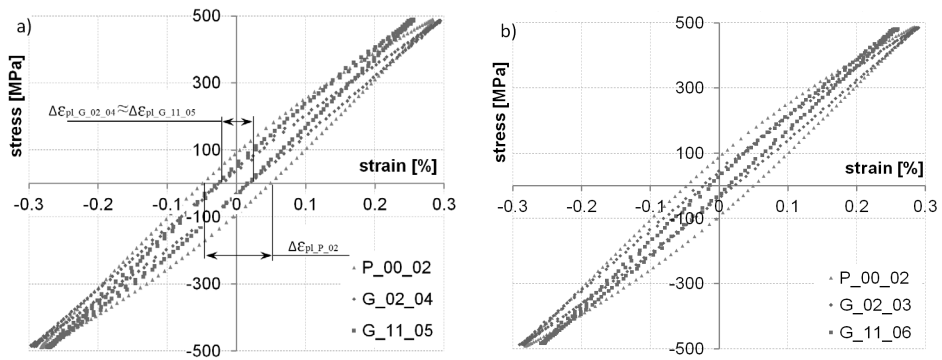

Fig. 6. Examples of hysteresis loops for half of the fatigue life for the stress amplitude level of 488.40 MPa for different samples a) P_00_02, G_02_04, G_11_05 and b) P_00_02, G_02_03, G_11_06

The strain was measured using an extensometer with gauge length of 12.5 mm. The weld zone, heat affected zone, and parent material were in the area of gauge length. The heterogeneity of the structure formed during the laser welding process caused differences in the shape of the analysed hysteresis loops (Fig. 6). The total strain range in comparison to the base material decreased in the case of the loop of G_11 and slightly increased in the case of the loop of

G_02. The plastic strain ranges (Fig. 6) were comparable for samples made with various welding parameters ($\Delta\varepsilon_{pl\_G\_02} \approx \Delta\varepsilon_{pl\_G\_11}$); however, they were significantly lower than the range of strain determined for samples of the parent material ($\Delta\varepsilon_{pl\_P\_00}$).

4. Research analysis

The statistical analysis was carried out based on the fatigue test results. To this end, the least squares method was applied and the fatigue life results were described in the log-log graphs in the form of a straight line. Considering the fact that the fatigue cracks of ground welded samples of G_02 and G_11 occurred in the base material, the results were described using one line. The effect was the square of the correlation coefficient $R^2 = 0.9872$ for the results obtained for the P_00 parent material and $R^2 = 0.9698$ for the results of the ground welded samples of G_02 and G_11 (Fig. 7).
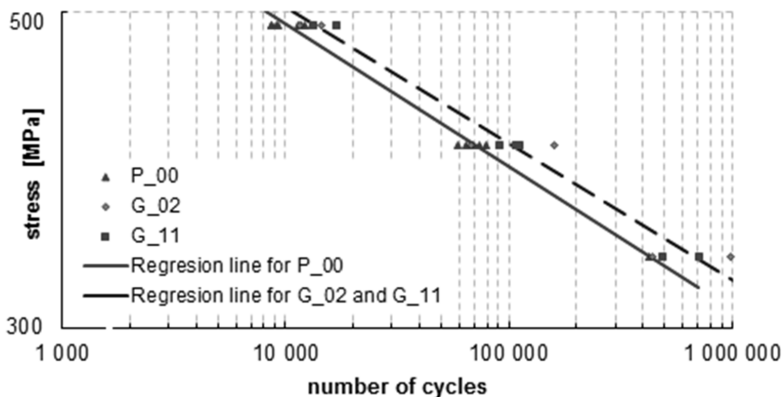

Fig. 7. Statistical results of the fatigue tests of parent material samples (P_00) and ground welded samples (G_02 and G_11)

For the parent material samples (P_00) and ground welded samples (G_02 and G_11), the fatigue category was determined based on the statistical results of fatigue tests (Fig. 7). According to Eurocode 3 [13], the fatigue category is expressed as the normative fatigue strength in [MPa] for $2\cdot10^6$ cycles. The results are listed in Table 4. The effect of the above is the percentage difference in the fatigue strength determined against the parent material samples (P_00), being about 5 [%] for the ground welded samples (G_02 and G_11).

The effect of the grinding operation on the fatigue strength/life can be observed after the analysis of the graph in Figure 7 and the results listed in Table 4. Grinding improves the fatigue strength/life, which agrees with the results of the studies included in the literature [14].

Table 4. Fatigue strength results

	Samples type	
	P_00	G_02 and G_11
Fatigue strength of specimens at $2 \cdot 10^6$ cycles [MPa]	288	303

Summary

Based on the previous tests of butt-welded joints in DUPLEX 2205 steel made using various laser-welding parameters, two joints were selected and subjected to fatigue testing. A comparative analysis was conducted for the results of the fatigue strength/life of laser-welded joints that had been ground against the fatigue strength/life of the parent material.

Based on the hysteresis loops, shape strengthening of the material was observed after the welding process compared to the base material. The strengthening may be caused by the increase in the hardness of the weld zone (about 290 HV0.1) and heat affected zone (about 275 HV0.1) compared to the base metal (about 265 HV0.1).

For the samples prepared in accordance with Fig. 3b made using two different welding parameters, which included ground face and root geometric notches, no changes were observed in the fatigue strength/life. The increase of the fatigue strength/life of ground and welded joints in relation to non-ground base material was observed. The grinding operation is better, especially for lower stress levels, and it increases the high cycle fatigue life. The grinding operation increased fatigue strength for $2 \cdot 10^6$ by about 5%.

References

1. Boehm L.: New Engineering Processes in Aircraft Construction, Application of Laser-Beam and Friction Stir Welding, Glass Physics and Chemistry, Vol. 31, No. 1, 2005, pp. 27–29.
2. Hobbacher A.: Kierunki rozwoju techniki spawania i łączenia w wykonaw- stwie wyrobów niezawodnych i ekonomicznych, Biuletyn Instytutu Spawalnictwa, Nr 2/2004, s. 22–33.
3. Konuk A.R, RGKM Aarts, Huis A.J in't Veld, Sibillano T., Rizzi D., Ancona A.: Process control of stainless steel laser welding using an optical spectroscopic sensor, Phys Procedia 2011; 12: 744–51.
4. Sołtysiak R.: Effect of laser welding parameters of DUPLEX 2205 steel welds on fatigue life. Solid State Phenomena Vol. 223 (2015) , pp. 11–18.
5. Cui C.Y., Cui X.G., Ren X.D., Liu TT., Hu J.D., Wang Y.M.: Microstructure and microhardness of fiber laser butt welded joint of stainless steel plates, Materials and Design 49 (2013), pp. 761–765.

6. Yang Y., Wang Z., Tan H., Hong J., Jiang Y., Jiang L., Li J.: Effect of a brief post-weld heat treatment on the microstructure evolution and pitting corrosion of laser beam welded UNS S31803 duplex stainless steel, Corrosion Science 65 (2012), pp. 472–480.
7. Taban E., Kaluc E.: Welding behaviour of DUPLEX and SUPERDUPLEX stainless steels using laser and plasma arc welding processes, Welding In The World, Peer-reviewed Section 07/08 2011 Vol. 55, pp. 48–57.
8. Muthupandi V., Srinivasan P.B., Seshadri S.K., Sunderasan S.: Effect of weld metal chemistry and heat input on the structure and properties of duplex stainless steel welds, Materials Science & Engineering: A, Structural Materials: Properties, Microstructure and Processing, 2003, vol. 358, no. 1–2, pp. 9–16.
9. Karlsson L., Tolling J.: Experiences and new possibilities in welding duplex stainless steels. Proc., IIW Regional Congress on Welding and Related Inspection Technologies, South Africa, 2006.
10. Saeid T., Abdollah-Zadeh A., Assadi H., Malek Ghaini F.: Effect of friction stir welding speed on the microstructure and mechanical properties of a duplex stainless steel, Materials Science & Engineering: A, Structural Materials: Properties, Microstructure and Processing, 2008, vol. 496, no. 1–2, pp. 262–268.
11. Stergiou V., Papadimitriou G.D.: Effect of an electron beam surface treatment on the microstructure and mechanical properties of SAF 2205 joints produced with electron beam welding, Journal of Materials Science, (2012) 47, pp. 2110–2121.
12. PN-EN ISO 15614-11: 2005 Specification and qualification of welding procedures for metallic materials – Welding procedure test – Part 11: Electron and laser beam welding.
13. PN-EN 1993-1-9: 2007 Eurocode 3: Design of steel structures – Part 1–9: Fatigue.
14. Vidal C., Infante V.: Fatigue Behavior of Friction Stir-Welded Joints Repaired by Grinding, Journal of Materials Engineering and Performance (2014) 23, pp. 1340–1349.

Wpływ parametrów spawania laserowego stali typu DUPLEX na trwałość zmęczeniową złączy z usuniętym karbem geometrycznym w postaci lica i grani

Słowa kluczowe

Spawanie laserowe, trwałość zmęczeniowa, stal duplex, stal nierdzewna, parametry spawania.

Streszczenie

W połączeniach spawanych występują lokalne spiętrzenia odkształceń spowodowane głównie geometrią złącza (karb geometryczny) jak również niejednorodnością strukturalną (karb strukturalny). Czynniki te mają znaczący wpływ na trwałość zmęczeniową złącza. W niniejszej pracy przedstawiono wyniki prób zmęczeniowych złączy spawanych laserowo ze stali typu DUPLEX 2205 z uwzględnieniem karbu strukturalnego. Karb geometryczny w postaci lica i grani spoiny usunięto. Złącza spawane czołowo wykonano przy użyciu lasera dyskowego typu Nd-YAG bez materiału dodatkowego dla dwóch różnych parametrów spawania. Parametry zostały dobrane na podstawie wcześniejszych badań (zgodnie z PN-EN ISO 15614-11: 2005) przeprowadzonych na złączach wykonanych kilkunastoma różnymi parametrami spawania. W badaniach trwałości zmęczeniowej połączeń spawanych laserowo pominięto karb geometryczny. Pozwoliło to na określenie optymalnych parametrów spawania laserowego stali typu DUPLEX 2205 ze względu na trwałość zmęczeniową powstałej podczas spawania struktury złącza. Dodatkowo otrzymane wyniki trwałości zmęczeniowych złączy spawanych odniesiono do trwałości zmęczeniowej próbek pobranych z materiału rodzimego.